BMAL1 modulates glutamine supply to control hematopoietic stem and progenitor cell expansion

Tim Petzold[1,2,3], Lydia K. Lutes[1], Keila Navarro I. Batista[1], Antonia Konle[2], Bastien Baechler[1], Stéphane Jemelin[1], Holger Gerhardt[2,3,4], Rachel Golub[5], Christoph Scheiermann[1,6,7,*], Julien Y. Bertrand[1,7,*,‡]

[1]University of Geneva, Faculty of Medicine, Department of Pathology and Immunology, Rue Michel-Servet 1, Geneva 4, Switzerland
[2]Integrative Vascular Biology Laboratory, Max Delbrück Center (MDC) for Molecular Medicine in the Helmholtz Association, Robert-Rössle-Strasse 10, 13125, Berlin, Germany
[3]DZHK (German Center for Cardiovascular Research), 10785, Berlin, Germany
[4]Charité - Universitätsmedizin Berlin, Berlin, Germany
[5]Institut Pasteur, Université Paris Cité, INSERM U1223, Lymphocyte and Immunity Unit, 75015 Paris, France
[6]Biomedical Center (BMC), Institute for Cardiovascular Physiology and Pathophysiology, Walter Brendel Center for Experimental Medicine (WBex), Faculty of Medicine, Ludwig-[6]Maximilians-Universität (LMU) Munich, Planegg-Martinsried, Germany
[7]Geneva Centre of Inflammation Research, University of Geneva, Faculty of Medicine, Rue Michel-Servet 1, Geneva 4, Switzerland

[*]Equal contribution
[‡]Author for correspondence: julien.bertrand@unige.ch

Abstract

Following specification in the dorsal aorta, hematopoietic stem and progenitor cells (HSPCs) proliferate in the HSPC niche, known as the caudal hematopoietic tissue (CHT) in zebrafish. Here we demonstrate that *bmal1a*, a core component of the circadian clock machinery, is expressed in CHT endothelial cells (ECs) and affects HSPCs in a non-cell autonomous manner. Using endothelial cell-specific dominant-negative Bmal1a zebrafish lines, we demonstrate a striking increase in HSPC numbers in the CHT, resulting from enhanced HSPC proliferation. RNA-sequencing of dominant-negative *bmal1a* ECs sorted from the CHT shows a downregulation of *glud1a*, resulting in increased glutamine levels in the CHT. This newly discovered *bmal1a-glud1a*-glutamine pathway fuels HSPC expansion. We demonstrate that this glutamine synthesis pathway controlling HSPC expansion is likely conserved in the

mouse fetal liver (FL) niche, in which hepatocytes are the likely source of glutamine. Together, our data uncover a novel mechanism of HSPC homeostasis, in which EC BMAL1, expressed by the niche, controls the amount of bioavailable glutamine for HSPCs by regulating the expression of genes involved in glutamine synthesis.

Keywords: HSPC, niche, expansion, glutamine, endothelial cell, zebrafish, mouse

Introduction

Circadian rhythms are biological oscillations which regulate most physiological and behavioural processes, allowing organisms to adapt to a fluctuating environment. In mammals, circadian rhythms are sustained by transcriptional translational feedback loops (TTFL) (Hurley et al., 2016). The core mammalian clock genes include *Bmal1* and *Clock*, which encode activator proteins of the TTFL. BMAL1 and CLOCK proteins form a heterodimer complex which binds to E-Box sequences in the promoters of target genes, including the TTFL repressor circadian genes *Per* and *Cry*. Transcription of *Per* and *Cry* genes results in heterodimerization of the PER/CRY transcription factor complex, which ultimately inhibits *Bmal1* and *Clock* expression (Scheiermann et al., 2013). Together with additional auxiliary *Rev-erba/Ror* regulatory loops of *Bmal1* and *Clock*, this TTFL mediates approximately 24-hour oscillations (Relogio et al., 2011, Ueda et al., 2005).

The zebrafish circadian clock architecture is very similar to that of mammals. However, due to a third round of teleost whole genome duplication in this species, additional copies of many genes are present, including those of the circadian clock (Liu et al., 2015). Zebrafish therefore possess two paralogues of *bmal1* (Wang, 2009), three of *clock* (Wang, 2008b), four of *Per* (Wang, 2008a) and seven of *Cry* (Liu et al., 2015), adding molecular complexity to the zebrafish clock. The precise functions of the individual gene paralogues are yet to be established (Froland Steindal and Whitmore, 2019).

BMAL1 and CLOCK proteins regulate the transcription of thousands of target genes. In mammals, it is thought that BMAL1 and CLOCK drive the expression of 15% of the transcriptome (Trott and Menet, 2018), including a plethora of genes involved in metabolism (Reinke and Asher, 2019). In fact, metabolism, including cellular and organellar metabolism (Neufeld-Cohen et al., 2016), as well as blood

nutrient homeostasis (Lamia et al., 2008), is one of the most rhythmic processes. Light-dark cycles have been shown to regulate hematopoietic stem and progenitor cell (HSPC) self-renewal and differentiation by cell intrinsic metabolic re-wiring of these cells (Golan et al., 2018). Furthermore, it was previously demonstrated that many genes involved in metabolism are under the control of BMAL1 and CLOCK in malignancies such as acute myeloid leukaemia (AML) (Puram et al., 2016). The expression of genes involved in the synthesis of amino acids such as glutamine, have been shown to be altered in the absence of a functional circadian clock in the context of cancer (Wang et al., 2024), while emerging evidence also shows that circadian clock genes are expressed in oocytes and during the development of the rat embryo and primate fetus (Seron-Ferre et al., 2007), suggesting that these genes play a role during embryogenesis.

In vertebrates, hematopoiesis takes place in successive waves, starting with primitive hematopoietic cells, followed by the emergence of erythro-myeloid progenitors, and culminating with the definitive wave in which hematopoietic stem and progenitor cells (HSPCs) are generated (Bertrand and Traver, 2009). HSPCs are specified from the dorsal aorta (Bertrand et al., 2010a, Boisset et al., 2010, Kissa and Herbomel, 2010), and many recent studies have demonstrated heterogeneity in terms of developmental potential among these aorta-derived progenitors. Work in zebrafish has, for example, pointed to the existence of lymphoid-restricted progenitors (Tian et al., 2017), lymphoid-erythroid primed progenitors and lympho-myeloid primed progenitors, among others (Ulloa et al., 2021, Torcq et al., 2025). The identities of such progenitors were determined using transcriptomics analysis of sorted progenitors, or *a posteriori*, after lineage-tracing, and currently there is a lack of transgenic marker lines to allow these sub-populations to be robustly characterized *in vivo* in zebrafish. Among these HSPCs, only a rare subset fulfils the criteria of true *bona fide* hematopoietic stem cells (HSCs) which can contribute to adult multilineage hematopoiesis (Bertrand et al., 2010a, Tian et al., 2017, Henninger et al., 2017). However, all these definitive progenitors share a number of common features; they are derived from the aorta, their generation is dependent on Notch signalling, and they all depend on the expression of *gata2b* (Butko et al., 2015). Following specification from the aorta, HSPCs colonize the caudal hematopoietic tissue (CHT) in zebrafish, or the fetal liver (FL) in mammals, via the blood circulation (Mahony and Bertrand, 2019). A crucial component of this

embryonic niche is the vascular endothelium (Tamplin et al., 2015, Khan et al., 2016), which provides HSPCs with highly regulated signals allowing them to expand. While some factors controlling the vascular HSPC niche have been discovered (Cacialli et al., 2021, Mahony et al., 2016, Xue et al., 2017), a complete picture of the molecular interplay involved is lacking. In particular, the role of the circadian clock in this process is unknown.

Previous work has shown that circadian clock genes are expressed in venous ECs of the zebrafish embryo at 24 hours post-fertilisation (hpf) (Gurung et al., 2022). We therefore reasoned that the clock may play a role in HSPC development in the CHT. Here, using newly generated EC-specific dominant-negative zebrafish lines, we report that the core circadian clock component *bmal1a* is a previously unknown regulator of HSPC expansion in zebrafish. We demonstrate that endothelial *bmal1a* acts as a negative regulator of HSPC proliferation in the vascular niche during zebrafish development, by controlling the expression of *glud1a*, a gene that plays a key role in the glutamine synthesis pathway. Glutamine plays an important role in cell proliferation (Yoo et al., 2020). In the context of hematopoiesis, glutamine has been shown to promote myeloid differentiation, augmenting the number of myeloid colonies in *in vitro* culture assays (Dass et al., 1984). More recently, glutamine was shown to be important for emergency myelopoiesis in the context of systemic inflammation, by promoting myeloid cell expansion and differentiation (Pizzato et al., 2023). In this process, glutamine is converted into glutamate, then α-ketoglutarate which can fuel the Krebs cycle in myeloid progenitors (Pizzato et al., 2023). Finally, glutamine is also important for erythroid development, since its conversion into succinyl-CoA is essential for heme production (Burch et al., 2018). This heme production, however, produces toxic ammonium which causes oxidative stress (Lyu et al., 2024). Detoxification of ammonium is brought about through the conversion of glutamate into glutamine via glutamine synthetase, which is upregulated in erythroid precursors (Lyu et al., 2024). Therefore, glutamine acts as an important amino acid in both steady state and malignant hematopoiesis. As such, targeting glutamine-related pathways may provide novel treatment routes for AML and related syndromes (Xiao et al., 2023).

Our data indicate that *bmal1a* controls the expansion rate of HSPCs, by regulating the glutamine concentration in the niche. While deletion of *Bmal1* in mouse ECs did not result in a similar HSPC phenotype, this is likely due to *Glud1*

being exclusively expressed by hepatocytes in the mammalian FL. When we increased the activity of Glud1 in *in toto* FL organ culture through addition of L-leucine, we observed a significant decrease in HSPC numbers, demonstrating that the role of this important metabolic pathway for HSPC expansion is also conserved in the mouse hematopoietic niche. Taken together, we have discovered a previously unknown, non-cell autonomous molecular mechanism controlling HSPC homeostasis: Bmal1 reprograms glutamine metabolism by regulating genes involved in glutamine synthesis, which governs the rate of HSPC expansion.

Results

The core circadian clock gene *bmal1a* is expressed in the CHT vasculature

To investigate the spatio-temporal expression patterns of circadian clock genes during zebrafish development, embryos were raised in 12hr light:dark cycles before whole mount *in situ* hybridisation (WISH) for *bmal1a*, *bmal1b* and *clocka* was performed every 6 hours between 24 and 84 hpf (*in situ* images shown between 24-66 hpf). *bmal1a* was expressed in the CHT region between 24 and 42 hpf but not at later stages (**Fig. 1A-B**). Furthermore, *bmal1a* expression in this region did not oscillate in a circadian manner (**Fig. 1B**). However, *bmal1a* showed oscillatory expression in the heads of embryos in the assessed timeframe, indicating tissue-specific expression patterns (**Supp. Fig. 1**). Compared to *bmal1a*, *bmal1b* was more broadly expressed along the entire trunk at 24 hpf (**Supp. Fig. 2A**), whereas *clocka* expression was specifically expressed in the CHT at 24 hpf (**Supp. Fig. 2B**). This indicates that the protein products of *bmal1a* and *clocka* may functionally interact in that region.

Since mouse *Bmal1* is the only non-redundant circadian clock gene (Scheiermann et al., 2018), we focused our subsequent investigations on *bmal1a* and *bmal1b*. In order to determine whether ECs are responsible for the expression observed by *in situ* hybridisation, we sorted ECs from *kdrl:EGFP* embryo tails at 24 hpf by fluorescence activated cell sorting (FACS, for gating strategy see **Supp. Fig. 2C**), before carrying out *bmal1a* and *bmal1b* qPCR (**Fig. 1C and Supp. Fig. 2D**). Expression of *bmal1a* and *bmal1b* were both found to be significantly enriched in tail ECs with *bmal1a* being more highly expressed than *bmal1b* (**Fig. 1C and Supp. Fig. 2D**). However, to avoid any potential functional redundancy, we designed a strategy

that would impair the activities of both Bmal1a and Bmal1b proteins in CHT-ECs, to study their contribution(s) to the hematopoietic niche.

Endothelial-specific dominant-negative Bmal1a results in a non-cell autonomous increase in HSPCs in the CHT

To specifically impair Bmal1a activity in ECs, we engineered a new dominant-negative (DN) *bmal1a* zebrafish line (*UAS:DN-bmal1a*). This DN *bmal1a* encodes a protein which contains the DNA-binding domain, a PAS domain required for heterodimerisation to CLOCK and a nuclear translocation domain (**Supp. Fig. 3A**). However, it lacks the C-terminal transactivation domain required by Bmal1a to induce transcription of its target genes (Gustafson et al., 2017). We reasoned that the *DN-Bmal1a* protein generated in the *UAS:DN-bmal1a* line would also occupy E-box elements and, as such, would prevent endogenous Bmal1 and Clock proteins from binding these DNA motifs.

We crossed the *UAS:DN-bmal1a* with *kdrl:GAL4* zebrafish adults, to specifically express *DN-bmal1a* in embryonic ECs. In *kdrl:GAL4;UAS:DN-bmal1a* embryos, we detected *bmal1a* throughout the whole vascular system, as determined by WISH (**Supp. Fig. 3B**), in contrast to CHT-specific *bmal1a* expression in wild-type controls No gross morphological alterations were present in these double transgenic embryos. In particular, aortic vascular specification and development was unaffected in *kdrl:GAL4;UAS:DN-bmal1a* embryos, as indicated by normal *dll4* expression at 28 hpf (**Supp. Fig. 3D**) and *kdrl:EGFP* expression at 48 hpf (**Supp. Fig. 3E**). To determine whether *DN-bmal1a* efficiently disrupted circadian clock function, we performed qPCR analysis of the expression of *per2*, a known Bmal1:Clock target gene and component of the circadian architecture in both mammals (Takahashi, 2017) and zebrafish (Ruggiero et al., 2021). *per2* mRNA expression was decreased in *kdrl:GAL4;UAS:DN-bmal1a* embryos compared to controls at 36 hpf (**Supp. Fig. 3C**), suggesting that the construct was indeed acting as a dominant-negative. *per2* expression was not totally abolished as our dominant-negative construct was only effective in ECs, while qPCR was performed on whole embryos.

We also generated a second *DN-bmal1a* line that targets the highly-conserved E-K-R-R motif, which is required for binding to the E-box consensus sequence CANNTG in the promoters of target genes (Hosoda et al., 2004). Substitution of the E-K-R-R arginine at position 91 with alanine in the mouse, results

in a dominant-negative BMAL1, since it is unable to support DNA binding, while still forming a heterodimer with CLOCK (Hasegawa et al., 2019). We identified the same arginine at position 88 in zebrafish *bmal1a* and mutated the codon to encode alanine (*UAS:R88A-DN-bmal1a*, **Supp. Fig. 4A**). Crossing the *UAS:R88A-DN-bmal1a* with *kdrl:GAL4* zebrafish adults yielded expression of *bmal1a* throughout the whole vascular system in double-positive embryos (**Supp. Fig. 4B**), phenocopying the *kdrl:GAL4;UAS:DN-bmal1a* line. Again, no gross morphological alterations were apparent and aortic vascular specification was unaffected, as indicated by normal *dll4* expression at 28 hpf (**Supp. Fig. 4C**).

We next investigated whether HSPC numbers were altered in *kdrl:GAL4;UAS:DN-bmal1a* embryos. We found no differences in *runx1* expression at 28 hpf (**Supp Fig. 5A**), or *cmyb* expression at 36 hpf (**Supp Fig. 5B**), indicating that HSPC specification was unaffected despite the expression of *DN-bmal1a* in all endothelial cells, showing that Bmal1a exerts no cell-autonomous role on HSPC emergence. We also found no differences in *cmyb*$^{+}$ cell numbers in the CHT region at 48 (**Supp Fig. 5C**) and 54 hpf (**Supp Fig. 5D**), indicating that HSPCs were able to colonize the CHT normally, at least at these timepoints. However, at 60 hpf, there was an increase in the number of *cmyb*$^{+}$ cells in the CHT of double transgenic embryos (**Fig. 2A**), which extended to larvae at 4.5 dpf (**Fig. 2B**), as determined by quantifying the *cmyb*$^{+}$ signal area. Similar observations were made when we used the second DN construct (*UAS:R88A-DN-bmal1a*), with no difference in *runx1* expression at 28 hpf (**Supp. Fig. 4D**) but an increase in *cmyb* expression in larvae at 4.5 dpf (**Supp. Fig. 4E**). Since both our dominant-negative *bmal1a* zebrafish lines gave identical phenotypes, we chose to continue with the *UAS:DN-bmal1a* line only, throughout the rest of the study.

The increase in HSPC numbers in the CHT was corroborated by using transgenic lines which fluorescently mark HSPCs. These lines (*cmyb:GFP*, *cd41:EGFP* and *runx1:NLS-mCherry*) were crossed with *kdrl:GAL4;UAS:DN-bmal1a* double-transgenic lines, and the resulting triple-transgenic larvae were analysed by microscopy. HSPC numbers were found to be significantly increased at 72 hpf in the CHT of triple-transgenic combinations relative to controls (**Fig. 2C, Supp. Fig. 6A** and **Supp. Fig. 6B**). The increase in HSPCs remained present at 7 dpf, as determined by *cmyb* WISH (**Supp. Fig. 6C**).

In order to exclude any cell-autonomous effect of our *DN-bmal1a*, we placed the construct under the control of *gata2b:KALTA4*, in order to drive *DN-bmal1a* expression specifically in HSPCs (Butko et al., 2015). We found no difference in CHT-HSPC numbers in double-transgenic larvae at 4.5 dpf (**Fig. 2D**). Finally, we investigated whether the EC-specific dominant-negative Bmal1a had an effect on the number of differentiated cells in the CHT. We found no difference in the numbers of neutrophils (as determined by *mpx*) (**Supp. Fig 7A**), erythrocytes (*gata1*) (**Supp. Fig 7B**), macrophages (*mfap4*) (**Supp. Fig 7C**) or T-cells (*rag1*) (**Supp. Fig 7D**) between *kdrl:GAL4;UAS:DN-bmal1a* larvae and controls at 4.5 dpf. This lack of difference in the number of differentiated cells in *kdrl:GAL4;UAS:DN-bmal1a* larvae may be attributed to the fact that the expanded HSPCs differentiate later, do not have the same differentiation potential or that their expansion rate exceeds the rate of differentiation. Nevertheless, these findings demonstrate a role of CHT-EC specific *bmal1a* in controlling HSPC expansion in a non-cell autonomous manner.

Endothelial-specific dominant-negative Bmal1a results in an increased HSPC proliferation rate

Vascular morphology such as expanded vascular plexus CHT has a direct impact on the number of HSPCs (Xue et al., 2017, Tamplin et al., 2015). Furthermore, many factors derived from the CHT vasculature are known to positively regulate HSPC expansion (Wattrus and Zon, 2018). Thus, we reasoned that vascular morphology or numbers of ECs in the CHT may be altered in *kdrl:GAL4;UAS:DN-bmal1a* embryos, resulting in the observed HSPC increase. However, we found no gross vascular morphological alterations in *kdrl:GAL4;UAS:DN-bmal1a;kdrl:EGFP* embryos (**Supp. Fig 3E**) and the number of CHT-ECs between *kdrl:GAL4;UAS:DN-bmal1a;kdrl:nls-EGFP* zebrafish and *kdrl:GAL4;kdrl:nls-EGFP* controls was similar at 48 hpf (**Supp. Fig 3F**), when some HSPCs in the CHT may still be EGFP positive following specification from the dorsal aorta endothelium, but also at 4.5 dpf (**Supp. Fig 3G**), when this is likely no longer the case.

We speculated that the increase in CHT resident HSPCs in *kdrl:GAL4;UAS:DN-bmal1a* larvae may be due to a reduced migration rate of these cells away from this niche to the kidney glomerulus, which represents the adult niche. To assess this, we performed *cmyb* WISH in *kdrl:GAL4;UAS:DN-bmal1a*

larvae and controls at 4.5 and 7 dpf, before imaging and quantifying *cmyb* signal in the kidney glomeruli. At 4.5 dpf, there was reduced *cmyb* WISH signal in the kidney glomeruli in *kdrl:GAL4;UAS:DN-bmal1a* larvae (**Supp. Fig 8A**), while at 7 dpf this difference was no longer present (**Supp. Fig 8B**). Together these data suggest that there is a transient delay in migration of HSPCs away from the CHT in the absence of functional endothelial Bmal1a.

We reasoned that the increase in HSPCs in the niche may also, at least in part, be due to a difference in their expansion rate in the CHT of *kdrl:GAL4;UAS:DN-bmal1a* animals. Therefore, we assessed the proliferation rate of CHT-HSPCs by staining for anti-phospho-histone 3 (PH3), a marker of mitotic cells (Hendzel et al., 1997), in *kdrl:GAL4;UAS:DN-bmal1a;cmyb:GFP* larvae and controls at 60 and 72 hpf. Triple-transgenic larvae showed a significant increase in the number of $GFP^{+}PH3^{+}$ cells in the CHT compared to controls at both 60 hpf (**Fig. 3A**) and 72 hpf (**Fig. 3B**). This indicated that the lack of functional Bmal1a in CHT-ECs results in an enhanced HSPC proliferation rate in the niche, which we decided to investigate further.

Endothelial-derived glutamine fuels definitive HSPC proliferation

We hypothesised that the lack of functional Bmal1a in CHT-ECs results in alterations in transcriptional output leading to enhanced HSPC proliferation. To investigate this, we dissected tails of *kdrl:GAL4;UAS:DN-bmal1a;kdrl:EGFP* embryos and of *UAS:DN-bmal1a;kdrl:EGFP* controls at 36 hpf and FACS-sorted $EGFP^{+}$ cells (**Fig 4A**, for sorting strategy, see **Supp. Fig. 9A**). We subsequently performed bulk RNA-sequencing (RNA-seq) on these ECs and found 95 differentially regulated genes between the two genotypes (**Fig. 4B-C**). The majority of differentially regulated genes were found to be downregulated in *kdrl:GAL4;UAS:DN-bmal1a;kdrl:EGFP* embryos (84/95). A known direct target gene of Bmal1a, *nr1d2a* (Cho et al., 2012, Amaral and Johnston, 2012), was markedly downregulated in our RNA-seq dataset (**Fig. 4B-C**), providing further evidence of disrupted circadian clock function induced by the DN-Bmal1a protein.

The RNA-seq data revealed that *glud1a* was downregulated in *kdrl:GAL4;UAS:DN-bmal1a;kdrl:EGFP* embryos (**Fig. 4B-C**), which was confirmed by qPCR (**Supp. Fig 10A**) and WISH (**Supp. Fig 10B**). Glutamate dehydrogenase 1A (GLUD1A or GDH1), is a hexameric enzyme which catalyses the conversion of glutamate to α-

ketoglutarate (Plaitakis et al., 2017, Shang et al., 2020). It counteracts the activity of GLUL (glutamate ammonia ligase), a second enzyme (glutamine synthetase) that produces glutamine *de novo* from glutamate and ammonia (**Fig. 4D**) (Eelen et al., 2018).

We reasoned that a down-regulation of *glud1a* in our endothelial-specific *DN-bmal1a* zebrafish embryos, could result in an accumulation of glutamate in ECs. This increase in the amount of available glutamate would ultimately result in an increase in glutamine production, due to an enhanced conversion of glutamate to glutamine by GLUL. To test this, we first examined the expression patterns of *glud1a* and *glul* in zebrafish by *in situ* hybridisation, to determine whether these genes are expressed in the CHT during the time of HSPC expansion. *glud1a* was found to be expressed in the CHT between 24 and 48 hpf (**Fig. 4E**), while *glula* (zebrafish possess three paralogues of the *glul* gene, *glula*, *glulb* and *glulc*) was expressed in the CHT between 24 and 60 hpf (**Fig. 4E**). Therefore, during and following aorta-derived HSPC colonisation of the CHT, *glula* may drive the production of glutamine in the niche. To investigate this hypothesis further, we quantified the amount of glutamine in the tails of 72 hpf *kdrl:GAL4;UAS:DN-bmal1a* larvae relative to controls. We observed a significant increase in the concentration of glutamine present in the EC-specific *DN-bmal1a* embryos in comparison to controls (**Fig. 5A**), suggesting that a reduction of Bmal1a function, and the resulting downregulation in *glud1a* expression, may ultimately account for an increased synthesis of glutamine.

Since glutamine is known to be necessary for the proliferation of many cell types, including malignant (Zhang et al., 2017, Nguyen and Duran, 2018) and stem cells (Shang et al., 2020, Yu et al., 2019), we hypothesised that the glutamine increase in the EC-specific *DN-bmal1a* embryos was the driver of the HSPC expansion phenotype observed in these animals. To investigate this, we supplemented wild-type zebrafish with 1mM glutamine, following HSPC specification, between 48 hpf and 4.5 dpf. Glutamine supplementation resulted in increased HSPC numbers in the CHT as determined by WISH (**Fig. 5D**), in line with previous *in vitro* data demonstrating the importance of glutamine for HSPC expansion (Ni et al., 2019). Together, this data suggests that the increase in glutamine production in *kdrl:GAL4;UAS:DN-bmal1a* embryos provides an explanation for the increased number of HSPCs in the CHT of these embryos.

We next investigated whether modulating GLUD1A activity affects HSPC numbers. We supplemented *kdrl:GAL4;UAS:DN-bmal1a* or wild-type zebrafish with the GLUD1A allosteric activators, BCH (Han et al., 2016, Sener et al., 1981) and ADP (Li et al., 2011, Koberstein and Sund, 1973), between 48 hpf and 4.5 dpf. Supplementation of *kdrl:GAL4;UAS:DN-bmal1a* embryos with 500μM BCH (**Fig. 5B**) or 100μM ADP (**Fig. 5C**) resulted in decreased CHT *cmyb* signal at 4.5 dpf. Similarly, supplementation of wild-type embryos with either 500μM BCH (**Fig. 5E**) or 100μM ADP (**Fig. 5F**) also resulted in decreased CHT *cmyb* signal at 4.5 dpf. Wild-type embryos were then also supplemented with another allosteric activator of GLUD1A, L-leucine (Sener and Malaisse, 1980, Couee and Tipton, 1989). Supplementation of wild-type embryos with 1mM L-leucine (**Fig. 5G**) also resulted in decreased CHT *cmyb* signal at 4.5 dpf.

Since the HSPC pool is very heterogeneous, we next wanted to understand which type(s) of progenitors are affected by GLUD1A activity and glutamine. To investigate this, we first treated *mindbomb* embryos with glutamine. *mindbomb* mutants are deficient for Notch signalling, and therefore lack all definitive HSPCs (Burns et al., 2005), but still produce erythromyeloid progenitors (Bertrand et al., 2010b). When treating *mindbomb* siblings with glutamine from 48 to 72 hpf, we found an increase in HSPC expansion, as determined by an increase in *cmyb* WISH signal at 72 hpf (**Supp. Fig 11A**). *mindbomb*$^{-/-}$ embryos lacked *cmyb* signal in the CHT (**Supp. Fig 11B**) and did not exhibit any increase following treatment with glutamine (**Supp. Fig 11B**), demonstrating that only Notch-dependent aorta-derived HSPCs are sensitive to glutamine addition. To corroborate this finding, we supplemented *gata2b:KALTA4*$^{+}$*;UAS:lifeact-GFP*$^{+}$ embryos with glutamine or L-leucine between 48 and 72 hpf. In line with our data using other HSPC reporter lines, we found more *gata2b:GFP*$^{+}$ HSPCs in the CHT of glutamine-treated embryos at 72 hpf (**Supp. Fig 11C**). *gata2b:KALTA4*$^{+}$*;UAS:lifeact-GFP*$^{+}$ embryos treated with L-leucine had fewer *gata2b:GFP*$^{+}$ cells in the CHT at 72 hpf (**Supp. Fig 11C**), providing evidence that glutamine is important for the expansion of aorta-derived definitive HSPCs.

Together, these results show that the *bmal1a-glud1a*-glutamine pathway can directly alter definitive (aorta-derived) HSPC expansion in the CHT, by modulating the amount of glutamine available to HSPCs.

Glutamine is transported by SLC channels

Amino acids such as glutamine induce cell proliferation by activating the mTOR pathway (Jewell et al., 2015, Gonzalez et al., 2020). Glutamine is primarily transported via Slc (solute carrier)-type channels (Bhutia and Ganapathy, 2016, Yoo et al., 2020), some of which are able to carry out the export of glutamine, while others facilitate glutamine import. A further subset can both export and import glutamine (Bhutia and Ganapathy, 2016). We thus analysed the expression of *slc* genes (pre-selected on their known capacity to transport glutamine) in CHT-ECs and HSPCs at 48 hpf, prior to the HSPC expansion phase. *kdrl:EGFP*$^{+}$ ECs and *ikaros:EGFP*^{low} HSPCs (Mahony et al., 2018) were sorted by FACS (for sorting strategies, see **Supp. Fig. 9A-B**) from 48 hpf embryos and qPCR was performed to determine the expression of selected *slc* genes in the sorted populations. *slc1a5* was determined to be the most highly expressed in CHT-ECs (**Supp. Fig. 12A**), while some other *slc* genes such as *slc38a5a* and *slc38a5b* were also detected, albeit at a lower level. In the HSPC population, expression of importing *slc* genes was analysed, as well as the expression of *slc* genes encoding transporters which carry out glutamine import and export. As in ECs, *slc1a5* was determined to be the most highly expressed of the *slc* genes examined in HSPCs, along with some expression of *slc38a5a*, *slc38a5b* and *slc38a2* (**Supp. Fig. 12B**). Together, the data demonstrates that genes encoding channels required for the transport of glutamine out of ECs and into HSPCs are expressed in the CHT at the beginning of HSPC expansion.

To probe whether SLC transporters do indeed play a role in HSPC expansion in the CHT, we treated wild-type embryos with the SLC blocker L-γ-glutamyl-*p*-nitroanilide (GPNA). GPNA was originally thought to be a specific Slc1a5 channel inhibitor (Esslinger et al., 2005), but has recently been shown to also block the activity of other sodium-dependent SLCs (Broer et al., 2016) and also system L transporters such as LAT1 and LAT2 (Chiu et al., 2017). Treating wild-type embryos with GPNA from 48 hpf to 4.5 dpf resulted in a complete loss of HSPCs in the CHT as determined by *cmyb* WISH (**Supp. Fig. 12F**), indicating that glutamine transport into HSPCs may indeed be critical not only for HSPC expansion but also for their survival.

Loss of fetal liver endothelial *Bmal1* does not affect HSPC numbers in the mouse

Finally, we wanted to determine whether the HSPC expansion phenotype observed in the absence of functional EC-Bmal1a in zebrafish is conserved in mammals. To investigate this, we used a tamoxifen-inducible EC-specific *Bmal1* KO line, *Cdh5*:*Cre*^{ERT2};*Bmal1*$^{flox/flox}$. Pregnant mice were injected i.p. with 1mg tamoxifen at embryonic day (E)10.5, following HSPC specification (**Supp. Fig. 13A**). Subsequently, embryo FLs were harvested at E13.5 and analyzed by flow cytometry. ECs as well as LSKs (lineage-negative Sca-1^{+} c-Kit^{+} HSPCs) were also sorted by FACS for gene expression analyses by qPCR (for FACS gating strategy, see **Supp. Fig. 14**) and the purity of these populations was confirmed by qPCR analysis of *Cdh5* (**Supp. Fig. 15A**) and *Cmyb* (**Supp. Fig. 15B**) expression. *Bmal1* expression was reduced in FACS-sorted *Cdh5*:*Cre*^{ERT2};*Bmal1*$^{flox/flox}$ FL-ECs relative to controls (**Supp. Fig. 13B**), but this was not the case in sorted FL-LSKs (**Supp. Fig. 13C**), demonstrating EC-specific *Bmal1* deficiency.

Next, we assessed the impact of the EC-specific *Bmal1* KO on FL LSK numbers in mouse embryos at E13.5. We did not observe differences in LSK numbers in *Cdh5*:*Cre*^{ERT2};*Bmal1*$^{flox/flox}$ embryos compared to controls (**Supp. Fig. 15C-D**). Furthermore, we found that expression of the cell proliferation markers, *Mki67* (**Supp. Fig. 15E**) and *Ccnb2* (*CyclinB2*) (**Supp. Fig. 15F**) were unchanged in FL-LSKs between the two genotypes. Together, these results suggest that the HSPC expansion phenotype observed in the zebrafish CHT is not conserved in the analogous region in the mouse embryo, the FL.

We focused on investigating whether the *Glud1*-glutamate-*Glul*-glutamine pathway was affected in EC-specific *Bmal1* KO mouse embryos. *Glud1* expression was quantified in sorted FL-ECs by qPCR. *Glud1* expression was unchanged in *Cdh5*:*Cre*^{ERT2};*Bmal1*$^{flox/flox}$ ECs, relative to controls (**Supp. Fig. 13D**). This lack of transcriptional control of *Glud1* by Bmal1 in mouse FL-ECs provides an explanation as to why the HSPC expansion phenotype present in *kdrl:GAL4;UAS:DN-bmal1a* zebrafish was not recapitulated in *Cdh5*:*Cre*^{ERT2};*Bmal1*$^{flox/flox}$ mouse embryos. Furthermore, when analysing previously published single-cell transcriptomic data of human FL cells (Popescu et al., 2019), including ECs (**Supp. Fig. 16A**) and hepatocytes (**Supp. Fig. 16B**), we found that *Glud1* is in fact specifically expressed by hepatocytes but not ECs (**Supp. Fig. 16C**).

The *Glud1*-glutamate-*Glul*-glutamine signalling axis is conserved in the mouse fetal liver

We next investigated whether the *Glud1*-glutamate-*Glul*-glutamine pathway is nevertheless conserved in the mouse FL. To assess this, we set up FL organ cultures in a glutamine-free medium before supplementing these with either glutamine or L-leucine, the allosteric activator of Glud1. After 48 hours in culture, FL pieces in each condition were pooled (see materials and methods section for details), and the resulting cell suspension was analysed by cytometry to measure the number of LSKs (**Fig. 6A**). All samples were fully acquired to determine the cell viability and total cell counts. Supplementation of FL organ cultures with glutamine or L-leucine did not affect cell viability (**Fig. 6B**) or total cell numbers (**Fig. 6C**) relative to glutamine-free controls. While the addition of glutamine did not alter the total number of LSKs (**Fig. 6D**) or their percentages (**Fig. 6E**), supplementation with L-leucine decreased the number of LSKs in organ cultures (**Fig. 6D-E**), similar to what was observed in zebrafish. Therefore, the importance of the *Glud1*-glutamate-*Glul*-glutamine axis in regulating HSPC expansion appears to be conserved in the mouse FL niche but is likely to be active in hepatocytes, rather than in ECs.

Discussion

A complete identification of genetic factors which govern HSPC expansion remains incomplete. Here, we have discovered a novel mechanism by which HSPC expansion is controlled in the hematopoietic niche through regulation of the quantity of glutamine available for HSPCs from the niche microenvironment. We have demonstrated that the precise control of bioavailable glutamine is, at least in part, carried out by the core circadian clock component *bmal1a* in zebrafish, through regulation of *glud1a* expression. Our data also suggests that Bmal1a promotes the migration of HSPCs away from the CHT. Whether Bmal1a also plays a role in the regulation of HSPC immigration into the CHT in zebrafish will be interesting to investigate in future work. Furthermore, subsequent investigations using high-resolution 3D imaging of HSPCs in the CHT, kidney glomeruli and thymus may also enhance our understanding of HSPCs in these structures in the context of EC Bmal1a loss of function. Nevertheless, this study contributes to an expanding body of work implicating circadian clock genes not only in metabolic control (Reinke and

Asher, 2019, Marcheva et al., 2013), but also in stem cell biology (Weger et al., 2017, Dierickx et al., 2018) and hematopoiesis (Golan et al., 2019, Mendez-Ferrer et al., 2009).

While previous studies focused on mechanisms which regulate HSPCs in a cell-autonomous manner, here, we demonstrate that Bmal1 in zebrafish exerts its control on HSPC expansion non-cell autonomously. As such, along with previously reported transcription factors which control the HSPCs in CHT, such as Tfec (Mahony et al., 2016), and Klf6a (Xue et al., 2017), we demonstrate that Bmal1a is a newly identified transcriptional regulator of HSPCs in the niche. Puram *et al*., previously showed that human HSPCs possess robust rhythmic expression of *Per2*, a direct target gene of BMAL1 (Puram et al., 2016). Contrary to this, our data in the zebrafish demonstrate that *bmal1a* expression in CHT-ECs does not cycle and is present only at 24-42 hpf. As such, the role of Bmal1a in regulating CHT-resident HSPCs occurs in a non-rhythmic manner. Interestingly non-rhythmic circadian clock gene expression has previously also been shown to also occur in the fetal liver in rats (Varcoe et al., 2013, Wharfe et al., 2011), suggesting that the lack of rhythmic circadian clock gene expression in the embryonic HSPC expansion niche is conserved across species. Further research will be required to better understand the mechanisms which induce rhythmic circadian clock gene expression in some tissues but not others.

Our study indicates that the *bmal1a-glud1a-glula*-glutamine pathway functions as a previously unidentified metabolic crosstalk between CHT-ECs and HSPCs, in line with a recent study showing a similar mechanism to enhance satellite cell proliferation during muscle regeneration (Shang et al., 2020). In their study, Shang and colleagues showed that *Glud1*-knock-out macrophages synthesise more glutamine, which is then exported out of these cells before being taken up by satellite cells, boosting their expansion and subsequent muscle regeneration. Their study was done in the context of muscle damage, in which the tissue must regenerate, and a downregulation in *Glud1* to generate additional glutamine was beneficial. Similarly, our research demonstrates how expression of *bmal1a* and its downstream target *glud1a* are lost in CHT-ECs prior to the arrival of HSPCs in the niche. This downregulation in *glud1a* expression then results in increased glutamine production at the time it is required by incoming HSPCs. We suggest that this *bmal1a-glud1a-glula*-glutamine axis, acting in a highly time-sensitive manner, represents a newly

identified homeostatic control mechanism to precisely regulate HSPC numbers in the CHT. With this in mind, it is tempting to speculate that the mis-regulation of *glud1a* expression or protein activity may be a contributing factor in uncontrolled hematopoietic cell expansion in blood cancers, since leukemic cells are known to be dependent on glutamine (Gregory et al., 2019, Sancerni et al., 2022).

Our *slc* gene expression data in ECs and HSPCs in the CHT suggests that the encoded channels may facilitate the export of glutamine out of ECs, before allowing uptake of glutamine into HSPCs. We found *slc1a5* to be the most highly expressed glutamine export gene in CHT-ECs. Previous reports also showed high expression of *slc1a5* in both human (Oburoglu et al., 2014) and mouse (Ni et al., 2019) HSPCs. While SLC1A5 has been shown to be important for HSPC commitment to the erythroid lineage (Oburoglu et al., 2014), we find it also plays an important role in HSPC expansion. SLC1A5-mediated cellular import of neutral amino acids such as glutamine is known to stimulate mammalian target of rapamycin complex 1 (mTORC1) signalling (Nicklin et al., 2009, Bhutia et al., 2015), a well-known driver of cell growth and proliferation, by activating anabolic processes such as DNA and protein synthesis (Valvezan and Manning, 2019, Mossmann et al., 2018, Saxton and Sabatini, 2017). In our study we used GPNA, which blocks SLC-mediated glutamine transport but also inhibits the uptake of other neutral amino acids (Bhutia and Ganapathy, 2016, Chiu et al., 2017, Fuchs and Bode, 2005), rendering it difficult to discern the relative contribution that a lack of glutamine export or uptake has on the phenotype observed. Recently however, Miklas *et al*., demonstrated that zebrafish and neonatal mouse hearts can regenerate through cardiomyocyte de-differentiation and proliferation, resulting from glutamine-driven mTORC1 activation (Miklas et al., 2022). Taken together, these previous findings and the data we present in this manuscript suggest that mTORC1 is likely to be a key component of the molecular pathway by which EC-derived glutamine induces HSPC proliferation, though further research will be required to confirm this hypothesis.

The data generated from our EC-specific *Bmal1*-KO mouse embryo experiments demonstrates that *Glud1* expression is not regulated by Bmal1 in FL-ECs, providing an explanation as to why FL LSK numbers were unaltered in these animals in comparison to controls. Our data indicate however that the *Bmal1-Glud1-Glul*-glutamine pathway is likely conserved in the FL, but that it is not predominantly

active in ECs as in the zebrafish CHT. Rather, single-cell transcriptome analyses of human FL cells suggests that this pathway is active in hepatocytes in mammals. Through evolution from teleosts, such as zebrafish, to mammals, HSPCs expand in a niche which has become increasingly more complex (Mahony and Bertrand, 2019): while the CHT in zebrafish is a transient vascularized tissue (Tamplin et al., 2015), the FL in mammals is a *bona fide* organ containing hepatocytes. Mouse FL hepatocytes have been shown to express *Bmal1* (Ceccacci et al., 2023), *Glud1* (Ceccacci et al., 2023) and *Glul* (Kuo et al., 1988), when glutamine is known to be present in, and exported from hepatocytes (Gebhardt and Coffer, 2013, Watford, 2000). The cell-type expression differences between key regulators of the HSPC niche in zebrafish and mammals was recently highlighted in another study in which we reported that *ifi30,* a gene that plays an important role in promoting HSPC expansion by detoxifying the niche from ROS, is specifically expressed in zebrafish CHT-ECs, but is only expressed in macrophages in the human FL (Cacialli et al., 2021). This, together with our findings in the present study demonstrates how although the HSPC niche has evolved in complexity over time, critical genetic pathways such as the *bmal1a-glud1a-glula*-glutamine axis have remained conserved.

In this manuscript, we have elucidated a molecular pathway where Bmal1 reprograms glutamine metabolism in the HSPC niche of both zebrafish and mouse, by controlling genes involved in glutamine synthesis. This ultimately changes glutamine availability in the niche, affecting HSPC expansion. Our findings reveal a novel, non-cell autonomous, homeostatic mechanism that controls embryonic HSPC proliferation. Our mouse data demonstrate sensitivity of the LSK population (containing *bona fide* HSCs) in response to Glud1 activity modulation. The lack of robust markers to discriminate HSCs from other progenitor subsets in the zebrafish model means we were unable to tease apart which of the definitive HSPC subsets respond to glutamine, which will be interesting and important to clarify in the future. Manipulation of the *bmal1a-glud1a-glula*-glutamine axis identified in this work may lead to new strategies to precisely control HSPC proliferation *ex vivo*, which could pave the way for greatly improved regenerative medicine protocols.

Acknowledgments

We would like to thank all lab members from the Neerman-Arbez, Scheiermann and Bertrand laboratories for their comments and suggestions during this project. We are also grateful to the animal facility staff and the flow cytometry, bioimaging and genomics platforms at UNIGE for all their assistance and suggestions during this project. This work was supported by a grant from the Fondation Privée des Hopitaux de Genève (RC05-03 to J.Y.B. and C.S.). T.P. benefitted from a grant from the Gabbiani Fund. J.Y.B. was funded by the Swiss National Fund (grant #320030-228027). C.S. was funded by the European Research Council (Consolidator grant 101001233, CIRCADYN), the Deutsche Forschungsgemeinschaft (DFG, German Research Foundation collaborative research grants TRR359 (491676693), project B07), the Swiss National Science Foundation (SNF, 310030_182417/1), the Swiss Cancer League (KLS-4836-08-2019) and the Geneva Cancer League (2106). Zebrafish and mouse figures were created using biorender.com.

Methods

Ethical statement

All animals, zebrafish and mice, were raised in accordance to FELASA and Swiss guidelines (Alestrom et al., 2020). All animal procedures and experiments were performed in strict accordance with all mandatory guidelines (EU and Swiss directives on the protection of animals used for scientific purposes) and approved and performed in accordance with the guidelines of the animal research committee of Geneva (Commission Cantonale pour les Expériences sur les Animaux (CCEA) and the Office fédéral de la santé alimentaire et des affaires vétérinaires (OSAV)), under licence GE/178/19. All efforts were made to comply to the 3R guidelines.

Mouse models and timed matings

Tg(*Cdh5*:*Cre*$^{ERT2+/-}$;*Bmal1*$^{flox/flox}$) (referred to as *Cdh5*:*Cre*$^{ERT2+/-}$;*Bmal1*$^{flox/flox}$ throughout) mice were generated by crossing *Tg*(*Cdh5*:*Cre*$^{ERT2+/+}$) (referred to as *Cdh5*:*Cre*^{ERT2} throughout) (B6) mice (a gift from R. Adams, Max Planck Institute for Molecular Biomedicine) with *Tg*(*Bmal1*$^{flox/flox}$) (referred to as *Bmal1*$^{flox/flox}$ throughout) (B6) mice (Jackson Laboratories) at ENVIGO. For timed matings, *Tg*(*Cdh5*:*Cre*$^{ERT2+/-}$;*Bmal1*$^{flox/flox}$, referred to as *Cdh5*:*Cre*^{ERT2}:*Bmal1*$^{flox/flox}$) mice were crossed with

Tg(*Bmal1*$^{flox/flox}$) mice to generate *Cdh5*:*Cre*^{ERT2} positive and negative littermate controls. One female mouse was placed with a single male for 12 hr overnight and subsequently examined for the presence of a copulation plug. This finding was used as an indicator of potential pregnancy, and marked as embryonic day (E) 0.5. At E10.5, pregnant females were intraperitoneally (i.p.) injected with 1mg tamoxifen (prepared as described below). At E13.5 pregnant females were sacrificed and the fetal livers of the embryos were harvested for FACS and qPCR analysis. A portion of the remaining embryonic tissue was also kept for genotyping of the embryos by PCR.

Fetal liver organ cultures

For fetal liver organ cultures, E13.5 FLs were dissected from wild-type C57BL/6 pregnant mice, and the culture was performed as previously (Bertrand et al., 2006, Bertrand et al., 2005). Briefly, each FL was cut into eight pieces, and each piece was placed into single wells of a 60-well Terasaki plate containing 30 microliters of medium composed of RPMI (deprived of glutamine), 10% Fetal Calf Serum, Pen/Strep (10 U/ml), 0.1% b-mercaptoethanol and HEPES (25mM). The plates were then inverted and placed in an incubator at 37°C for 48 hours. Glutamine (Sigma-Aldrich) was supplemented to produce a final medium concentration of either 2mM or 10mM. L-leucine (Sigma-Aldrich) was supplemented to a final medium concentration of 10mM. Each condition was tested on 6 different FL and two independent experiments were performed. At the end of the culture, all the 8 pieces originating from the same FL were consolidated for FACS analysis. Since no differences were found for the readouts tested between the 2mM or 10mM glutamine conditions, data for these were collated.

Tamoxifen preparation

Tamoxifen powder was purchased from Sigma (Catalog No. T5648-5G). The power was first dissolved in ethanol at 50mg/mL, then diluted with castor oil to 25mg/mL. Before injection, the tamoxifen solution was further diluted to 5mg/mL with 1x phosphate-buffered saline (PBS). Pregnant females were i.p. injected with 200uL of the 5mg/mL tamoxifen solution at E10.5.

Zebrafish husbandry

AB* zebrafish, as well as transgenic zebrafish lines were kept in a 14/10 hr light/dark cycle at 28.5°C. Embryos were obtained as described previously (Westerfield, 2000). Embryos were staged by hours-post fertilization (hpf) as described previously (Kimmel et al., 1995). In this study, the zebrafish *mindbomb*^{ta52b} (Itoh et al., 2003) mutant was used, as well as the following transgenic zebrafish lines: *Tg(kdrl:GAL4)*^{bw9} (Kim et al., 2014) (referred to as *kdrl:GAL4*), *Tg(gata2b:KALTA4)*^{sd32} (Butko et al., 2015) (referred to as *gata2b:KALTA4*), *Tg(kdrl:EGFP)*^{s843} (Jinn et al., 2005) (referred to as *kdrl:EGFP*), *Tg(kdrl:EGFP-NLS)* (Blum et al., 2008) (referred to as *kdrl:nls-EGFP*), *Tg(cmyb:GFP)*^{zf169} (North et al., 2007) (referred to as *cmyb:GFP*), *Tg(Mmu.Runx1:NLS-mCherry)*^{cz2010} (Tamplin et al., 2015) (referred to as *runx1:mCherry*), *Tg(CD41:EGFP)* (Lin et al., 2005) (referred to as *cd41:EGFP*), *Tg(ikaros:EGFP)*^{fr101} (referred to as *ikaros:EGFP*) and *Tg(UAS:lifeact-GFP)*^{mu271} (Butko et al., 2015). Zebrafish embryos were treated with 0.003% 1-phenyl-2-thiourea (PTU, Sigma P7629) starting at 24 hpf to prevent pigmentation.

Generation of transgenic animals

For *Tg(UAS:DN-bmal1a)* and *Tg(UAS:R88A-DN-bmal1a)* zebrafish generation, a Tol2 vector containing 4xUAS promoter, the coding sequence (including a STOP codon), and a poly-adenylation signal sequence was generated by subcloning. The Tol2 *UAS:R88A-DN-bmal1a* construct was generated by first generating a *UAS:full-length bmal1a* construct, before carrying out site directed mutagenesis of this using a QuikChange II kit (Agilent). AB* zebrafish embryos were co-injected with 50pg of the final Tol2 vector along with 50pg of *tol2 transposase* mRNA. Injected F0s were mated with AB* zebrafish, and the resulting F1 offspring were screened by PCR to assess germline integration of the Tol2 construct. Primers used for the generation of the *UAS:DN-bmal1a* and *UAS:R88A-DN-bmal1a* constructs and for genotyping of UAS lines are listed in Supplementary Table 2 and 3 respectively.

Whole-mount *in situ* hybridisation and analyses

Whole-mount *in situ* hybridisation was performed on 4% paraformaldehyde-fixed embryos as described previously (Thisse and Thisse, 2008). Digoxigenin-labelled *runx1, cmyb, dll4, mpx, gata1, mfap4,* and *rag1* probes were previously described

(Mahony et al., 2016, Petzold et al., 2025). *bmal1a*, *bmal1b, clocka, glula, glud1a, slc1a5, slc38a5a* and *slc38a5b* digoxigenin-labelled probes were synthesized using an RNA labelling kit (SP6/T7; Roche), using primers listed in Supplementary Table 1. RNA probes were generated by linearization of TOPO-TA or ZeroBlunt vectors (Invitrogen) containing the PCR-amplified cDNA sequences.

Immunofluorescence

Transgenic fluorescent embryos were embedded in 1% agarose in a glass-bottom dish. Immunofluorescence double staining was performed as described previously (Gao et al., 2015), with chicken anti-GFP (1:400; Life Technologies) and rabbit anti-phospho-histone 3 (PH3) antibodies (1:250; Abcam). AlexaFluor 488-conjugated anti-chicken secondary antibody (1:1000; Life Technologies) and AlexaFluor 594-conjugated anti-rabbit secondary antibody (1:1000; Life Technologies) were used to reveal the primary antibodies.

Zebrafish chemical treatments

All compounds used in this study were purchased from Sigma-Aldrich. Zebrafish were treated with glutamine at a final concentration of 1mM, BCH at 500µM, ADP at 100µM, L-leucine at 1mM and GPNA at 500µM. Zebrafish were exposed to compounds in 0.003% 1-phenyl-2-thiourea (PTU, Sigma, P7629) E3 (fish) water in multiwell plates between 48 hpf to 4.5 dpf, unless stated otherwise. Compound water was replaced every 12 hours. Following exposure, embryos were fixed in 4% paraformaldehyde.

Glutamine assay

Tails of 72 hpf *kdrl:GAL4;UAS:DN-bmal1a* larvae and *kdrl:GAL4* controls were dissected. Three independent experiments were carried out using clutches of ~35 embryos per condition. The glutamine concentration per embryo tail was then quantified using a colorimetric glutamine assay kit following the protocol (Abcam, ab197011).

Microscopy

Whole mount *in situ* hybridisation images were taken on an Olympus MVX10 microscope in 100% glycerol. Fluorescent images were taken with an Olympus IX83 microscope. Representative fluorescent confocal images in **Fig. 3A** were taken using an upright 3i spinning-disc confocal microscope and a Zeiss Plan-Apochromat water-dipping objective. Representative fluorescent confocal images in **Fig. 3B** were taken using a Nikon inverted A1r spectral microscope. Fluorescent confocal images in **Fig. 3A** are 3D maximum projection images from Z-stack acquisitions, while fluorescent confocal images in **Fig. 3B** were taken in 2D. All images were taken using the CellSens Dimension software (Olympus) apart from confocal images which were taken using the NIS-Elements Advanced Research software (Nikon).

Image processing and quantification

All images were processed using Fiji ImageJ (NIH) (Schindelin et al., 2012). *bmal1a*, *runx1* and *cmyb in situ* hybridisation signal intensity of the desired region was quantified as described previously (Dobrzycki et al., 2018). Quantification of *cmyb*, *mpx* and *mfap4* positive cell numbers in the desired region in *in situ* hybridisation images was carried out manually using the counter tool following image inversion, sharpening and enlarging the region of interest of each image in Fiji ImageJ, as was done previously (Cacialli et al., 2021, Cacialli et al., 2022). *cmyb*, *gata1* and *rag1 in situ* hybridisation expression area in particular regions was measured manually in Fiji ImageJ, as has been done previously (Lundin et al., 2020, Soto et al., 2021, Klaus et al., 2022, Ghersi et al., 2023, Cacialli et al., 2021, Aleman et al., 2026). In all *in situ* hybridisation quantifications, aortic signals along the trunk to the end of the yolk tube extension, and CHT signals from the end of the yolk tube extension to the end of the tail were quantified respectively. *kdrl:nls-EGFP*, *cmyb:GFP*, *cd41:EGFP*^{low} and *runx1:nls-mCherry* positive cell numbers in the CHT were quantified manually from 2D images using the counter tool following image inversion, sharpening and enlarging the region of interest of each image in Fiji ImageJ, as was done previously (Cacialli et al., 2021, Cacialli et al., 2022). Positive cells from the end of the yolk tube extension to the end of the tail were quantified.

Fluorescence activated cell sorting

Whole zebrafish embryos or tail dissections were incubated with a liberase-blendzyme 3 (Roche) solution for 90 min at 33 °C, then dissociated and resuspended in 0.9x PBS-1% fetal calf serum, as described previously (Cacialli et al., 2021). We distinguished and excluded dead cells by staining them with SYTOX-red (Life Technologies) or DRAQ7 (Thermo Fischer Scientific). Cell sorting was performed using an Aria II (BD Biosciences, software diva v6.1.3) or BIORAD S3 cell sorter. Cell suspensions were passed through a 40mm filter prior to FACS. Data were acquired on a LSR2Fortessa (BD Biosciences, software diva8.0.2) and analysed with FlowJo. Fetal livers were dissociated into 1% BSA in PBS by pipetting, and then underwent red blood cell lysis using RBC Lysis Buffer (Biolegend; Catalog No. 420302) for 5 minutes at room temperature. Cells were then washed and blocked with FcR Blocking Reagent (mouse; 1:50) from Miltenyi Biotec (Catalog No. 130-092-75) for 15 minutes at room temperature. Cells were surface stained with CD31 (clone MEC13.3), Sca1 (clone D7), CD45 (clone 30-F11), cKit (CD117; clone2B8), and lineage (CD19, clone 6D5; GR1, clone RB6-8C5; TER119, clone TER-119; and CD3, clone 145-2C11) antibodies (1:100) for 15 minutes on ice. DAPI was used to distinguish live cells (2ug per 1 million cells; AppliChem Catalog No. A4099). Cells were analysed and sorted using an Aria Fusion cell sorter (BD Biosciences) and flow cytometry data analysed using FlowJo software (BD). For qPCR, cells were directly sorted into Qiagen RLT lysis buffer (Catalog No. 79216).

Quantitative real-time PCR and analyses

Total RNA was extracted using RNeasy minikit (Qiagen) and reverse transcribed into cDNA using a Superscript III kit (Invitrogen). Quantitative real-time PCR (qPCR) was performed using a KAPA SYBR FAST Universal qPCR Kit (KAPA BIOSYSTEMS) and run on a CFX connect real-time system (Bio-Rad). All qPCR primers used for gene expression in zebrafish and mouse are listed in Supplementary Tables 4. All qPCR experiments were performed using technical triplicates. Experiments were each repeated three times and fold-change averages from each experiment were combined.

Bulk RNA-sequencing and analyses

The total RNAs of sorted GPF$^+$ cells from the tails of 36 hpf *kdrl:EGFP* embryos were extracted using a QIAGEN RNeasy Mini Kit. The mRNA sequencing libraries were generated using a SMARTer Nextera kit for Illumina. The library preparations were sequenced on an Illumina Hiseq 4000 platform and 150 bp paired-end reads were generated. The fastq files were mapped to the UCSC Danio rerio danRer10 (GRCz10) genome with STAR v2.7.0f (Dobin et al., 2013). The biological QC was performed with picard tools. The number of reads mapping to each gene feature of the UCSC Danio rerio danRer10 reference was prepared with HTSeq v0.9.1 (HTseq-count) (Putri et al., 2022, Anders et al., 2015). The differential expression analysis was performed with the statistical analysis R/Bioconductor package edgeR 1.34.1 (Robinson et al., 2010), with a multiple testing Benjamini and Hochberg correction FDR 5% and a fold-change threshold of 2. Differentially expressed genes are listed in Supplementary Table 5.

Data analyses

Statistical significance between two samples was calculated using unpaired two-tailed Student's *t*-tests assuming unequal variance. At least three independent experiments were carried out in all cases, unless stated otherwise. In all experiments, normality was assumed, and variance was comparable between groups. Sample size was selected empirically according to previous experience in the assessment of experimental variability. The investigators were blinded for all transgenic zebrafish and mouse flow cytometry experiments, both during the experiments and the quantification. Circadian rhythmicity in Supp. Fig. 1 was determined by cosinor analysis (Spadaro et al., 2020, Refinetti et al., 2007). Numerical data are the mean ± s.e.m., unless stated otherwise. Statistical calculations and the graphs for the numerical data were performed using Prism 10 software (GraphPad Software). Details of the statistical analyses for the bulk RNA-seq experiment are provided in the corresponding section.

Data Availability

All raw data will become freely accessible on the Yareta repository databank following publication (10.26037/yareta:2l3zxli34zdd3pgeq4cst75q5u).

Author contributions

T.P. performed all zebrafish experiments and analyses and generated the *Tg(UAS:DN-bmal1a)* and *Tg(UAS:R88A-DN-bmal1a)* zebrafish lines. T.P. also performed all mouse qPCR experiments and analyses. A.K. contributed to experiments for Fig. 3A. J.Y.B and R.G. designed the mouse fetal liver organ culture experiments, and J.Y.B. performed these experiments. L.K.L. and K.N.I.B. performed all remaining mouse experiments and analyses. B.B. performed some *in situ* hybridization experiments. S.J. performed all mouse genotyping. H.G. provided resources. T.P., L.K.L., K.N.I.B., C.S., and J.Y.B. designed experiments. T.P. wrote the original draft of the manuscript. T.P., C.S., and J.Y.B. edited and wrote the final version of the manuscript.

Competing interests

The authors declare that they have no competing interests.

References

ALEMAN, A. G., ULLOA, B., NAYAK, R., FORD, C., POTTS, K. S., DE SENA-TOMAS, C., VICIOSO, C., RANGASWAMY, U., ELIAS, H. K., KHARAS, M. G., SANGES, R., BOWMAN, T. & TARGOFF, K. L. 2026. Crip2 preserves hematopoietic stem and progenitor cell production through inhibition of Notch signals. *Development*.

ALESTROM, P., D'ANGELO, L., MIDTLYNG, P. J., SCHORDERET, D. F., SCHULTE-MERKER, S., SOHM, F. & WARNER, S. 2020. Zebrafish: Housing and husbandry recommendations. *Laboratory Animals,* 54**,** 213-224.

AMARAL, I. P. G. & JOHNSTON, I. A. 2012. Circadian expression of clock and putative clock-controlled genes in skeletal muscle of the zebrafish. *American Journal of Physiology-Regulatory Integrative and Comparative Physiology,* 302**,** R193-R206.

ANDERS, S., PYL, P. T. & HUBER, W. 2015. HTSeq-a Python framework to work with high-throughput sequencing data. *Bioinformatics,* 31**,** 166-169.

BERTRAND, J. Y., CHI, N. C., SANTOSO, B., TENG, S., STAINIER, D. Y. & TRAVER, D. 2010a. Haematopoietic stem cells derive directly from aortic endothelium during development. *Nature,* 464**,** 108-11.

BERTRAND, J. Y., CISSON, J. L., STACHURA, D. L. & TRAVER, D. 2010b. Notch signaling distinguishes 2 waves of definitive hematopoiesis in the zebrafish embryo. *Blood,* 115**,** 2777-83.

BERTRAND, J. Y., DESANTI, G. E., LO-MAN, R., LECLERC, C., CUMANO, A. & GOLUB, R. 2006. Fetal spleen stroma drives macrophage commitment. *Development,* 133**,** 3619-28.

BERTRAND, J. Y., JALIL, A., KLAINE, M., JUNG, S., CUMANO, A. & GODIN, I. 2005. Three pathways to mature macrophages in the early mouse yolk sac. *Blood,* 106**,** 3004-11.

BERTRAND, J. Y. & TRAVER, D. 2009. Hematopoietic cell development in the zebrafish embryo. *Curr Opin Hematol,* 16**,** 243-8.

BHUTIA, Y. D., BABU, E., RAMACHANDRAN, S. & GANAPATHY, V. 2015. Amino Acid Transporters in Cancer and Their Relevance to "Glutamine Addiction": Novel Targets for the Design of a New Class of Anticancer Drugs. *Cancer Research,* 75**,** 1782-1788.

BHUTIA, Y. D. & GANAPATHY, V. 2016. Glutamine transporters in mammalian cells and their functions in physiology and cancer. *Biochimica Et Biophysica Acta-Molecular Cell Research,* 1863**,** 2531-2539.

BLUM, Y., BELTING, H. G., ELLERTSDOTTIR, E., HERWIG, L., LUDERS, F. & AFFOLTER, M. 2008. Complex cell rearrangements during intersegmental vessel sprouting and vessel fusion in the zebrafish embryo. *Developmental Biology,* 316**,** 312-322.

BOISSET, J. C., VAN CAPPELLEN, W., ANDRIEU-SOLER, C., GALJART, N., DZIERZAK, E. & ROBIN, C. 2010. In vivo imaging of haematopoietic cells emerging from the mouse aortic endothelium. *Nature,* 464**,** 116-20.

BROER, A., RAHIMI, F. & BROER, S. 2016. Deletion of Amino Acid Transporter ASCT2 (SLC1A5) Reveals an Essential Role for Transporters SNAT1 (SLC38A1) and SNAT2 (SLC38A2) to Sustain Glutaminolysis in Cancer Cells. *Journal of Biological Chemistry,* 291**,** 13194-13205.

BURCH, J. S., MARCERO, J. R., MASCHEK, J. A., COX, J. E., JACKSON, L. K., MEDLOCK, A. E., PHILLIPS, J. D. & DAILEY, H. A., JR. 2018. Glutamine via alpha-ketoglutarate dehydrogenase provides succinyl-CoA for heme synthesis during erythropoiesis. *Blood,* 132**,** 987-998.

BURNS, C. E., TRAVER, D., MAYHALL, E., SHEPARD, J. L. & ZON, L. I. 2005. Hematopoietic stem cell fate is established by the Notch-Runx pathway. *Genes Dev,* 19**,** 2331-42.

BUTKO, E., DISTEL, M., POUGET, C., WEIJTS, B., KOBAYASHI, I., NG, K., MOSIMANN, C., POULAIN, F. E., MCPHERSON, A., NI, C. W., STACHURA, D. L., DEL CID, N., ESPIN-PALAZON, R., LAWSON, N. D., DORSKY, R., CLEMENTS, W. K. & TRAVER, D. 2015. Gata2b is a restricted early regulator of hemogenic endothelium in the zebrafish embryo. *Development,* 142**,** 1050-1061.

CACIALLI, P., MAHONY, C. B., PETZOLD, T., BORDIGNON, P., ROUGEMONT, A. L. & BERTRAND, J. Y. 2021. A connexin/ifi30 pathway bridges HSCs with their niche to dampen oxidative stress. *Nature Communications,* 12.

CACIALLI, P., MAILHE, M. P., WAGNER, I., MERKLER, D., GOLUB, R. & BERTRAND, J. Y. 2022. Synergistic prostaglandin E synthesis by myeloid and endothelial cells promotes fetal hematopoietic stem cell expansion in vertebrates. *EMBO J,* 41**,** e108536.

CECCACCI, E., VILLA, E., SANTORO, F., MINUCCI, S., RUHRBERG, C. & FANTIN, A. 2023. A Refined Single Cell Landscape of Haematopoiesis in the Mouse Foetal Liver. *J Dev Biol,* 11.

CHIU, M., SABINO, C., TAURINO, G., BIANCHI, M. G., ANDREOLI, R., GIULIANI, N. & BUSSOLATI, O. 2017. GPNA inhibits the sodium-independent transport system L for neutral amino acids. *Amino Acids,* 49**,** 1365-1372.

CHO, H., ZHAO, X., HATORI, M., YU, R. T., BARISH, G. D., LAM, M. T., CHONG, L. W., DITACCHIO, L., ATKINS, A. R., GLASS, C. K., LIDDLE, C., AUWERX, J., DOWNES, M., PANDA, S. & EVANS, R. M. 2012. Regulation of circadian behaviour and metabolism by REV-ERB-alpha and REV-ERB-beta. *Nature,* 485**,** 123-127.

COUEE, I. & TIPTON, K. F. 1989. Activation of glutamate dehydrogenase by L-leucine. *Biochim Biophys Acta,* 995**,** 97-101.

DASS, P. D., MURDOCH, F. E. & WU, M. C. 1984. Glutamine promotes colony formation in bone marrow and HL-60 cells; accelerates myeloid differentiation in induced HL-60 cells. *In Vitro,* 20**,** 869-75.

DIERICKX, P., VAN LAAKE, L. W. & GEIJSEN, N. 2018. Circadian clocks: from stem cells to tissue homeostasis and regeneration. *Embo Reports,* 19**,** 18-28.

DOBIN, A., DAVIS, C. A., SCHLESINGER, F., DRENKOW, J., ZALESKI, C., JHA, S., BATUT, P., CHAISSON, M. & GINGERAS, T. R. 2013. STAR: ultrafast universal RNA-seq aligner. *Bioinformatics,* 29**,** 15-21.

DOBRZYCKI, T., KRECSMARIK, M., BONKHOFER, F., PATIENT, R. & MONTEIRO, R. 2018. An optimised pipeline for parallel image-based quantification of gene expression and genotyping after in situ hybridisation. *Biology Open,* 7.

EELEN, G., DUBOIS, C., CANTELMO, A. R., GOVEIA, J., BRUNING, U., DERAN, M., JARUGUMILLI, G., VAN RIJSSEL, J., SALADINO, G., COMITANI, F., ZECCHIN, A., ROCHA, S., CHEN, R. Y., HUANG, H. L., VANDEKEERE, S., KALUCKA, J., LANGE, C., MORALES-RODRIGUEZ, F., CRUYS, B., TREPS, L., RAMER, L., VINCKIER, S., BREPOELS, K., WYNS, S., SOUFFREAU, J., SCHOONJANS, L., LAMERS, W. H., WU, Y., HAUSTRAETE, J., HOFKENS, J., LIEKENS, S., CUBBON, R., GHESQUIERE, B., DEWERCHIN, M., GERVASIO, F. L., LI, X. R., VAN BUUL, J. D., WU, X. & CARMELIET, P. 2018. Role of glutamine synthetase in angiogenesis beyond glutamine synthesis. *Nature,* 561**,** 63-+.

ESSLINGER, C. S., CYBULSKI, K. A. & RHODERICK, J. F. 2005. N-gamma-Aryl glutamine analogues as probes of the ASCT2 neutral amino acid transporter binding site. *Bioorganic & Medicinal Chemistry,* 13**,** 1111-1118.

FROLAND STEINDAL, I. A. & WHITMORE, D. 2019. Circadian Clocks in Fish-What Have We Learned so far? *Biology (Basel),* 8.

FUCHS, B. C. & BODE, B. P. 2005. Amino acid transporters ASCT2 and LAT1 in cancer: Partners in crime? *Seminars in Cancer Biology,* 15**,** 254-266.

GAO, L., LI, D. T., MA, K., ZHANG, W. J., XU, T., FU, C., JING, C. B., JIA, X. E., WU, S., SUN, X., DONG, M., DENG, M., CHEN, Y., ZHU, W. G., PENG, J. R., WAN, F. Y., ZHOU, Y., ZON, L. I. & PAN, W. J. 2015. TopBP1 Governs Hematopoietic Stem/Progenitor Cells Survival in Zebrafish Definitive Hematopoiesis. *Plos Genetics,* 11.

GEBHARDT, R. & COFFER, P. J. 2013. Hepatic autophagy is differentially regulated in periportal and pericentral zones - a general mechanism relevant for other tissues? *Cell Commun Signal,* 11**,** 21.

GHERSI, J. J., BALDISSERA, G., HINTZEN, J., LUFF, S. A., CHENG, S., XIA, I. F., STURGEON, C. M. & NICOLI, S. 2023. Haematopoietic stem and progenitor cell heterogeneity is inherited from the embryonic endothelium. *Nat Cell Biol,* 25**,** 1135-1145.

GOLAN, K., KOLLET, O., MARKUS, R. P. & LAPIDOT, T. 2019. Daily light and darkness onset and circadian rhythms metabolically synchronize hematopoietic stem cell differentiation and maintenance: The role of bone marrow norepinephrine, tumor necrosis factor, and melatonin cycles. *Experimental Hematology,* 78**,** 1-10.

GOLAN, K., KUMARI, A., KOLLET, O., KHATIB-MASSALHA, E., SUBRAMANIAM, M. D., FERREIRA, Z. S., AVEMARIA, F., RZESZOTEK, S., GARCIA-GARCIA, A., XIE, S., FLORES-FIGUEROA, E., GUR-COHEN, S., ITKIN, T., LUDIN-TAL, A., MASSALHA, H., BERNSHTEIN, B., CIECHANOWICZ, A. K., BRANDIS, A., MEHLMAN, T., BHATTACHARYA, S., BERTAGNA, M., CHENG, H., PETROVICH-KOPITMAN, E., JANUS, T., KAUSHANSKY, N., CHENG, T., SAGI, I., RATAJCZAK, M. Z., MENDEZ-FERRER, S., DICK, J. E., MARKUS, R. P. & LAPIDOT, T. 2018. Daily Onset of Light and Darkness Differentially Controls Hematopoietic Stem Cell Differentiation and Maintenance. *Cell Stem Cell,* 23**,** 572-585 e7.

GONZALEZ, A., HALL, M. N., LIN, S. C. & HARDIE, D. G. 2020. AMPK and TOR: The Yin and Yang of Cellular Nutrient Sensing and Growth Control. *Cell Metabolism,* 31**,** 472-492.

GREGORY, M. A., NEMKOV, T., PARK, H. J., ZABEREZHNYY, V., GEHRKE, S., ADANE, B., JORDAN, C. T., HANSEN, K. C., D'ALESSANDRO, A. & DEGREGORI, J. 2019. Targeting Glutamine Metabolism and Redox State for Leukemia Therapy. *Clin Cancer Res,* 25**,** 4079-4090.

GURUNG, S., RESTREPO, N. K., CHESTNUT, B., KLIMKAITE, L. & SUMANAS, S. 2022. Single-cell transcriptomic analysis of vascular endothelial cells in zebrafish embryos. *Sci Rep,* 12**,** 13065.

GUSTAFSON, C. L., PARSLEY, N. C., ASIMGIL, H., LEE, H. W., AHLBACH, C., MICHAEL, A. K., XU, H., WILLIAMS, O. L., DAVIS, T. L., LIU, A. C. & PARTCH, C. L. 2017. A Slow Conformational Switch in the BMAL1 Transactivation Domain Modulates Circadian Rhythms. *Mol Cell,* 66**,** 447-457 e7.

HAN, S. J., CHOI, S. E., YI, S. A., JUNG, J. G., JUNG, I. R., SHIN, M., KANG, S., OH, H., KIM, H. J., KIM, D. J., KWON, J. E., CHOI, C. S., LEE, K. W. & KANG, Y. 2016. Glutamate dehydrogenase activator BCH stimulating reductive amination prevents high fat/high fructose diet-induced steatohepatitis and hyperglycemia in C57BL/6J mice. *Scientific Reports,* 6.

HASEGAWA, S., FUKUSHIMA, H., HOSODA, H., SERITA, T., ISHIKAWA, R., ROKUKAWA, T., KAWAHARA-MIKI, R., ZHANG, Y., OHTA, M., OKADA, S., TANIMIZU, T., JOSSELYN, S. A., FRANKLAND, P. W. & KIDA, S. 2019. Hippocampal clock regulates memory retrieval via Dopamine and PKA-induced GluA1 phosphorylation. *Nat Commun,* 10**,** 5766.

HENDZEL, M. J., WEI, Y., MANCINI, M. A., VAN HOOSER, A., RANALLI, T., BRINKLEY, B. R., BAZETT-JONES, D. P. & ALLIS, C. D. 1997. Mitosis-specific phosphorylation of histone H3 initiates primarily within pericentromeric heterochromatin during G2 and spreads in an ordered fashion coincident with mitotic chromosome condensation. *Chromosoma,* 106**,** 348-60.

HENNINGER, J., SANTOSO, B., HANS, S., DURAND, E., MOORE, J., MOSIMANN, C., BRAND, M., TRAVER, D. & ZON, L. 2017. Corrigendum: Clonal fate mapping quantifies the number of haematopoietic stem cells that arise during development. *Nat Cell Biol,* 19**,** 142.

HOSODA, H., MOTOHASHI, J., KATO, H., MASUSHIGE, S. & KIDA, S. 2004. A BMAL1 mutant with arginine 91 substituted with alanine acts as a dominant negative inhibitor. *Gene,* 338**,** 235-41.

HURLEY, J. M., LOROS, J. J. & DUNLAP, J. C. 2016. Circadian Oscillators: Around the Transcription-Translation Feedback Loop and on to Output. *Trends Biochem Sci,* 41**,** 834-846.

ITOH, M., KIM, C. H., PALARDY, G., ODA, T., JIANG, Y. J., MAUST, D., YEO, S. Y., LORICK, K., WRIGHT, G. J., ARIZA-MCNAUGHTON, L., WEISSMAN, A. M., LEWIS, J., CHANDRASEKHARAPPA, S. C. & CHITNIS, A. B. 2003. Mind bomb is a ubiquitin ligase that is essential for efficient activation of Notch signaling by Delta. *Dev Cell,* 4**,** 67-82.

JEWELL, J. L., KIM, Y. C., RUSSELL, R. C., YU, F. X., PARK, H. W., PLOUFFE, S. W., TAGLIABRACCI, V. S. & GUAN, K. L. 2015. Differential regulation of mTORC1 by leucine and glutamine. *Science,* 347**,** 194-198.

JINN, S. W., BEISL, D., MITCHELL, T., CHEN, J. N. & STAINIER, D. Y. R. 2005. Cellular and molecular analyses of vascular tube and lumen formation in zebrafish. *Development,* 132**,** 5199-5209.

KHAN, J. A., MENDELSON, A., KUNISAKI, Y., BIRBRAIR, A., KOU, Y., ARNAL-ESTAPE, A., PINHO, S., CIERO, P., NAKAHARA, F., MA'AYAN, A., BERGMAN, A., MERAD, M. & FRENETTE, P. S. 2016. Fetal liver hematopoietic stem cell niches associate with portal vessels. *Science,* 351**,** 176-80.

KIM, A. D., MELICK, C. H., CLEMENTS, W. K., STACHURA, D. L., DISTEL, M., PANAKOVA, D., MACRAE, C., MORK, L. A., CRUMP, J. G. & TRAVER, D. 2014. Discrete Notch signaling requirements in the specification of hematopoietic stem cells. *Embo Journal,* 33**,** 2363-2373.

KIMMEL, C. B., BALLARD, W. W., KIMMEL, S. R., ULLMANN, B. & SCHILLING, T. F. 1995. Stages of Embryonic-Development of the Zebrafish. *Developmental Dynamics,* 203**,** 253-310.

KISSA, K. & HERBOMEL, P. 2010. Blood stem cells emerge from aortic endothelium by a novel type of cell transition. *Nature,* 464**,** 112-5.

KLAUS, A., CLAPES, T., YVERNOGEAU, L., BASU, S., WEIJTS, B., MAAS, J., SMAL, I., GALJART, N. & ROBIN, C. 2022. CLASP2 safeguards hematopoietic stem cell properties during mouse and fish development. *Cell Rep,* 39**,** 110957.

KOBERSTEIN, R. & SUND, H. 1973. Studies of Glutamate Dehydrogenase - Influence of Adp, Gtp, and L-Glutamate on Binding of Reduced Coenzyme to Beef-Liver Glutamate Dehydrogenase. *European Journal of Biochemistry,* 36**,** 545-552.

KUO, C. F., PAULSON, K. E. & DARNELL, J. E., JR. 1988. Positional and developmental regulation of glutamine synthetase expression in mouse liver. *Mol Cell Biol,* 8**,** 4966-71.

LAMIA, K. A., STORCH, K. F. & WEITZ, C. J. 2008. Physiological significance of a peripheral tissue circadian clock. *Proc Natl Acad Sci U S A,* 105**,** 15172-7.

LI, M., LI, C. H., ALLEN, A., STANLEY, C. A. & SMITH, T. J. 2011. The structure and allosteric regulation of glutamate dehydrogenase. *Neurochemistry International,* 59**,** 445-455.

LIN, H. F., TRAVER, D., ZHU, H., DOOLEY, K., PAW, B. H., ZEN, L. I. & HANDIN, R. I. 2005. Analysis of thrombocyte development in CD41-GFP transgenic zebrafish. *Blood,* 106**,** 3803-3810.

LIU, C., HU, J., QU, C., WANG, L., HUANG, G., NIU, P., ZHONG, Z., HONG, F., WANG, G., POSTLETHWAIT, J. H. & WANG, H. 2015. Molecular evolution and functional divergence of zebrafish (Danio rerio) cryptochrome genes. *Sci Rep,* 5**,** 8113.

LUNDIN, V., SUGDEN, W. W., THEODORE, L. N., SOUSA, P. M., HAN, A., CHOU, S., WRIGHTON, P. J., COX, A. G., INGBER, D. E., GOESSLING, W., DALEY, G. Q. & NORTH, T. E. 2020. YAP Regulates Hematopoietic Stem Cell Formation in Response to the Biomechanical Forces of Blood Flow. *Dev Cell,* 52**,** 446-460 e5.

LYU, J., GU, Z., ZHANG, Y., VU, H. S., LECHAUVE, C., CAI, F., CAO, H., KEITH, J., BRANCALEONI, V., GRANATA, F., MOTTA, I., CAPPELLINI, M. D., HUANG, L. J., DEBERARDINIS, R. J., WEISS, M. J., NI, M. & XU, J. 2024. A glutamine metabolic switch supports erythropoiesis. *Science,* 386**,** eadh9215.

MAHONY, C. B. & BERTRAND, J. Y. 2019. How HSCs Colonize and Expand in the Fetal Niche of the Vertebrate Embryo: An Evolutionary Perspective. *Front Cell Dev Biol,* 7**,** 34.

MAHONY, C. B., FISH, R. J., PASCHE, C. & BERTRAND, J. Y. 2016. tfec controls the hematopoietic stem cell vascular niche during zebrafish embryogenesis. *Blood,* 128**,** 1336-1345.

MAHONY, C. B., PASCHE, C. & BERTRAND, J. Y. 2018. Oncostatin M and Kit-Ligand Control Hematopoietic Stem Cell Fate during Zebrafish Embryogenesis. *Stem Cell Reports,* 10**,** 1920-1934.

MARCHEVA, B., RAMSEY, K. M., PEEK, C. B., AFFINATI, A., MAURY, E. & BASS, J. 2013. Circadian clocks and metabolism. *Handb Exp Pharmacol*, 127-55.

MENDEZ-FERRER, S., CHOW, A., MERAD, M. & FRENETTE, P. S. 2009. Circadian rhythms influence hematopoietic stem cells. *Current Opinion in Hematology,* 16, 235-242.

MIKLAS, J. W., LEVY, S., HOFSTEEN, P., MEX, D. I., CLARK, E., MUSTER, J., ROBITAILLE, A. M., SIVARAM, G., ABELL, L., GOODSON, J. M., PRANOTO, I., MADAN, A., CHIN, M. T., TIAN, R., MURRY, C. E., MOON, R. T., WANG, Y. & RUOHOLA-BAKER, H. 2022. Amino acid primed mTOR activity is essential for heart regeneration. *iScience,* 25, 103574.

MOSSMANN, D., PARK, S. & HALL, M. N. 2018. mTOR signalling and cellular metabolism are mutual determinants in cancer. *Nature Reviews Cancer,* 18, 744-757.

NEUFELD-COHEN, A., ROBLES, M. S., AVIRAM, R., MANELLA, G., ADAMOVICH, Y., LADEUIX, B., NIR, D., ROUSSO-NOORI, L., KUPERMAN, Y., GOLIK, M., MANN, M. & ASHER, G. 2016. Circadian control of oscillations in mitochondrial rate-limiting enzymes and nutrient utilization by PERIOD proteins. *Proc Natl Acad Sci U S A,* 113, E1673-82.

NGUYEN, T. L. & DURAN, R. V. 2018. Glutamine metabolism in cancer therapy. *Cancer Drug Resistance,* 1, 126-138.

NI, F., YU, W. M., LI, Z. G., GRAHAM, D. K., JIN, L. T., KANG, S. M., ROSSI, M. R., LI, S. Y., BROXMEYER, H. E. & QU, C. K. 2019. Critical role of ASCT2-mediated amino acid metabolism in promoting leukaemia development and progression. *Nature Metabolism,* 1, 390-403.

NICKLIN, P., BERGMAN, P., ZHANG, B. L., TRIANTAFELLOW, E., WANG, H., NYFELER, B., YANG, H. D., HILD, M., KUNG, C., WILSON, C., MYER, V. E., MACKEIGAN, J. P., PORTER, J. A., WANG, Y. K., CANTLEY, L. C., FINAN, P. M. & MURPHY, L. O. 2009. Bidirectional Transport of Amino Acids Regulates mTOR and Autophagy. *Cell,* 136, 521-534.

NORTH, T. E., GOESSLING, W., WALKLEY, C. R., LENGERKE, C., KOPANI, K. R., LORD, A. M., WEBER, G. J., BOWMAN, T. V., JANG, I. H., GROSSER, T., FITZGERALD, G. A., DALEY, G. Q., ORKIN, S. H. & ZON, L. I. 2007. Prostaglandin E2 regulates vertebrate haematopoietic stem cell homeostasis. *Nature,* 447, 1007-U7.

OBUROGLU, L., TARDITO, S., FRITZ, V., DE BARROS, S. C., MERIDA, P., CRAVEIRO, M., MAMEDE, J., CRETENET, G., MONGELLAZ, C., AN, X. L., KLYSZ, D., TOUHAMI, J., BOYER-CLAVEL, M., BATTINI, J. L., DARDALHON, V., ZIMMERMANN, V. S., MOHANDAS, N., GOTTLIEB, E., SITBON, M., KINET, S. & TAYLOR, N. 2014. Glucose and Glutamine Metabolism Regulate Human Hematopoietic Stem Cell Lineage Specification (vol 15, pg 169, 2014). *Cell Stem Cell,* 15**,** 666-668.

PETZOLD, T., BRIVIO, S., LINNERZ, T., WATANABE, M., GERHARDT, H. & BERTRAND, J. Y. 2025. Connexin 41.8 governs timely haematopoietic stem and progenitor cell specification. *Biol Open,* 14.

PIZZATO, H. A., WANG, Y., WOLFGANG, M. J., FINCK, B. N., PATTI, G. J. & BHATTACHARYA, D. 2023. Mitochondrial pyruvate metabolism and glutaminolysis toggle steady-state and emergency myelopoiesis. *J Exp Med,* 220.

PLAITAKIS, A., KALEF-EZRA, E., KOTZAMANI, D., ZAGANAS, I. & SPANAKI, C. 2017. The Glutamate Dehydrogenase Pathway and Its Roles in Cell and Tissue Biology in Health and Disease. *Biology-Basel,* 6.

POPESCU, D. M., BOTTING, R. A., STEPHENSON, E., GREEN, K., WEBB, S., JARDINE, L., CALDERBANK, E. F., POLANSKI, K., GOH, I., EFREMOVA, M., ACRES, M., MAUNDER, D., VEGH, P., GITTON, Y., PARK, J. E., VENTO-TORMO, R., MIAO, Z., DIXON, D., ROWELL, R., MCDONALD, D., FLETCHER, J., POYNER, E., REYNOLDS, G., MATHER, M., MOLDOVAN, C., MAMANOVA, L., GREIG, F., YOUNG, M. D., MEYER, K. B., LISGO, S., BACARDIT, J., FULLER, A., MILLAR, B., INNES, B., LINDSAY, S., STUBBINGTON, M. J. T., KOWALCZYK, M. S., LI, B., ASHENBERG, O., TABAKA, M., DIONNE, D., TICKLE, T. L., SLYPER, M., ROZENBLATT-ROSEN, O., FILBY, A., CAREY, P., VILLANI, A. C., ROY, A., REGEV, A., CHEDOTAL, A., ROBERTS, I., GOTTGENS, B., BEHJATI, S., LAURENTI, E., TEICHMANN, S. A. & HANIFFA, M. 2019. Decoding human fetal liver haematopoiesis. *Nature,* 574**,** 365-371.

PURAM, R. V., KOWALCZYK, M. S., DE BOER, C. G., SCHNEIDER, R. K., MILLER, P. G., MCCONKEY, M., TOTHOVA, Z., TEJERO, H., HECKL, D., JARAS, M., CHEN, M. C., LI, H. B., TAMAYO, A., COWLEY, G. S., ROZENBLATT-ROSEN, O., AL-SHAHROUR, F., REGEV, A. & EBERT, B. L. 2016. Core Circadian Clock Genes Regulate Leukemia Stem Cells in AML. *Cell,* 165**,** 303-316.

PUTRI, G. H., ANDERS, S., PYL, P. T., PIMANDA, J. E. & ZANINI, F. 2022. Analysing high-throughput sequencing data in Python with HTSeq 2.0. *Bioinformatics,* 38**,** 2943-2945.

REFINETTI, R., LISSEN, G. C. & HALBERG, F. 2007. Procedures for numerical analysis of circadian rhythms. *Biol Rhythm Res,* 38**,** 275-325.

REINKE, H. & ASHER, G. 2019. Crosstalk between metabolism and circadian clocks. *Nature Reviews Molecular Cell Biology,* 20**,** 227-241.

RELOGIO, A., WESTERMARK, P. O., WALLACH, T., SCHELLENBERG, K., KRAMER, A. & HERZEL, H. 2011. Tuning the mammalian circadian clock: robust synergy of two loops. *PLoS Comput Biol,* 7**,** e1002309.

ROBINSON, M. D., MCCARTHY, D. J. & SMYTH, G. K. 2010. edgeR: a Bioconductor package for differential expression analysis of digital gene expression data. *Bioinformatics,* 26**,** 139-140.

RUGGIERO, G., BEN-MOSHE LIVNE, Z., WEXLER, Y., GEYER, N., VALLONE, D., GOTHILF, Y. & FOULKES, N. S. 2021. Period 2: A Regulator of Multiple Tissue-Specific Circadian Functions. *Front Mol Neurosci,* 14**,** 718387.

SANCERNI, T., RENOULT, O., LUBY, A., CARADEUC, C., LENOIR, V., CROYAL, M., RANSY, C., AGUILAR, E., POSTIC, C., BERTHO, G., DENTIN, R., PRIP-BUUS, C., PECQUEUR, C. & ALVES-GUERRA, M. C. 2022. UCP2 silencing restrains leukemia cell proliferation through glutamine metabolic remodeling. *Front Immunol,* 13**,** 960226.

SAXTON, R. A. & SABATINI, D. M. 2017. mTOR Signaling in Growth, Metabolism, and Disease. *Cell,* 168**,** 960-976.

SCHEIERMANN, C., GIBBS, J., INCE, L. & LOUDON, A. 2018. Clocking in to immunity. *Nat Rev Immunol,* 18**,** 423-437.

SCHEIERMANN, C., KUNISAKI, Y. & FRENETTE, P. S. 2013. Circadian control of the immune system. *Nat Rev Immunol,* 13**,** 190-8.

SCHINDELIN, J., ARGANDA-CARRERAS, I., FRISE, E., KAYNIG, V., LONGAIR, M., PIETZSCH, T., PREIBISCH, S., RUEDEN, C., SAALFELD, S., SCHMID, B., TINEVEZ, J. Y., WHITE, D. J., HARTENSTEIN, V., ELICEIRI, K., TOMANCAK, P. & CARDONA, A. 2012. Fiji: an open-source platform for biological-image analysis. *Nature Methods,* 9**,** 676-682.

SENER, A. & MALAISSE, W. J. 1980. L-leucine and a nonmetabolized analogue activate pancreatic islet glutamate dehydrogenase. *Nature,* 288**,** 187-9.

SENER, A., MALAISSELAGAE, F. & MALAISSE, W. J. 1981. Stimulation of Pancreatic-Islet Metabolism and Insulin Release by a Non-Metabolizable Amino-Acid. *Proceedings of the National Academy of Sciences of the United States of America-Biological Sciences,* 78**,** 5460-5464.

SERON-FERRE, M., VALENZUELA, G. J. & TORRES-FARFAN, C. 2007. Circadian clocks during embryonic and fetal development. *Birth Defects Res C Embryo Today,* 81**,** 204-14.

SHANG, M., CAPPELLESSO, F., AMORIM, R., SERNEELS, J., VIRGA, F., EELEN, G., CAROBBIO, S., RINCON, M. Y., MAECHLER, P., DE BOCK, K., HO, P. C., SANDRI, M., GHESQUIERE, B., CARMELIET, P., DI MATTEO, M., BERARDI, E. & MAZZONE, M. 2020. Macrophage-derived glutamine boosts satellite cells and muscle regeneration. *Nature,* 587**,** 626-+.

SOTO, R. A., NAJIA, M. A. T., HACHIMI, M., FRAME, J. M., YETTE, G. A., LUMMERTZ DA ROCHA, E., STANKUNAS, K., DALEY, G. Q. & NORTH, T. E. 2021. Sequential regulation of hemogenic fate and hematopoietic stem and progenitor cell formation from arterial endothelium by Ezh1/2. *Stem Cell Reports,* 16**,** 1718-1734.

SPADARO, G., GIURATO, G., STELLATO, C., MARONE, G. & CASOLARO, V. 2020. Basophil degranulation in response to IgE ligation is controlled by a distinctive circadian clock in asthma. *Allergy,* 75**,** 158-168.

TAKAHASHI, J. S. 2017. Transcriptional architecture of the mammalian circadian clock. *Nat Rev Genet,* 18**,** 164-179.

TAMPLIN, O. J., DURAND, E. M., CARR, L. A., CHILDS, S. J., HAGEDORN, E. J., LI, P. L., YZAGUIRRE, A. D., SPECK, N. A. & ZON, L. I. 2015. Hematopoietic Stem Cell Arrival Triggers Dynamic Remodeling of the Perivascular Niche. *Cell,* 160**,** 241-252.

THISSE, C. & THISSE, B. 2008. High-resolution in situ hybridization to whole-mount zebrafish embryos. *Nature Protocols,* 3**,** 59-69.

TIAN, Y., XU, J., FENG, S., HE, S., ZHAO, S., ZHU, L., JIN, W., DAI, Y., LUO, L., QU, J. Y. & WEN, Z. 2017. The first wave of T lymphopoiesis in zebrafish arises from aorta endothelium independent of hematopoietic stem cells. *J Exp Med,* 214**,** 3347-3360.

TORCQ, L., VIVIER, C., SCHMUTZ, S., LOE-MIE, Y. & SCHMIDT, A. A. 2025. Single-cell and in situ spatial analyses reveal the diversity of newly born hematopoietic stem cells and of their niches. *Development,* 152.

TROTT, A. J. & MENET, J. S. 2018. Regulation of circadian clock transcriptional output by CLOCK:BMAL1. *PLoS Genet,* 14**,** e1007156.

UEDA, H. R., HAYASHI, S., CHEN, W., SANO, M., MACHIDA, M., SHIGEYOSHI, Y., IINO, M. & HASHIMOTO, S. 2005. System-level identification of transcriptional circuits underlying mammalian circadian clocks. *Nat Genet,* 37**,** 187-92.

ULLOA, B. A., HABBSA, S. S., POTTS, K. S., LEWIS, A., MCKINSTRY, M., PAYNE, S. G., FLORES, J. C., NIZHNIK, A., FELIZ NORBERTO, M., MOSIMANN, C. & BOWMAN, T. V. 2021. Definitive hematopoietic stem cells minimally contribute to embryonic hematopoiesis. *Cell Rep,* 36**,** 109703.

VALVEZAN, A. J. & MANNING, B. D. 2019. Molecular logic of mTORC1 signalling as a metabolic rheostat. *Nature Metabolism,* 1**,** 321-333.

VARCOE, T. J., BODEN, M. J., VOULTSIOS, A., SALKELD, M. D., RATTANATRAY, L. & KENNAWAY, D. J. 2013. Characterisation of the maternal response to chronic phase shifts during gestation in the rat: implications for fetal metabolic programming. *PLoS One,* 8**,** e53800.

WANG, H. 2008a. Comparative analysis of period genes in teleost fish genomes. *J Mol Evol,* 67**,** 29-40.

WANG, H. 2008b. Comparative analysis of teleost fish genomes reveals preservation of different ancient clock duplicates in different fishes. *Mar Genomics,* 1**,** 69-78.

WANG, H. 2009. Comparative genomic analysis of teleost fish bmal genes. *Genetica,* 136**,** 149-61.

WANG, Z., MA, L., MENG, Y., FANG, J., XU, D. & LU, Z. 2024. The interplay of the circadian clock and metabolic tumorigenesis. *Trends Cell Biol,* 34**,** 742-755.

WATFORD, M. 2000. Glutamine and glutamate metabolism across the liver sinusoid. *J Nutr,* 130**,** 983S-7S.

WATTRUS, S. J. & ZON, L. I. 2018. Stem cell safe harbor: the hematopoietic stem cell niche in zebrafish. *Blood Adv,* 2**,** 3063-3069.

WEGER, M., DIOTEL, N., DORSEMANS, A. C., DICKMEIS, T. & WEGER, B. D. 2017. Stem cells and the circadian clock. *Developmental Biology,* 431**,** 111-123.

WESTERFIELD, M. 2000. The Zebrafish Book. A Guide for the Laboratory Use of Zebrafish (Danio rerio). 4th edition. *University of Oregon Press, Eugene, Oregon 2000*.

WHARFE, M. D., MARK, P. J. & WADDELL, B. J. 2011. Circadian variation in placental and hepatic clock genes in rat pregnancy. *Endocrinology,* 152**,** 3552-60.

XIAO, Y., HU, B., GUO, Y., ZHANG, D., ZHAO, Y., CHEN, Y., LI, N. & YU, L. 2023. Targeting Glutamine Metabolism as an Attractive Therapeutic Strategy for Acute Myeloid Leukemia. *Curr Treat Options Oncol,* 24**,** 1021-1035.

XUE, Y. Y., LV, J. H., ZHANG, C. X., WANG, L., MA, D. Y. & LIU, F. 2017. The Vascular Niche Regulates Hematopoietic Stem and Progenitor Cell Lodgment and Expansion via klf6a-ccl25b. *Developmental Cell,* 42**,** 349-+.

YOO, H. C., YU, Y. C., SUNG, Y. & HAN, J. M. 2020. Glutamine reliance in cell metabolism. *Experimental and Molecular Medicine,* 52**,** 1496-1516.

YU, Y. L., NEWMAN, H., SHEN, L. Y., SHARMA, D., HU, G. L., MIRANDO, A. J., ZHANG, H. Y., KNUDSEN, E., ZHANG, G. F., HILTON, M. J. & KARNER, C. M. 2019. Glutamine Metabolism Regulates Proliferation and Lineage Allocation in Skeletal Stem Cells. *Cell Metabolism,* 29**,** 966-+.

ZHANG, J., PAVLOVA, N. N. & THOMPSON, C. B. 2017. Cancer cell metabolism: the essential role of the nonessential amino acid, glutamine. *Embo Journal,* 36**,** 1302-1315.

Figures

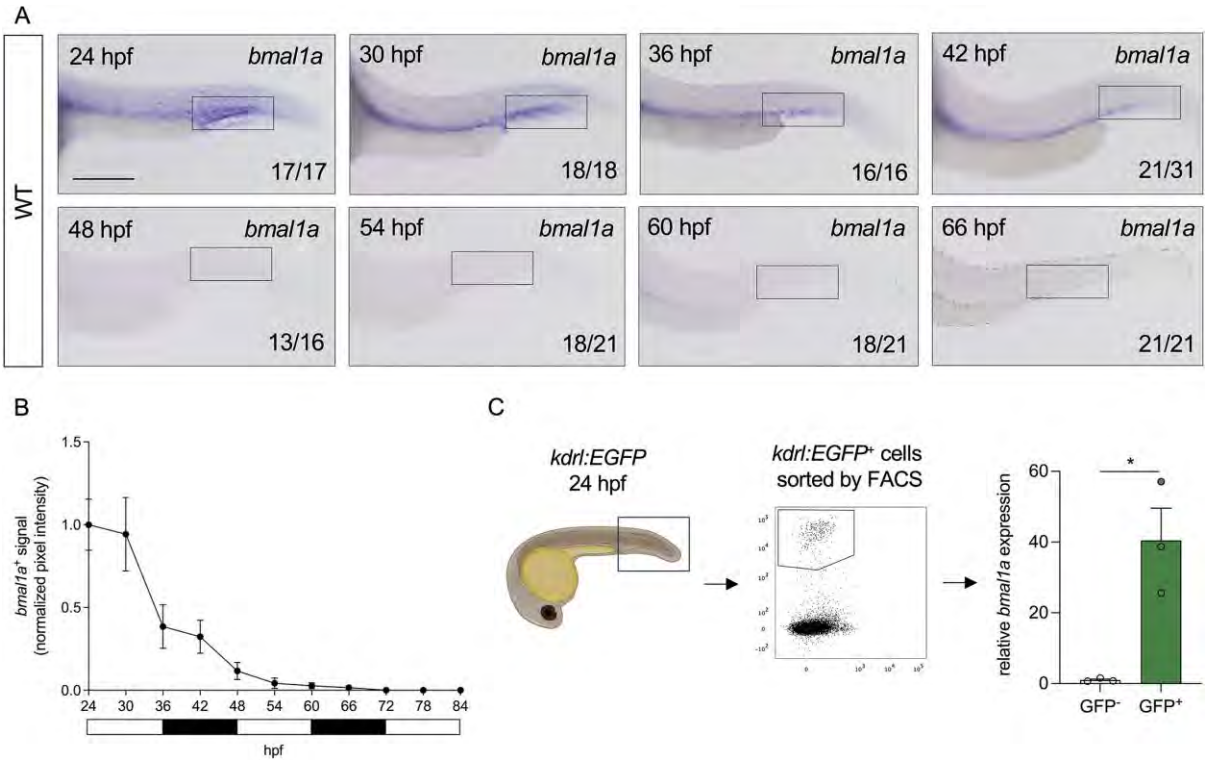

Fig. 1. *bmal1a* is expressed in endothelial cells of the CHT but its expression in this region is not rhythmic in embryos raised in light-dark cycles. A. *in situ* hybridisation of *bmal1a* from 24-66 hpf in the tails of zebrafish embryos raised in light-dark cycles. **B.** Quantification of normalised *bmal1a in situ* hybridisation signal between 24-84 hpf in the CHT of wild-type zebrafish raised in light-dark cycles. *bmal1a* expression diminishes over time and is not rhythmic; *n*=9-10 embryos for each timepoint. **C.** *kdrl:EGFP* tails were dissected at 24 hpf before endothelial cells were sorted by FACS and *bmal1a* expression was quantified by qPCR. *bmal1a* expression is enriched in endothelial cells; *n*=~50 embryos in triplicate. Statistical significance between two groups was calculated using unpaired two-tailed Student's *t*-tests assuming equal variance. Rectangles in **A** indicate the CHT area. Scale bar: 200 μm. White and black rectangles in **B** denote light and dark periods.

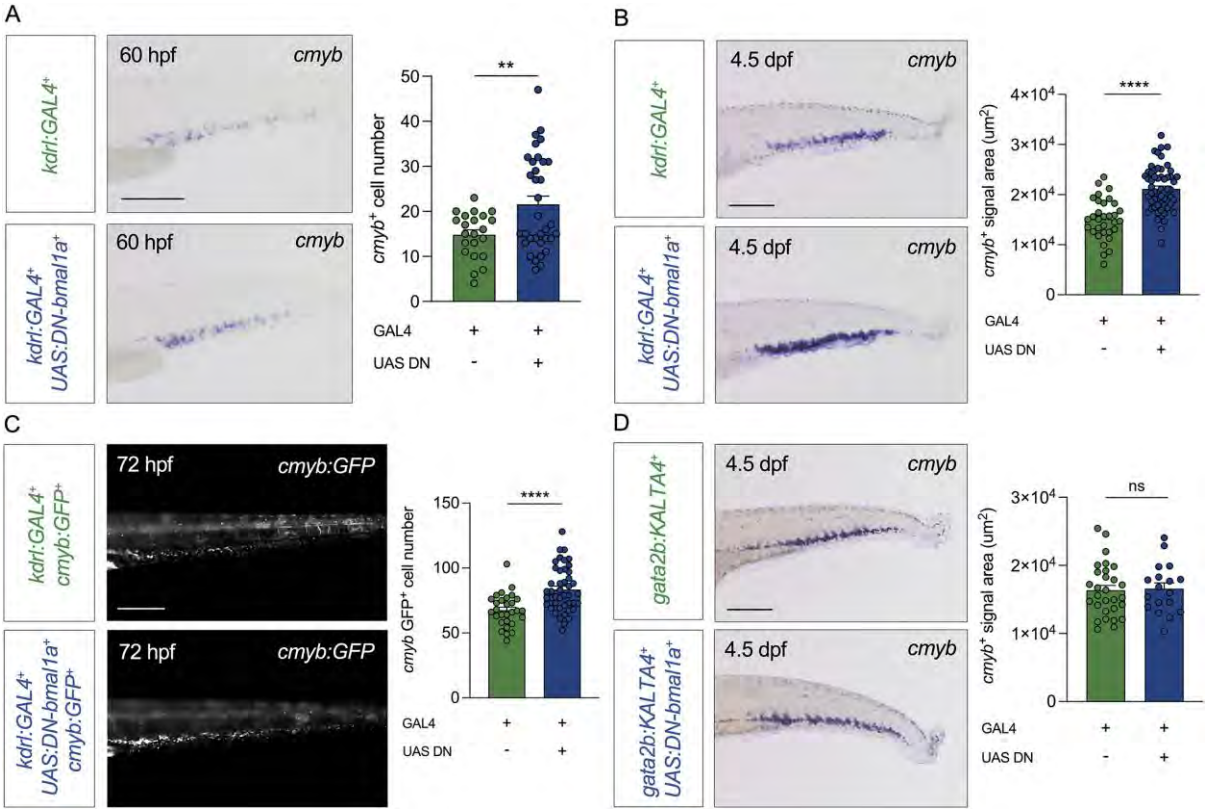

Fig. 2. Endothelial-specific dominant-negative *bmal1a* results in a non-cell autonomous increase in HSPC numbers in the CHT. A. *cmyb in situ* hybridisation and quantification in *kdrl:GAL4;UAS:DN-bmal1a* embryos and controls at 60 hpf. **B.** *cmyb in situ* hybridisation and quantification in *kdrl:GAL4;UAS:DN-bmal1a* larvae and controls at 4.5 dpf. **C.** *cmyb:GFP*$^{+}$ cells and quantification in *kdrl:GAL4;UAS:DN-bmal1a;cmyb:GFP* larvae and controls at 72 hpf. **D.** *cmyb in situ* hybridisation and quantification in *gata2b:KALTA4;UAS:DN-bmal1a* larvae and controls at 4.5 dpf. Statistical significance between two groups was calculated using unpaired two-tailed Student's *t*-tests assuming equal variance. Scale bars: 200 μm.

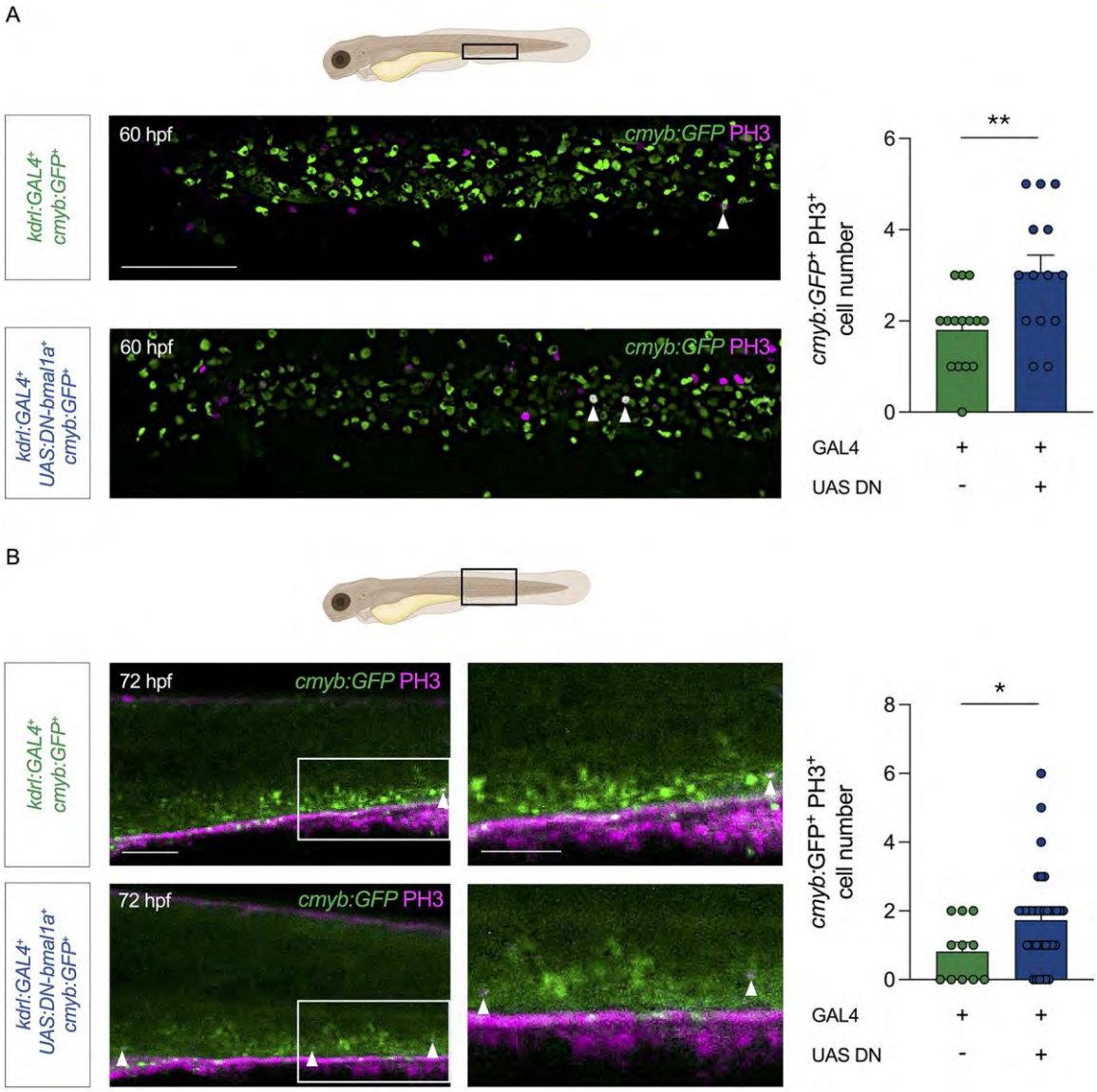

Fig. 3. Endothelial-specific dominant-negative *bmal1a* embryos display an increased HSPC proliferation rate in the CHT. A. Immunohistochemistry and quantification of *cmyb*:*GFP* and Phospho-Histone 3 (PH3) double-positive HSPCs in the CHT of *kdrl:GAL4;UAS:DN-bmal1a;cmyb:GFP* zebrafish larvae and controls at 60 hpf. **B.** Immunohistochemistry and quantification of *cmyb*:*GFP* and PH3 double-positive HSPCs in the CHT of *kdrl:GAL4;UAS:DN-bmal1a;cmyb:GFP* zebrafish larvae and controls at 72 hpf. Statistical significance between two groups was calculated using unpaired two-tailed Student's *t*-tests assuming equal variance. Schematic diagrams of embryos in **A** and **B** indicate the CHT regions imaged in each respective panel. Scale bars: 200 μm (**A** and **B**, left) and 50 μm (in enlargement, **B**, right).

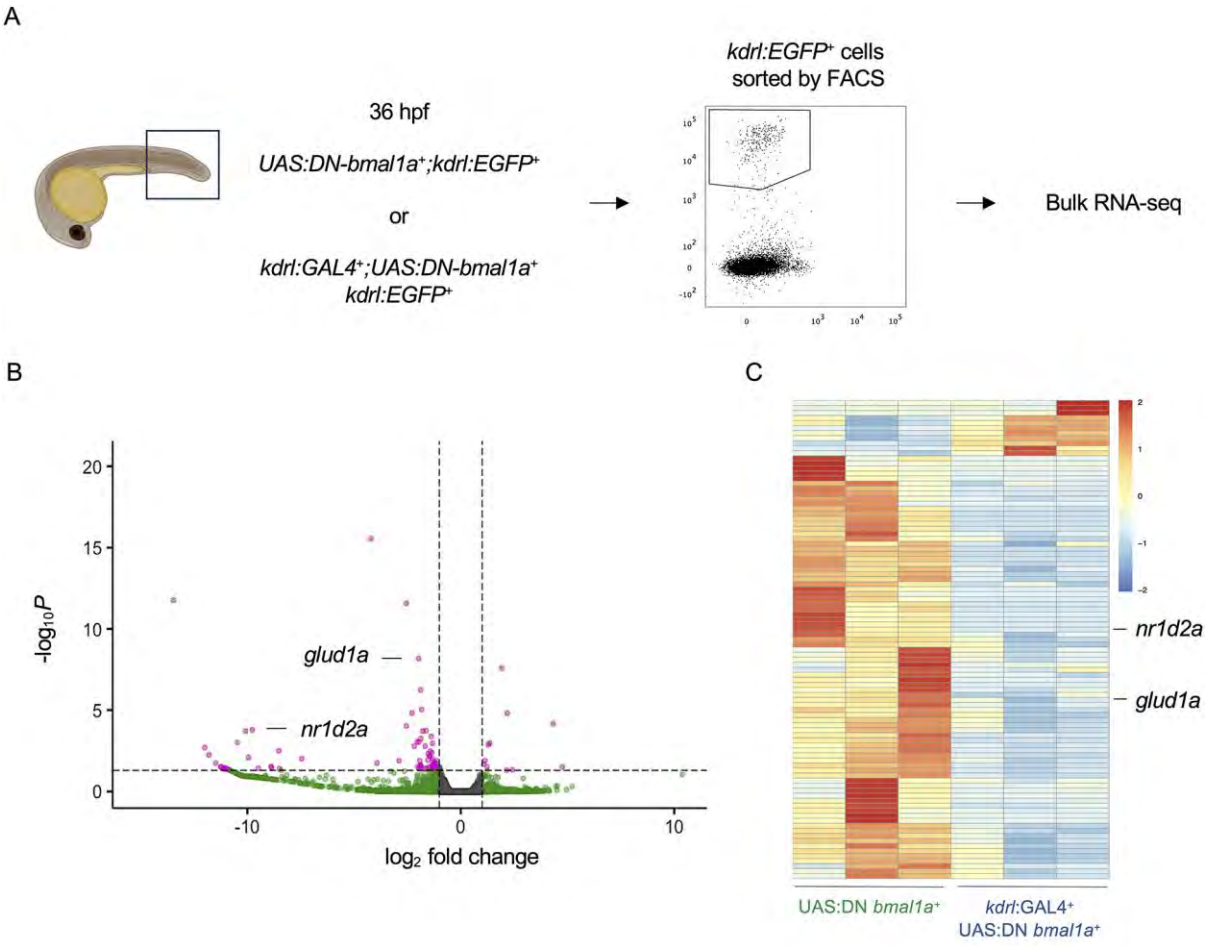

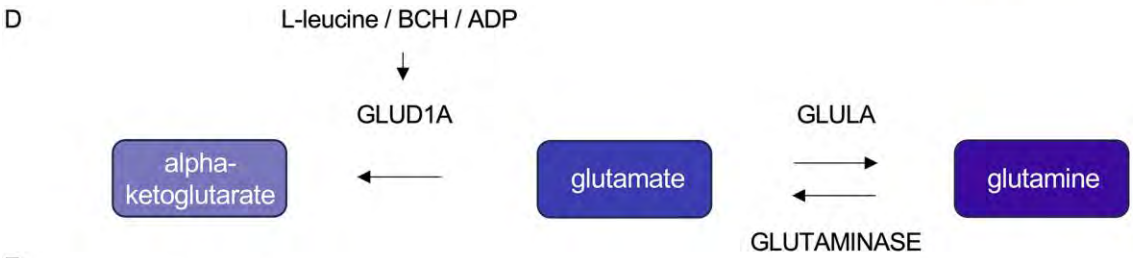

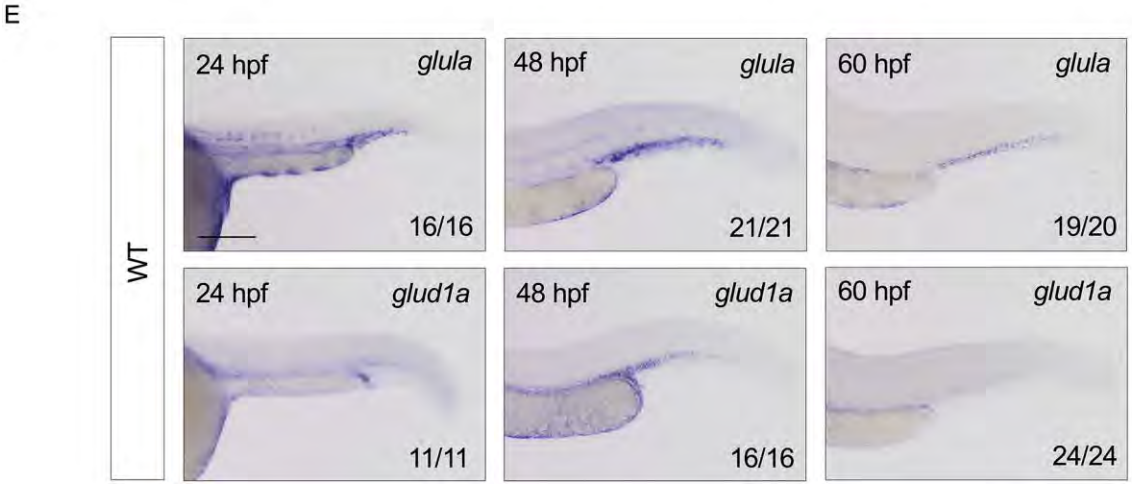

Fig. 4. Endothelial-specific dominant-negative *bmal1a* results in a decrease in *glud1a* expression in CHT endothelial cells. A. ECs were sorted by fluorescence activated cell sorting (FACS) from *kdrl:GAL4;UAS:DN-bmal1a;cmyb:GFP* zebrafish embryos and controls at 36 hpf, before HSPC emergence and migration to the CHT, and subjected to bulk RNA-sequencing; *n*=~60 embryos in triplicate for each genotype. **B.** Volcano plot depicting the 95 genes which were differentially expressed in tail endothelial cells of *kdrl:GAL4;UAS:DN-bmal1a;cmyb:GFP* embryos and controls, with *glud1a* and *nr1d2a* indicated. **C.** Heatmap depicting the 95 genes differentially expressed genes with *glud1a* and *nr1d2a* indicated. **D.** Schematic depicting the conversion of glutamate to α-ketoglutarate and glutamine via the enzymes GLUD1A, GLULA and GLUTAMINASE. Allosteric activators of GLUD1A (L-leucine, BCH and ADP) are also depicted. **E.** *In situ* hybridization of *glula* and *glud1a* at 24, 48 and 60 hpf in wild-type embryos. The two genes are expressed in the CHT at times compatible with a role in developmental hematopoiesis. Scale bars: 200 μm.

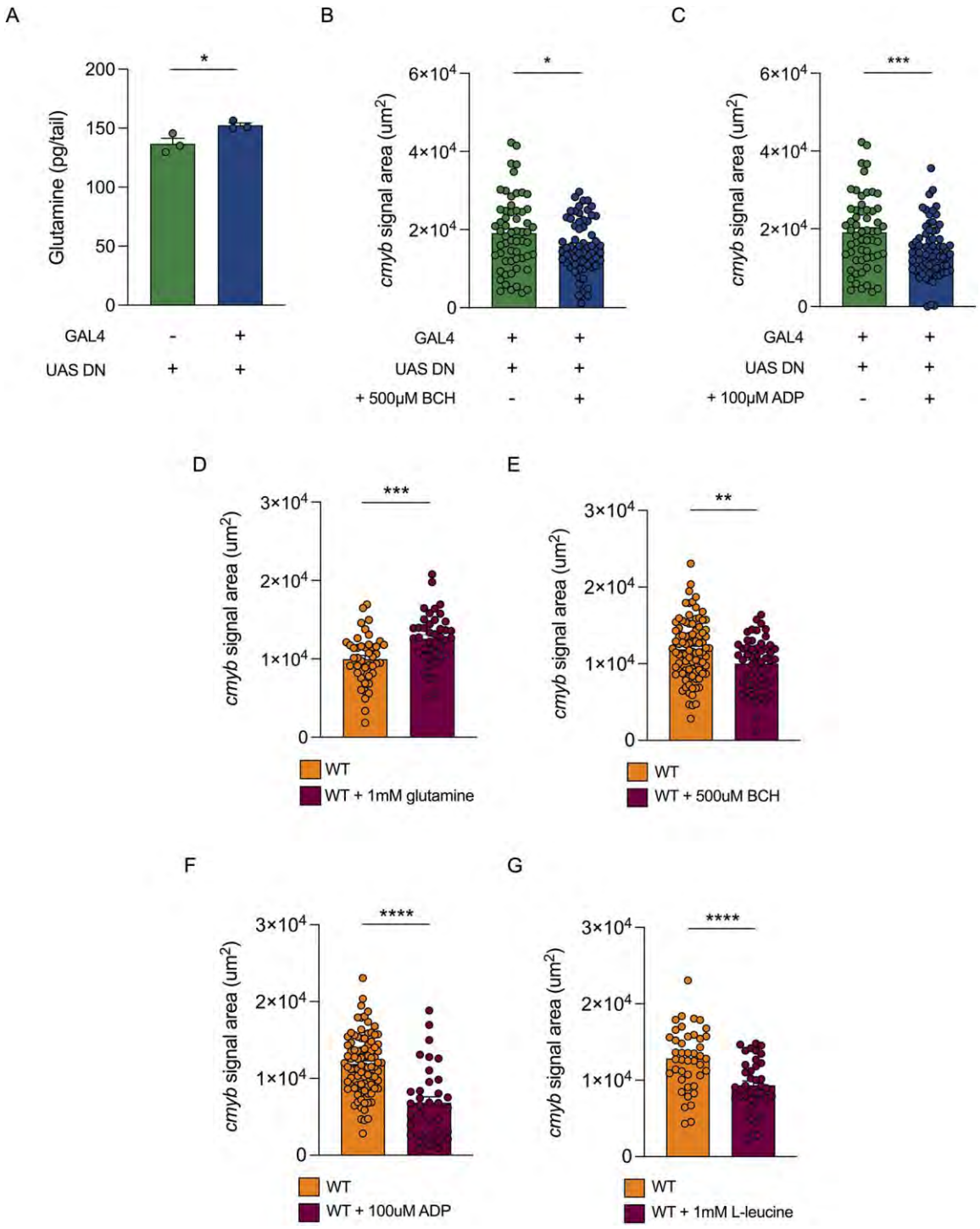

Fig. 5. Glutamine concentration is increased in endothelial-specific dominant-negative *bmal1a* zebrafish embryo tails and results in increased HSPC numbers. A. Quantification of glutamine concentrations in dissected tails of *kdrl:GAL4;UAS:DN-bmal1a* larvae and controls. **B.** Quantification of *cmyb in situ* hybridisation signal in *kdrl:GAL4;UAS:DN-bmal1a* larvae treated with 500μM BCH

and controls at 4.5 dpf. **C.** Quantification of *cmyb in situ* hybridisation signal in *kdrl:GAL4;UAS:DN-bmal1a* larvae treated with 100μM ADP and controls at 4.5 dpf. **D.** Quantification of *cmyb in situ* hybridisation signal in wild-type larvae treated with 1mM glutamine and controls at 4.5 dpf. **E.** Quantification of *cmyb in situ* hybridisation signal in wild-type larvae treated with 1mM L-leucine and controls at 4.5 dpf. **F.** Quantification of *cmyb in situ* hybridisation signal in wild-type larvae treated with 500μM BCH and controls at 4.5 dpf. **G.** Quantification of *cmyb in situ* hybridisation signal in wild-type larvae treated with 100μM ADP and controls at 4.5 dpf. Statistical significance between two groups was calculated using unpaired two-tailed Student's *t*-tests assuming equal variance.

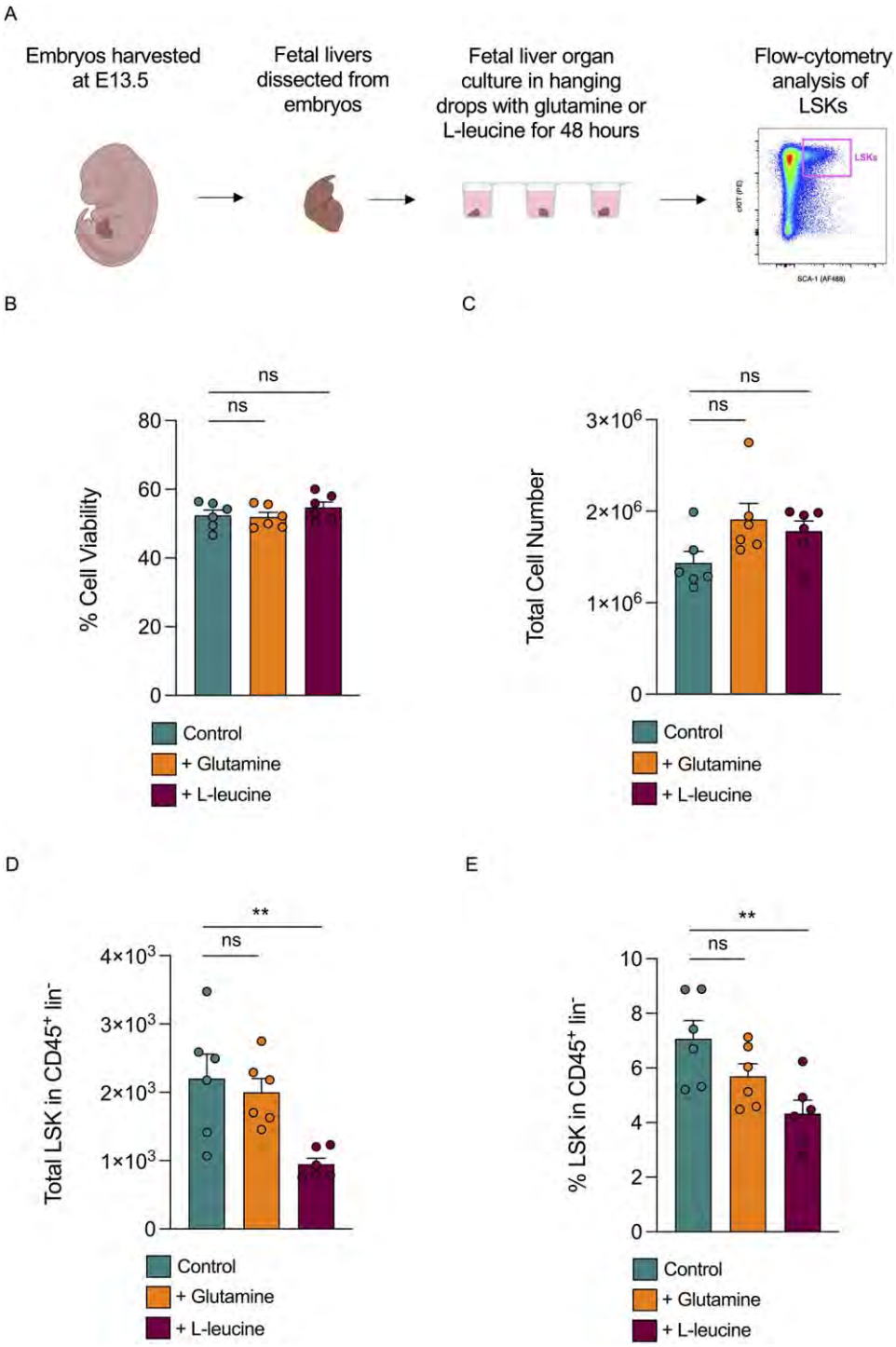

Fig. 6. Increasing GLUD1 activity in mouse fetal liver organ culture results in a decrease in LSK (HSPCs) numbers. A. Schematic of fetal liver organ culture experiments. Dissected fetal liver pieces were cultured with glutamine, L-leucine or without either (controls) for 48 hours prior to flow cytometry analysis. **B.** Viability (percentage of live cells) of fetal liver organ culture cells in controls or when

supplemented with glutamine (2mM or 10mM, see methods) or 10mM L-leucine. **C.** Total fetal liver organ culture cell numbers in controls or when supplemented with glutamine (2mM or 10mM) or 10mM L-leucine. **D.** Total LSKs in $CD45^+$ lin^- cells in controls or when supplemented with glutamine (2mM or 10mM) or 10mM L-leucine. **E.** %LSKs of $CD45^+$ lin^- cells in controls or when supplemented with glutamine (2mM or 10mM) or 10mM L-leucine.

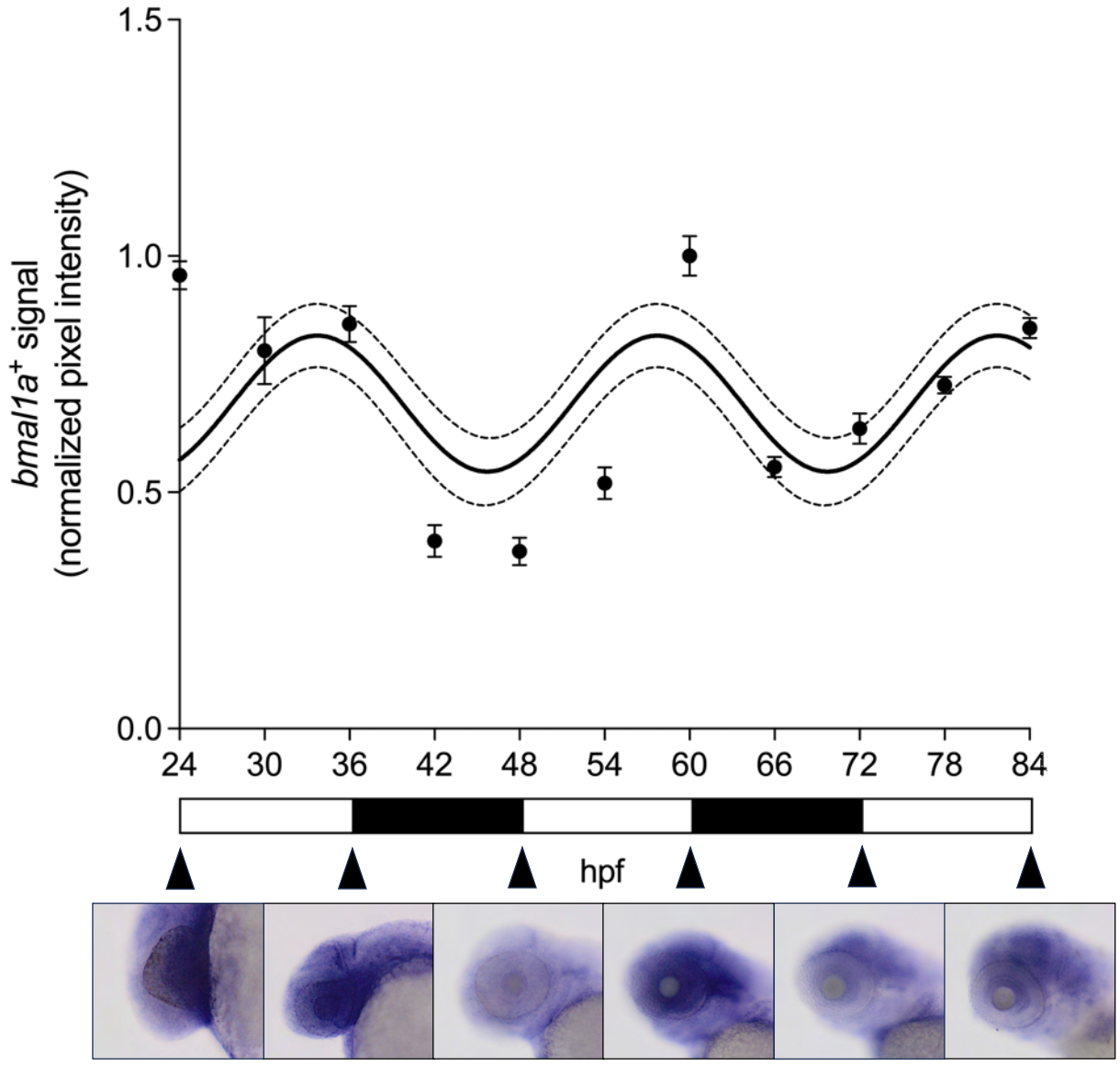

Fig. S1. *bmal1a* is expressed rhythmically in the heads of zebrafish embryos raised in light-dark cycles. Quantification of normalised *bmal1a in situ* hybridisation signal between 24-84 hpf in the heads of wild-type zebrafish raised in light-dark cycles; *n*=9-10 embryos or larvae for each timepoint. Images under the graph are representative *in situ* images of embryo / larvae heads every 12 hours. Circadian rhythmicity was determined by cosinor analysis.

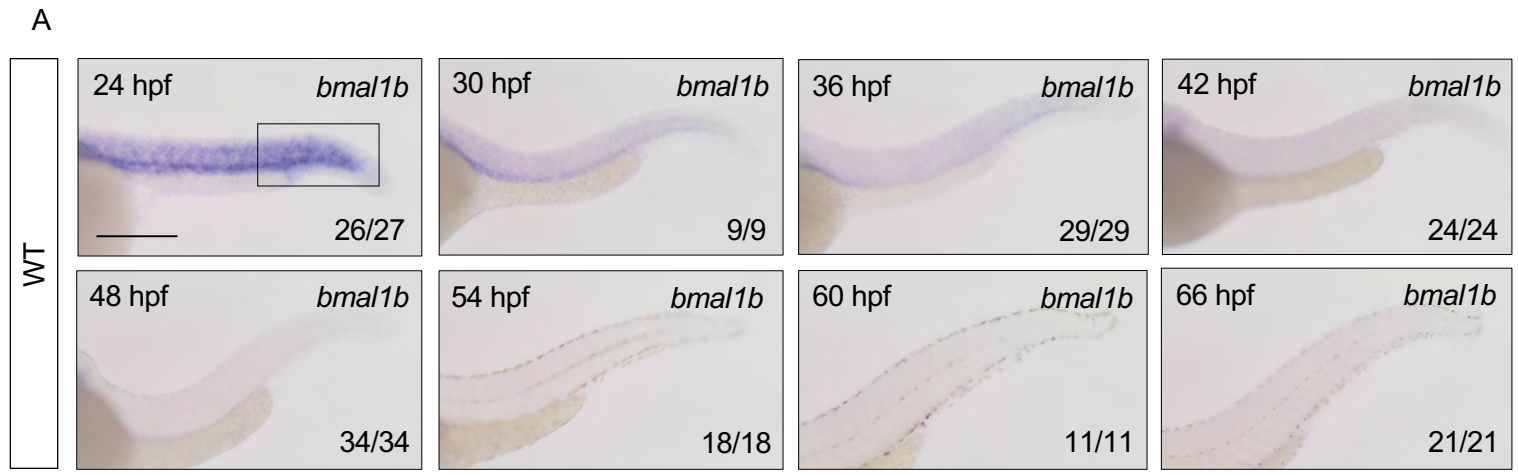

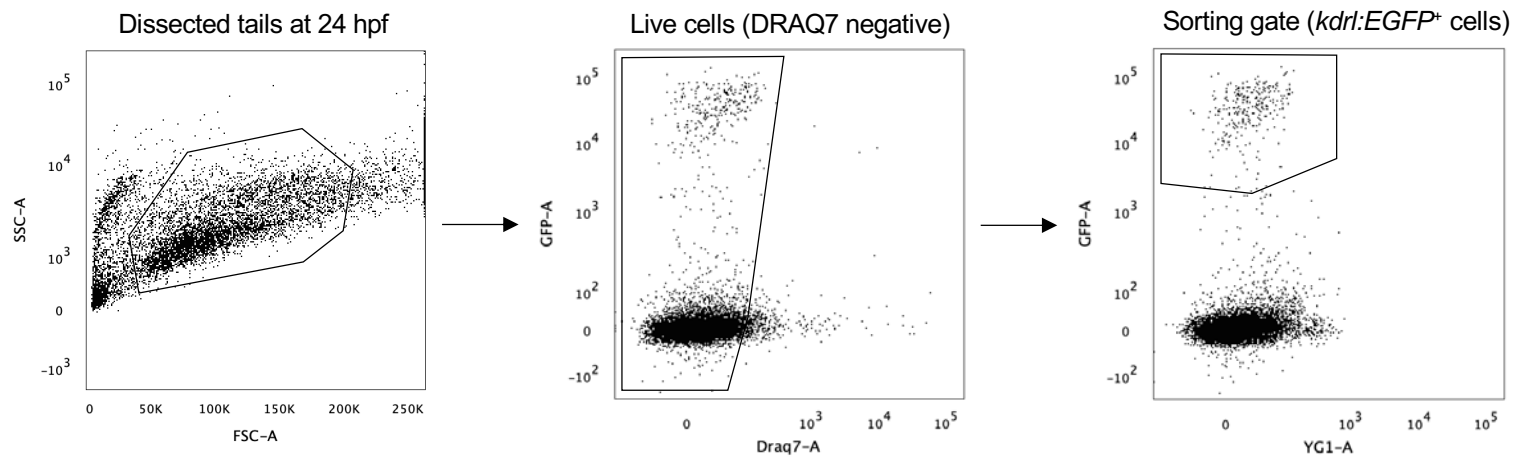

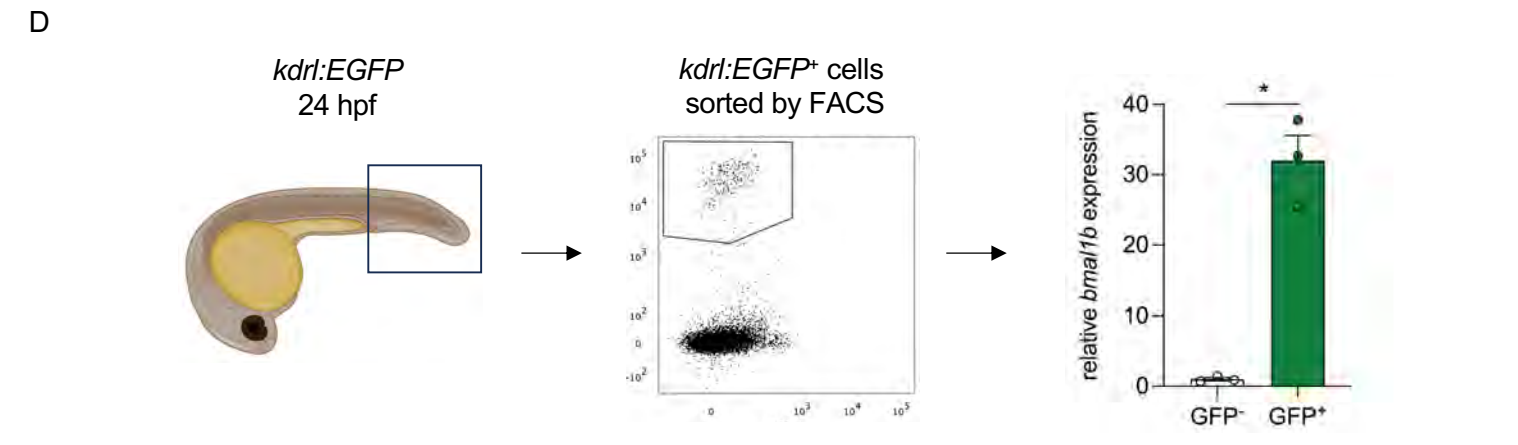

Fig. S2. Circadian clock genes are expressed in the CHT at 24 hpf. A. *in situ* hybridisation of *bmal1b* from 24-66 hpf in the tails of zebrafish embryos raised in light-dark cycles. **B.** *in situ* hybridisation of *clocka* from 24-66 hpf in the tails of zebrafish embryos raised in light-dark cycles. **C.** Fluorescence activated cell sorting (FACS) plots to depict the strategy used to sort endothelial cells from the tails of *kdrl:EGFP* embryos at 24 hpf. **D.** *kdrl:EGFP* tails were dissected at 24 hpf before endothelial cells were sorted by FACS and *bmal1b* expression was quantified by qPCR; *n*=~50 embryos in triplicate. Rectangles in **A** and **B** indicate the CHT area. Statistical significance between two groups was calculated using unpaired two-tailed Student's *t*-tests assuming equal variance. Scale bars: 200 μm.

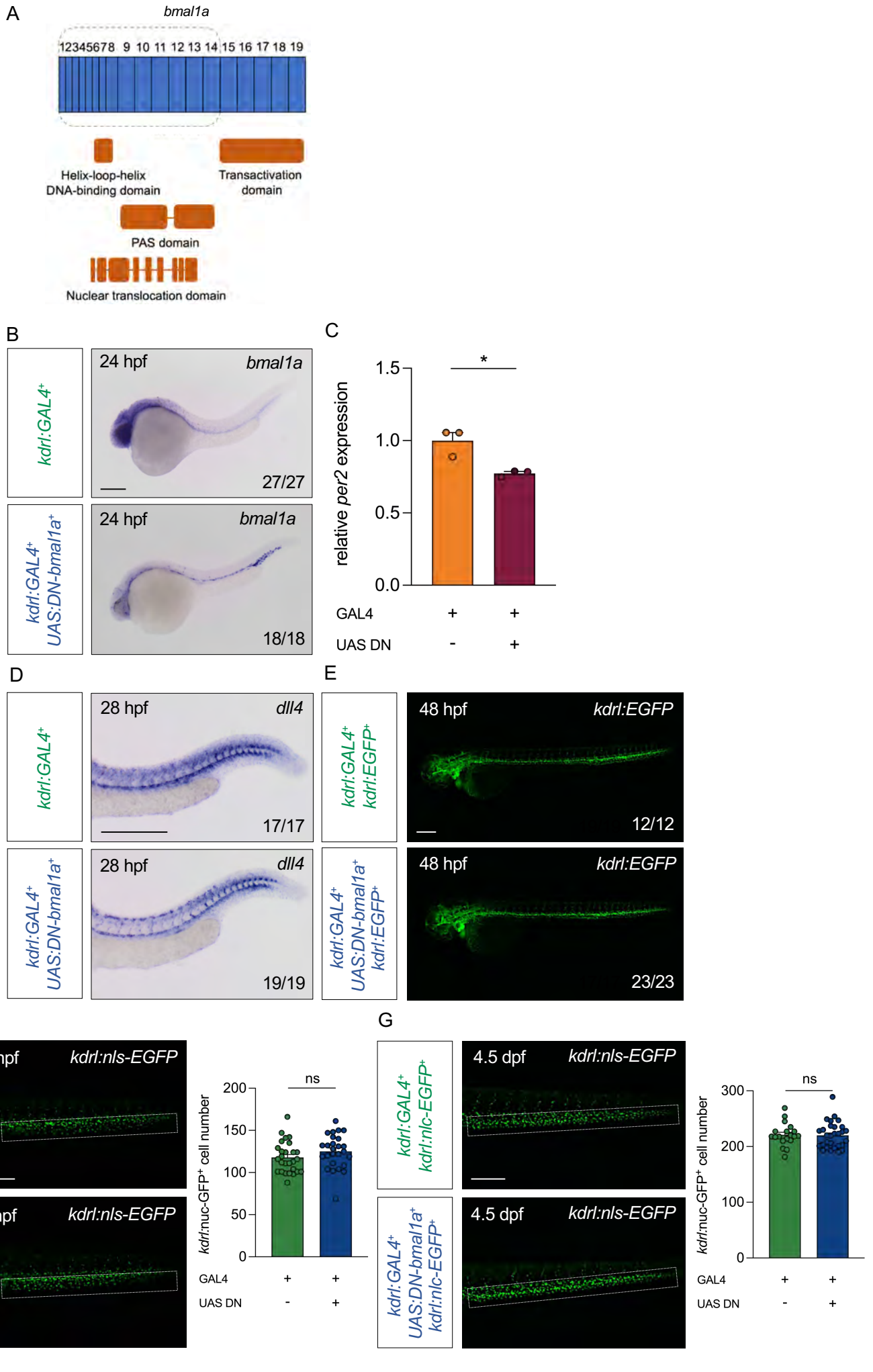
A
bmal1a
12345678 9 10 11 12 13 14 15 16 17 18 19
Helix-loop-helix DNA-binding domain
Transactivation domain
PAS domain
Nuclear translocation domain
B
kdrl:GAL4+
24 hpf
bmal1a
27/27
kdrl:GAL4+ UAS:DN-bmal1a+
24 hpf
bmal1a
18/18
C
relative per2 expression
1.5
1.0
0.5
0.0
*
GAL4 + +
UAS DN - +
D
kdrl:GAL4+
28 hpf
dll4
17/17
kdrl:GAL4+ UAS:DN-bmal1a+
28 hpf
dll4
19/19
E
kdrl:GAL4+ kdrl:EGFP+
48 hpf
kdrl:EGFP
12/12
kdrl:GAL4+ UAS:DN-bmal1a+ kdrl:EGFP+
48 hpf
kdrl:EGFP
23/23
F
kdrl:GAL4+ kdrl:nlc-EGFP+
48 hpf
kdrl:nls-EGFP
kdrl:GAL4+ UAS:DN-bmal1a+ kdrl:nlc-EGFP+
48 hpf
kdrl:nls-EGFP
kdrl:nuc-GFP+ cell number
200
150
100
50
0
ns
GAL4 + +
UAS DN - +
G
kdrl:GAL4+ kdrl:nlc-EGFP+
4.5 dpf
kdrl:nls-EGFP
kdrl:GAL4+ UAS:DN-bmal1a+ kdrl:nlc-EGFP+
4.5 dpf
kdrl:nls-EGFP
kdrl:nuc-GFP+ cell number
300
200
100
0
ns
GAL4 + +
UAS DN - +

Fig. S3. Loss of the Bmal1a transactivation domain in endothelial-specific dominant-negative Bmal1a zebrafish embryos reduces target gene expression but does not alter vascular development. A. Schematic showing the region of the *bmal1a* gene (within the dotted line) that was cloned from cDNA for the generation of the *UAS:DN-bmal1a* zebrafish line. Exons are indicated in blue (numbered 1-19) and protein domains are indicated in orange. Note the exclusion of the transactivation domain in the cloned fragment. **B.** *in situ* hybridisation of *bmal1a* in *kdrl:GAL4;UAS:DN-bmal1a* embryos and controls at 24 hpf. **C.** qPCR analysis of *per2* expression in whole *kdrl:GAL4;UAS:DN-bmal1a* embryos and controls at 36 hpf; *n*=~30 embryos in triplicate for each genotype. **D.** *in situ* hybridisation of *dll4* in *kdrl:GAL4;UAS:DN-bmal1a* embryos and controls at 28 hpf. **E.** *kdrl:EGFP* fluorescence in *kdrl:GAL4;UAS:DN-bmal1a;kdrl:EGFP* embryos and controls at 48 hpf. **F.** *kdrl:nls-EGFP* fluorescence and GFP^+ cell quantification in the CHT of *kdrl:GAL4;UAS:DN-bmal1a;kdrl:nls-EGFP* embryos and controls at 48 hpf. **G.** *kdrl:nls-EGFP* fluorescence and GFP^+ cell quantification in the CHT of *kdrl:GAL4;UAS:DN-bmal1a;kdrl:nls-EGFP* larvae and controls at 4.5 dpf. Rectangles in **F** and **G** indicate the CHT area in which cells were quantified. Statistical significance between two groups was calculated using unpaired two-tailed Student's *t*-tests assuming equal variance. Scale bars: 200 μm.

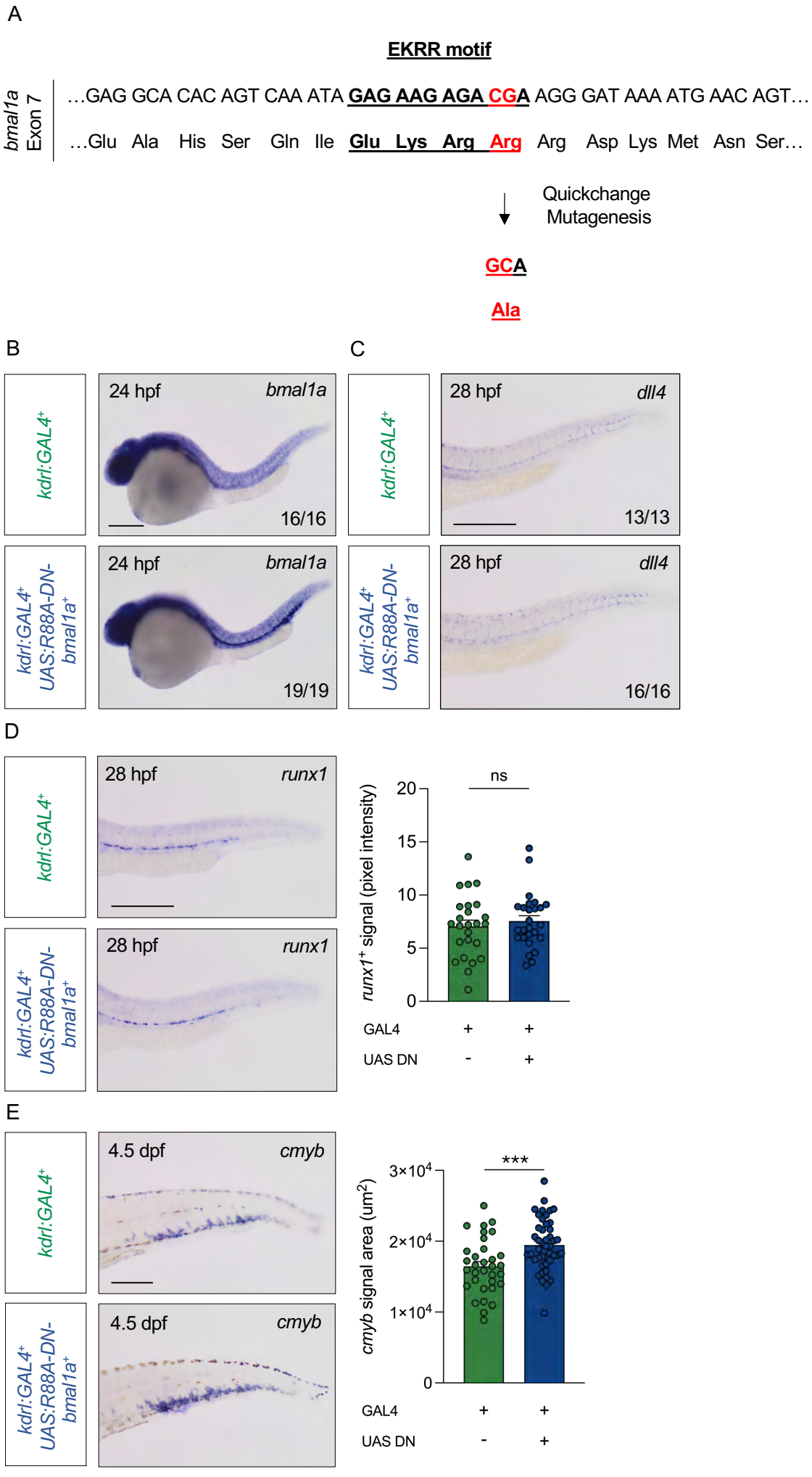

Fig. S4. Endothelial-specific R88A-*DN-bmal1a* results in an increase in the number of HSPCs in the CHT at 4.5 dpf. A. Experimental schematic showing the R88A amino acid change in the *bmal1a* EKRR motif induced by quickchange mutagenesis. **B.** *in situ* hybridisation of *bmal1a* in *kdrl:GAL4;UAS:R88A-DN-bmal1a* zebrafish embryos and controls at 24 hpf. **C.** *in situ* hybridisation of *dll4* in *kdrl:GAL4;UAS:R88A-DN-bmal1a* embryos and controls at 28 hpf. **D.** *runx1 in situ* hybridisation and quantification in *kdrl:GAL4;UAS:R88A-DN-bmal1a* embryos and controls at 28 hpf. **E.** *cmyb in situ* hybridisation and quantification in *kdrl:GAL4;UAS:R88A-DN-bmal1a* larvae and controls at 4.5 dpf. Statistical significance between two groups was calculated using unpaired two-tailed Student's *t*-tests assuming equal variance. Scale bars: 200 μm.

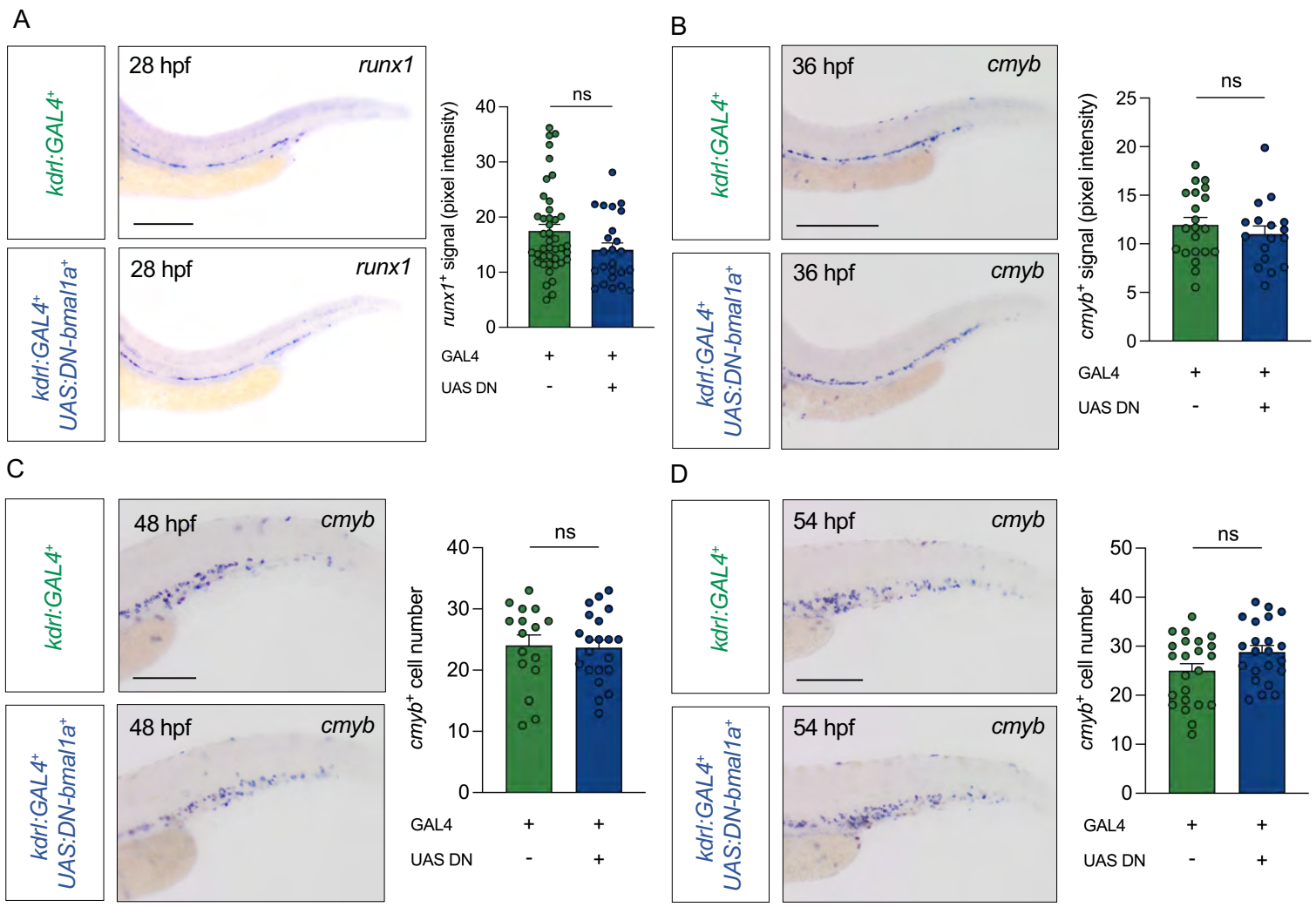

Fig. S5. Endothelial-specific dominant-negative *bmal1a* does not result in an increase in HSPC numbers in the CHT between 28 and 54 hpf. A. *runx1 in situ* hybridisation and quantification in *kdrl:GAL4;UAS:DN-bmal1a* zebrafish embryos and controls at 28 hpf. **B.** *cmyb in situ* hybridisation and quantification in *kdrl:GAL4;UAS:DN-bmal1a* embryos and controls at 36 hpf. **C.** *cmyb in situ* hybridisation and quantification in *kdrl:GAL4;UAS:DN-bmal1a* embryos and controls at 48 hpf. **D.** *cmyb in situ* hybridisation and quantification in *kdrl:GAL4;UAS:DN-bmal1a* embryos and controls at 54 hpf.

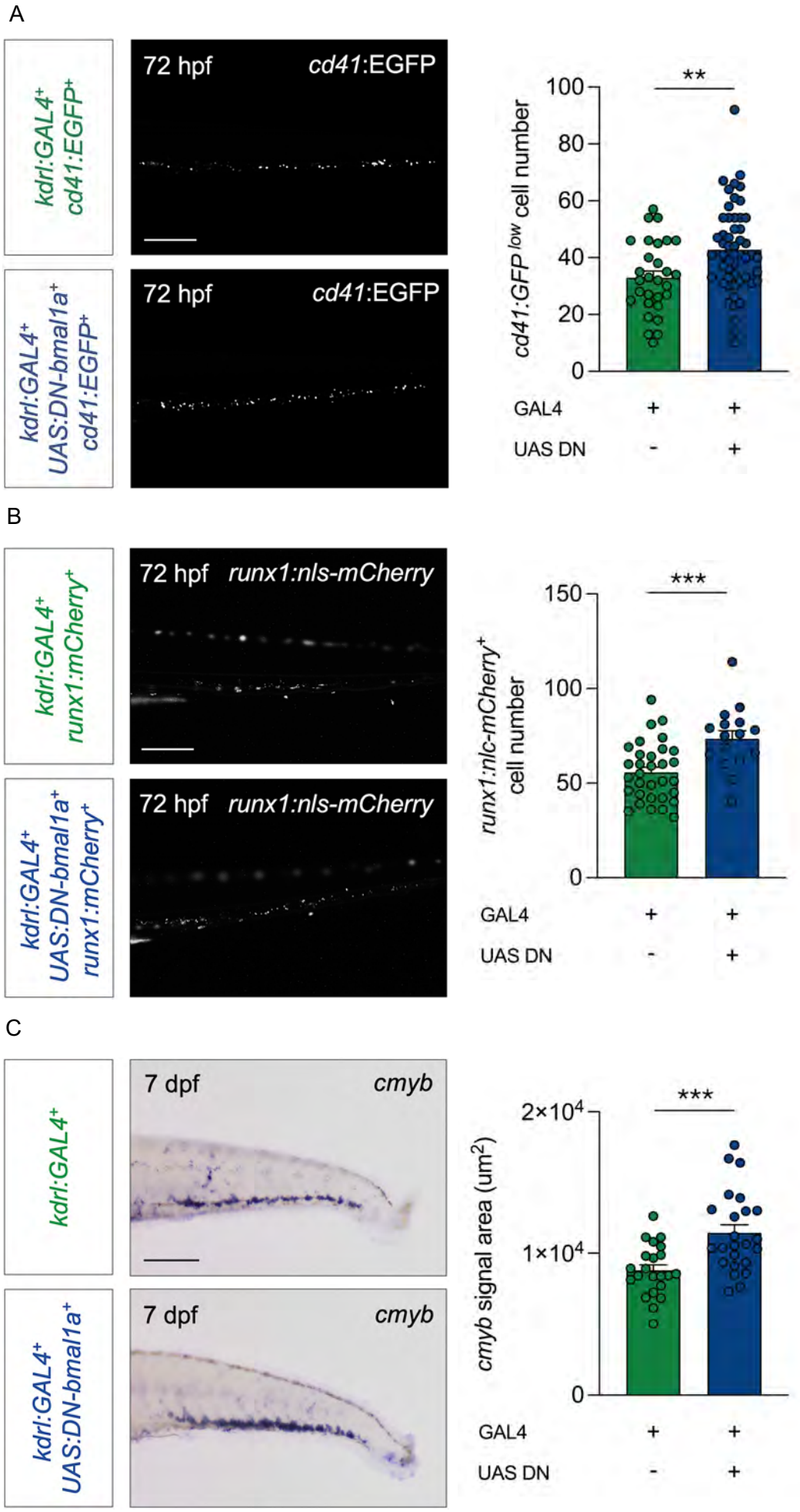

Fig. S6. Endothelial-specific DN-*bmal1a* larvae have an increased number of HSPCs in the CHT. A. *cd41:EGFP*$^{+}$ cells and quantification of *cd41:EGFP*^{low} cells in the CHT of *kdrl:GAL4;UAS:DN-bmal1a;cd41:EGFP* zebrafish larvae and controls at 72 hpf. **B.** *runx1:nls-mCherry*$^{+}$ cells and quantification in the CHT of *kdrl:GAL4;UAS:DN-bmal1a;runx1:nls-mCherry* larvae and controls at 72 hpf. **C.** *cmyb in situ* hybridisation and quantification in *kdrl:GAL4;UAS:DN-bmal1a;cmyb:GFP* larvae and controls at 7 dpf. Statistical significance between two groups was calculated using unpaired two-tailed Student's *t*-tests assuming equal variance. Scale bars: 200 μm.

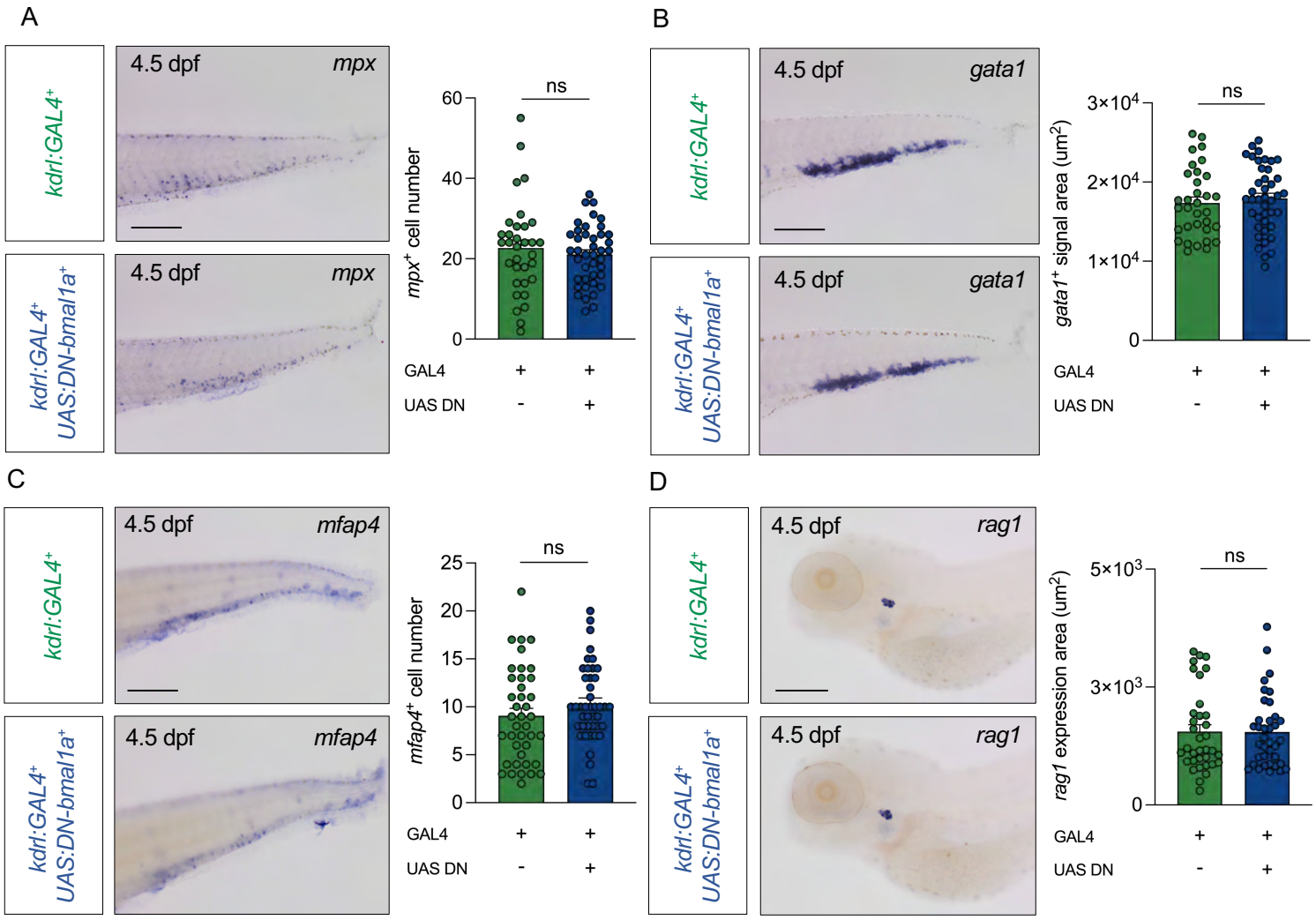

Fig. S7. Endothelial-specific *DN-bmal1a* does not alter neutrophil, erythrocyte, macrophage or T-cell numbers at 4.5 dpf. A. *mpx in situ* hybridisation and quantification in *kdrl:GAL4;UAS:DN-bmal1a* zebrafish larvae and controls at 4.5 dpf. **B.** *gata1 in situ* hybridisation and quantification in *kdrl:GAL4;UAS:DN-bmal1a* larvae and controls at 4.5 dpf. **C.** *mfap4 in situ* hybridisation and quantification in *kdrl:GAL4;UAS:DN-bmal1a* larvae and controls at 4.5 dpf. **D.** *rag1 in situ* hybridisation and quantification in *kdrl:GAL4;UAS:DN-bmal1a* larvae and controls at 4.5 dpf. Statistical significance between two groups was calculated using unpaired two-tailed Student's *t*-tests assuming equal variance. Scale bars: 200 µm.

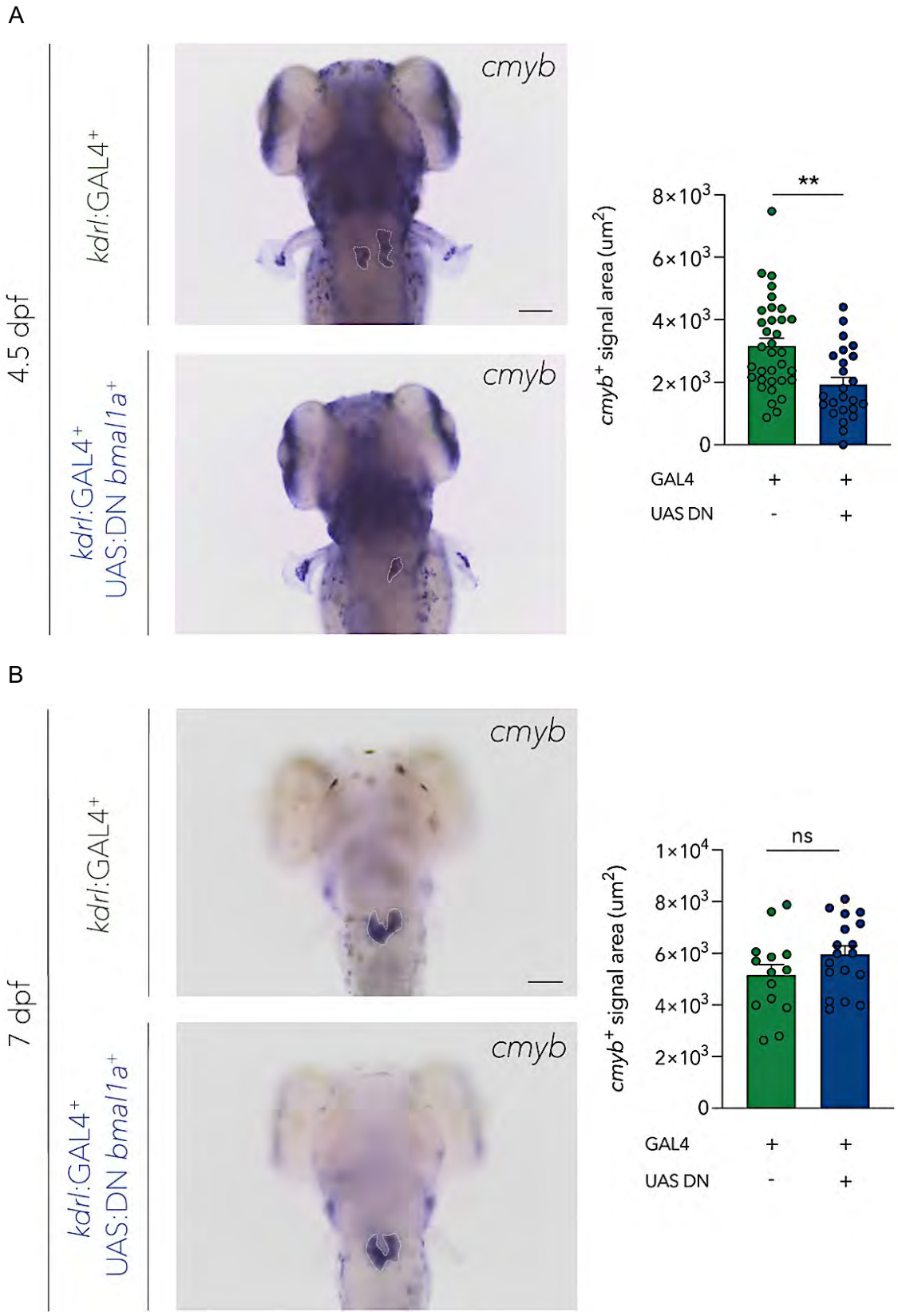

Fig. S8. Endothelial-specific dominant-negative Bmal1a reduces HSPC numbers in the kidney glomeruli at 4.5 dpf but not at 7 dpf. A. *cmyb in situ* hybridisation and quantification in *kdrl:GAL4*;*UAS:DN-bmal1a* embryos and controls at 4.5 dpf. **B.** *cmyb in situ* hybridisation and quantification in *kdrl:GAL4*;*UAS:DN-bmal1a* embryos and controls at 7 dpf. *cmyb*+ cells measured in the kidney glomeruli are marked by white dotted lines in both **A** and **B.** Two independent experiments were carried out for the experiment at 4.5 dpf. One experiment was performed at 7 dpf. Scale bars: 100 µm.

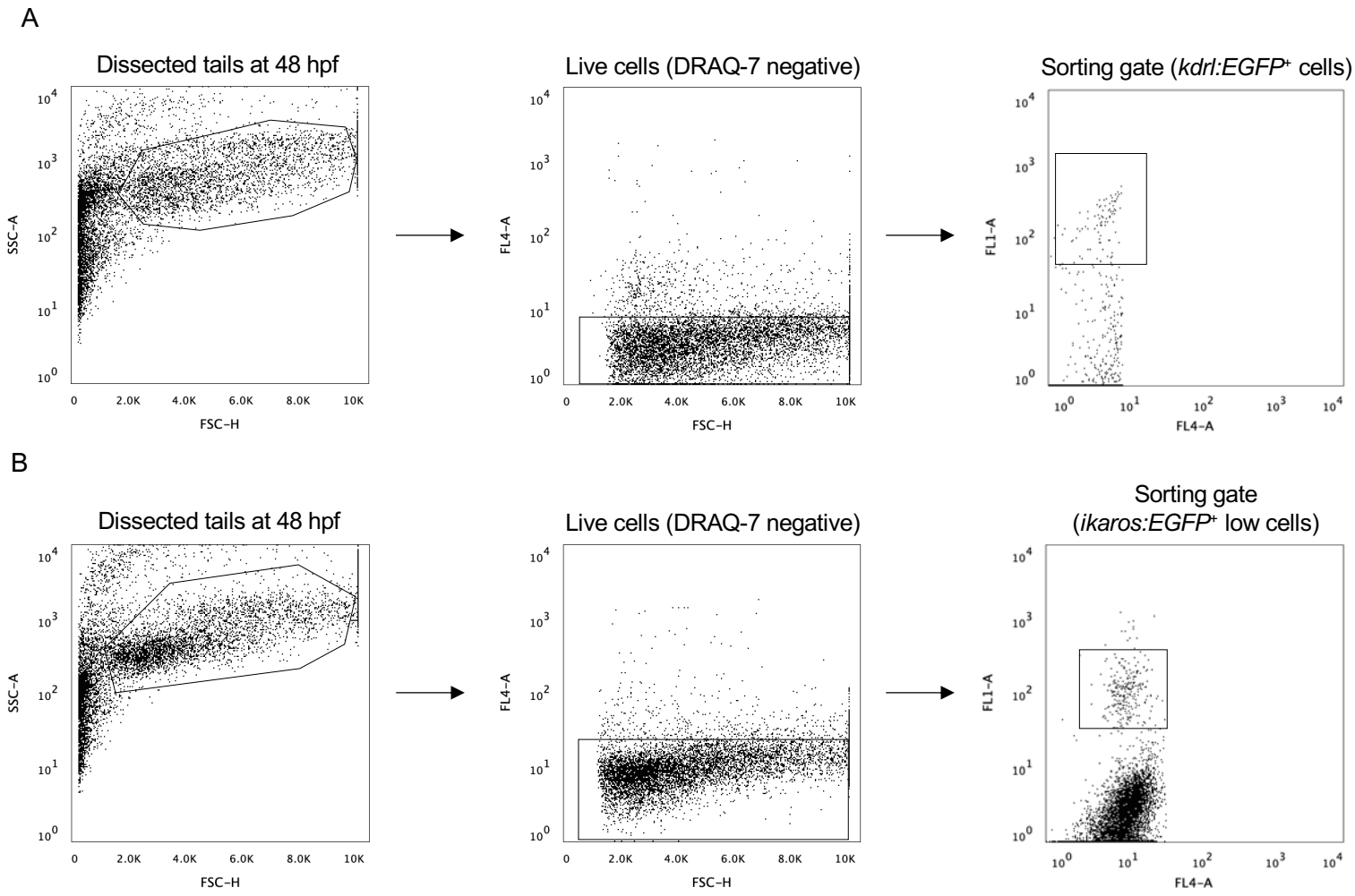

Fig. S9. Fluorescence activated cell sorting (FACS) strategy for sorting endothelial cells and HSPCs from tails of zebrafish embryos at 48 hpf. A. FACS plots to depict the strategy used to sort endothelial cells from the tails of *kdrl:EGFP* embryos at 48 hpf. **B.** FACS plots to depict the strategy used to sort HSPCs from the tails of *ikaros:EGFP* embryos at 48 hpf.

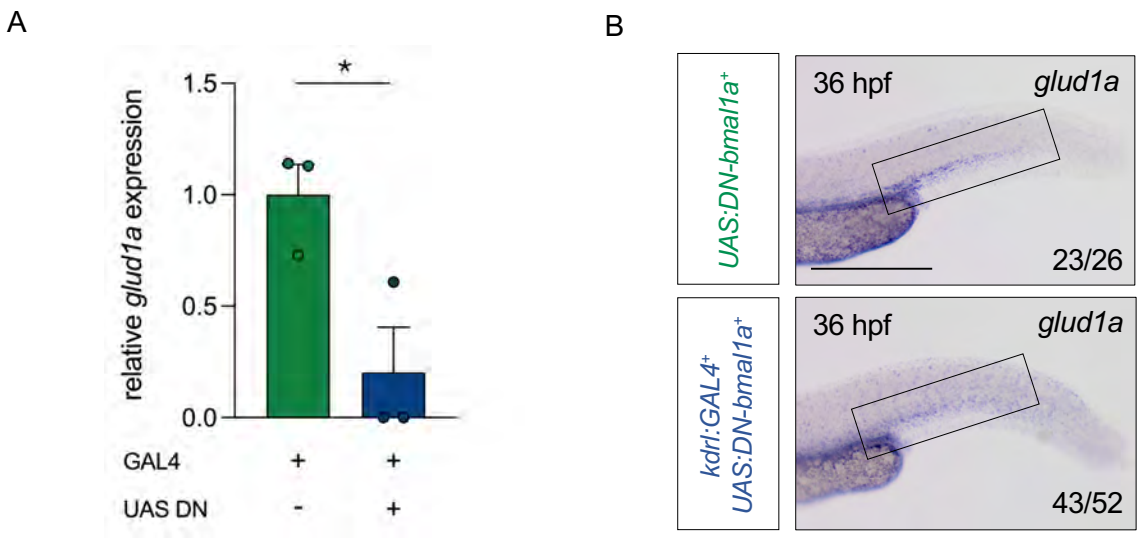

Fig. S10. *glud1a* expression is significantly reduced in endothelial-specific *DN-bmal1a* embryo tail endothelial cells. **A.** qPCR analysis of *glud1a* expression in tail endothelial cells of *kdrl:GAL4;UAS:DN-bmal1a* zebrafish embryos and controls at 36 hpf; *n*=~60 embryos in triplicate for each genotype. **B**. *glud1a in situ* hybridisation in *kdrl:GAL4;UAS:DN-bmal1a* embryos and controls at 36 hpf. Statistical significance between two groups was calculated using unpaired two-tailed Student's *t*-tests assuming equal variance. Scale bar: 200 μm.

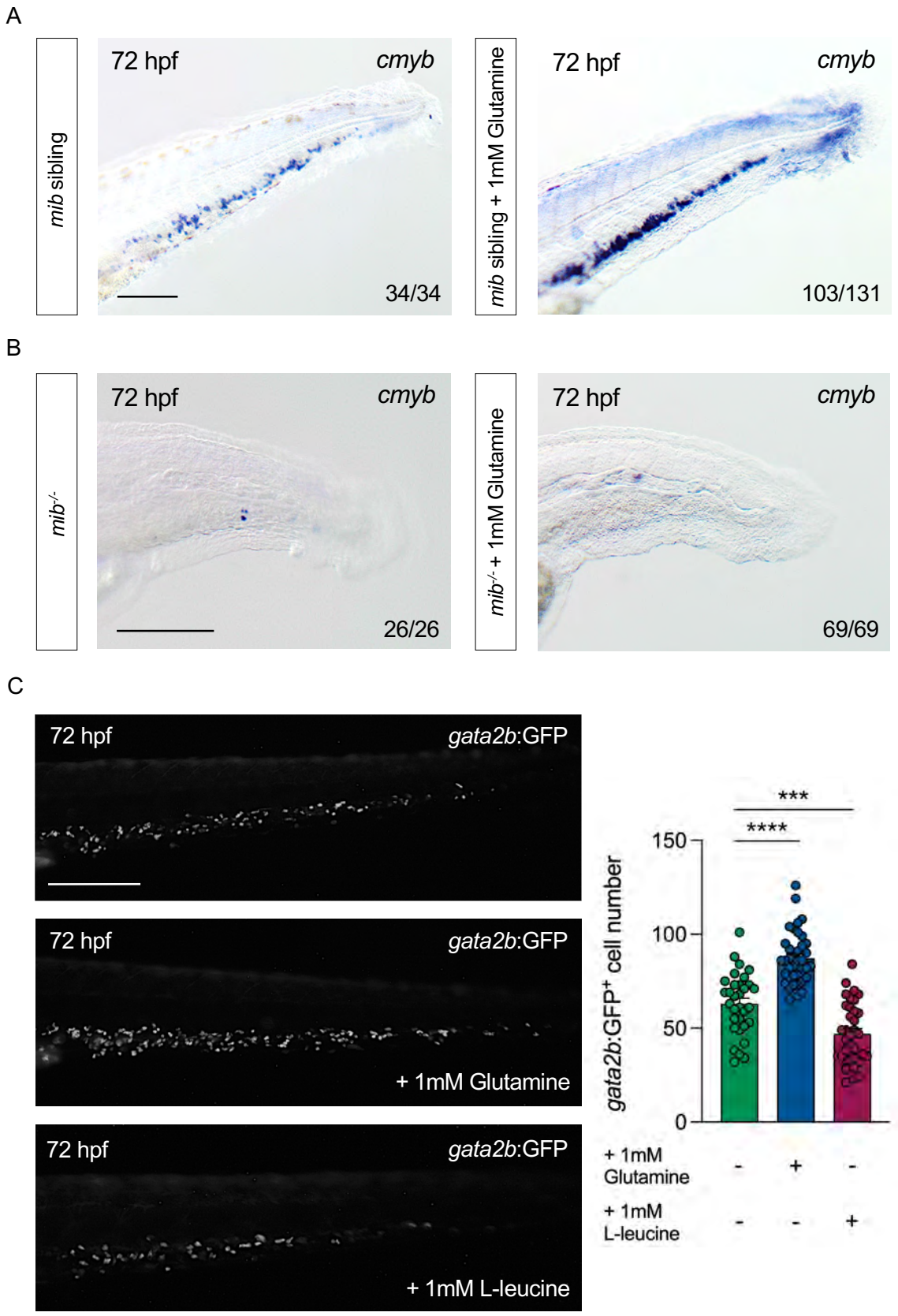

Fig. S11. Definitive HSPC expansion is affected by glutamine and GLUD1A modulation. A. Representative image of *cmyb in situ* hybridisation in *mib* sibling zebrafish embryos at 72 hpf with 1mM glutamine supplementation and controls. **B.** Representative image of *cmyb in situ* hybridisation in *mib*$^{-/-}$ mutant zebrafish embryos at 72 hpf with 1mM glutamine supplementation and controls. **C.** *gata2b*:GFP^{+} cells and quantification in the CHT of *gata2b:KALTA4*$^{+}$*;UAS:lifeact-GFP*$^{+}$ larvae at 72 hpf in controls and when supplemented with 1mM glutamine or 1mM L-leucine. Fractions in **A** and **B** represent the proportion of embryos with WISH signal as in the representative image. Statistical significance between two groups in **C** was calculated using unpaired two-tailed Student's *t*-tests assuming equal variance. Scale bars: 200 µm.

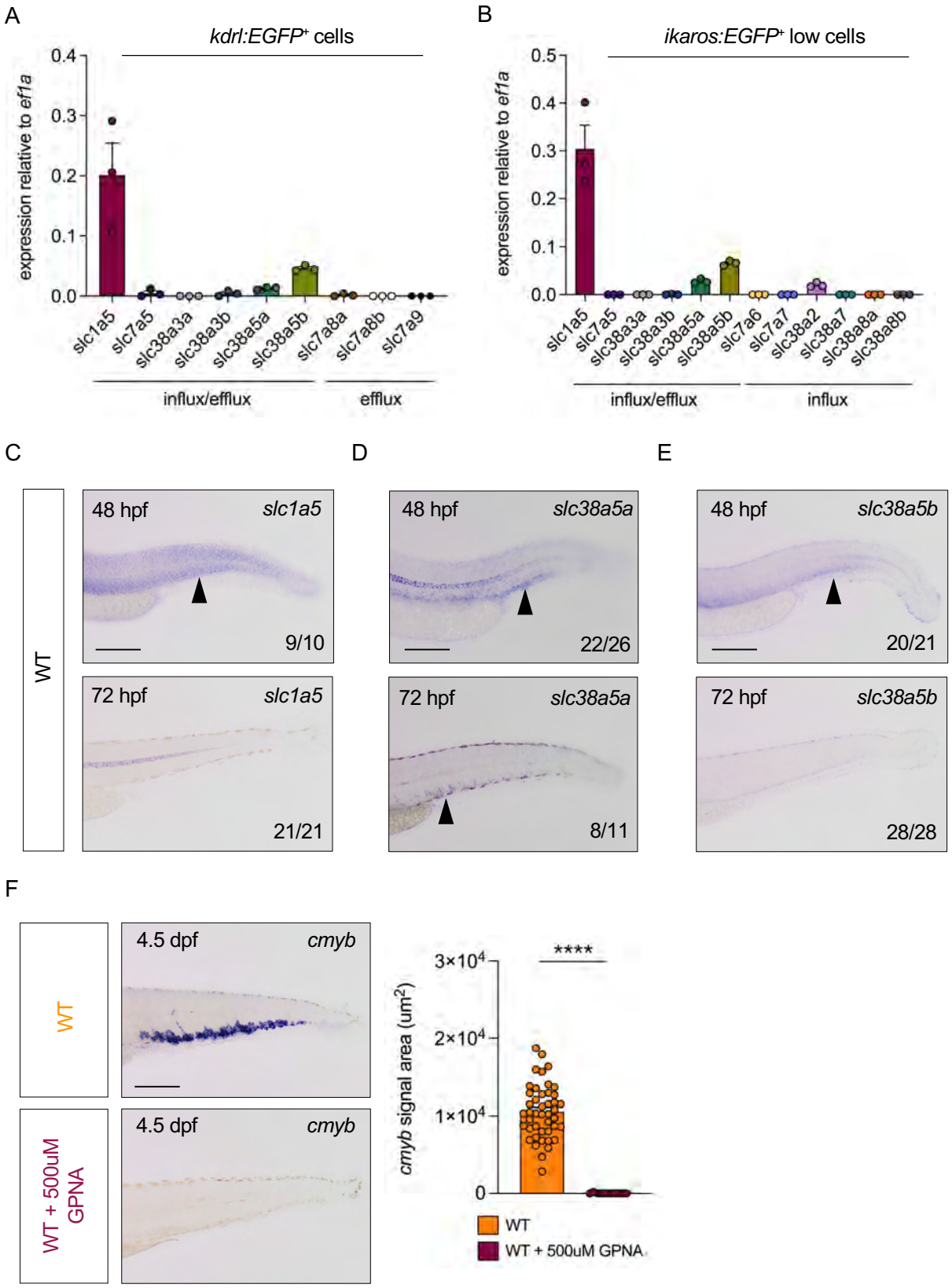

Fig. S12. Glutamine transporter genes are expressed in both endothelial cells and HSPCs. A. qPCR analyses of *slc* gene expression of SLCs able to carry out glutamine efflux in endothelial cells sorted from *kdrl:EGFP* zebrafish embryo tails at 48 hpf; *n*=~80 embryos in triplicate. **B.** qPCR analyses of *slc* gene expression of SLCs genes able to carry out glutamine influx into HSPCs sorted from *ikaros:GFP* tails at 48 hpf; *n*=~80 embryos in triplicate. **C.** *slc1a5 in situ* hybridisation at 48 and 72 hpf in wild-type zebrafish. **D.** *slc38a5a in situ* hybridisation at 48 and 72 hpf in wild-type zebrafish. **E.** *slc38a5b in situ* hybridisation at 48 and 72 hpf in wild-type zebrafish. **F.** *cmyb in situ* hybridisation and quantification in wild-type larvae treated with 500μM GPNA and controls at 4.5 dpf. Statistical significance between two groups in **F** was calculated using unpaired two-tailed Student's *t*-tests assuming equal variance. Scale bars: 200 μm.

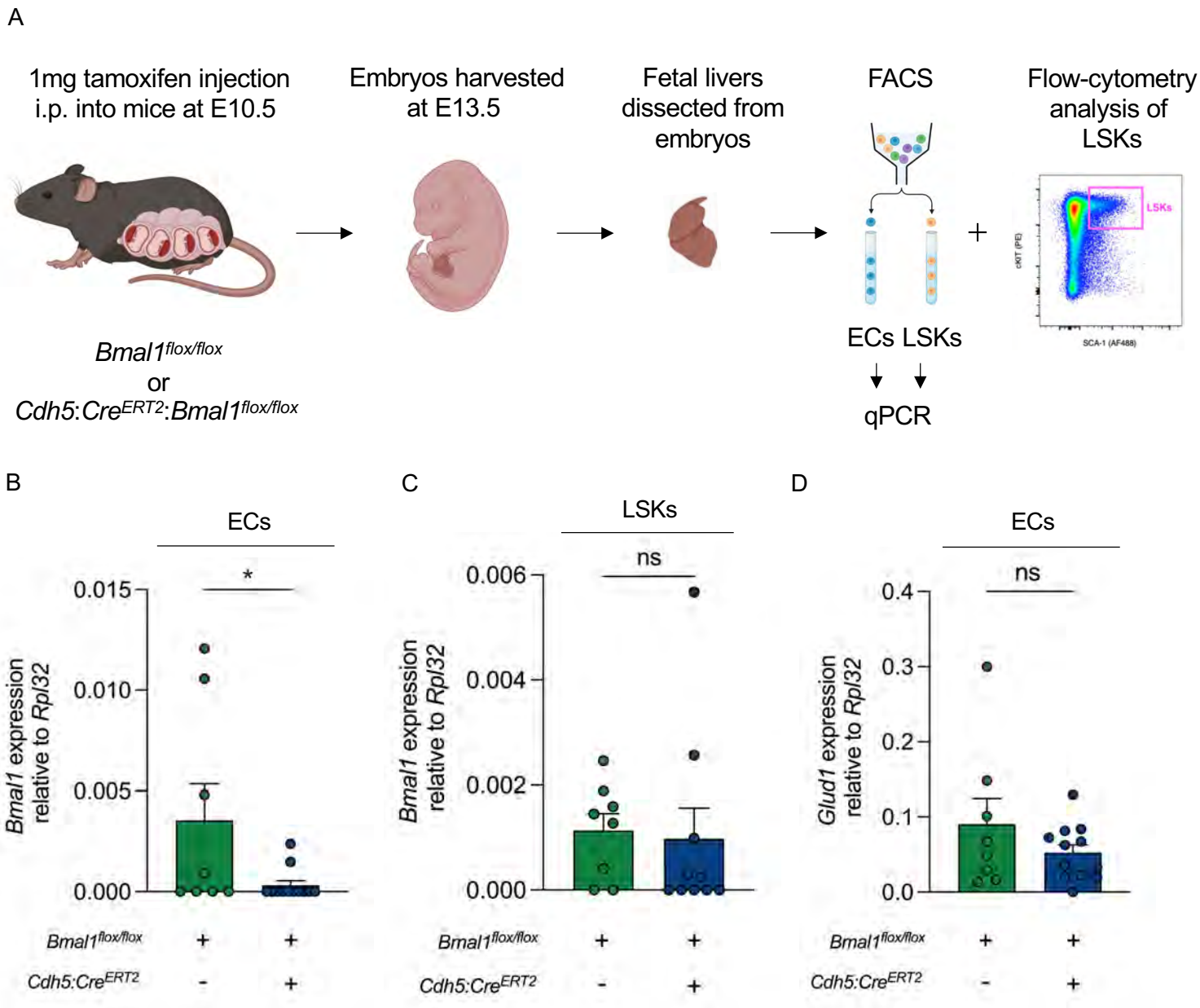

Fig. S13. Endothelial-specific deletion of *Bmal1* in mouse does not result in a difference in HSPC numbers in the fetal liver. A. Schematic of murine experiments. **B.** *Bmal1* expression in fetal liver endothelial cells of *Cdh5*:*Cre*^{ERT2}:*Bmal1*$^{flox/flox}$ embryos and controls at E13.5, as measured by qPCR. **C.** *Bmal1* expression in fetal liver LSKs (HSPCs) of *Cdh5*:*Cre*^{ERT2}:*Bmal1*$^{flox/flox}$ embryos and controls at E13.5, as measured by qPCR. **D.** *Glud1* expression expression in fetal liver endothelial cells of *Cdh5*:*Cre*^{ERT2}:*Bmal1*$^{flox/flox}$ embryos and controls at E13.5, as measured by qPCR. Statistical significance between two groups was calculated using unpaired two-tailed Student's *t*-tests assuming equal variance.

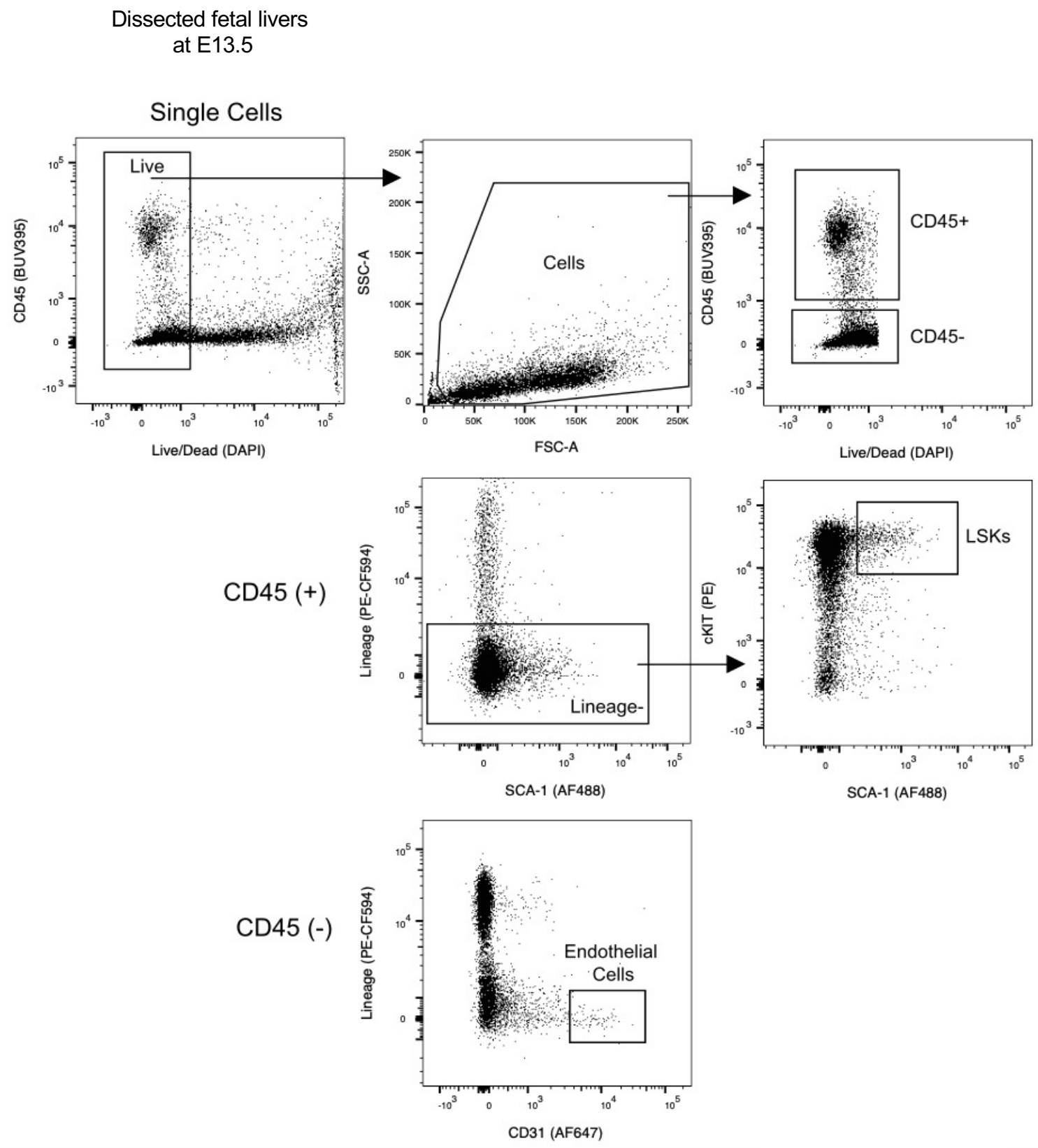

Fig. S14. Fluorescence activated cell sorting (FACS) strategy for sorting LSKs (HSPCs) and endothelial cells from mouse embryo fetal livers at E13.5. FACS plots to depict the strategy used to sort Lin$^-$SCA-1$^+$ cKIT$^+$ LSKs and CD31$^+$ endothelial cells from mouse embryo fetal livers at E13.5.

A

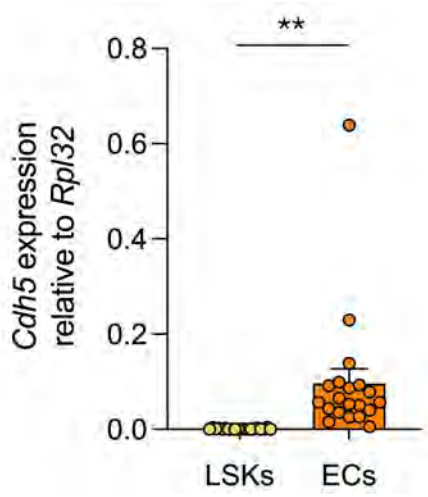
**
0.8
0.6
0.4
0.2
0.0
Cdh5 expression relative to Rpl32
LSKs
ECs

B

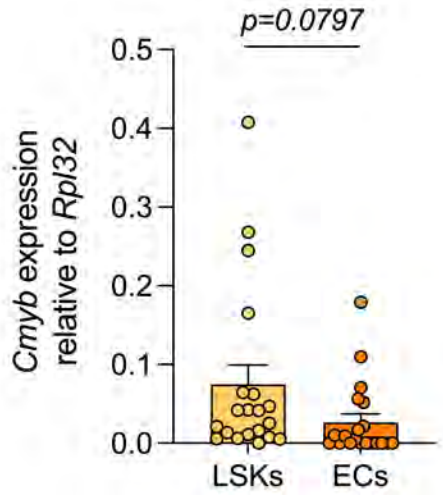
p=0.0797
0.5
0.4
0.3
0.2
0.1
0.0
Cmyb expression relative to Rpl32
LSKs
ECs

C

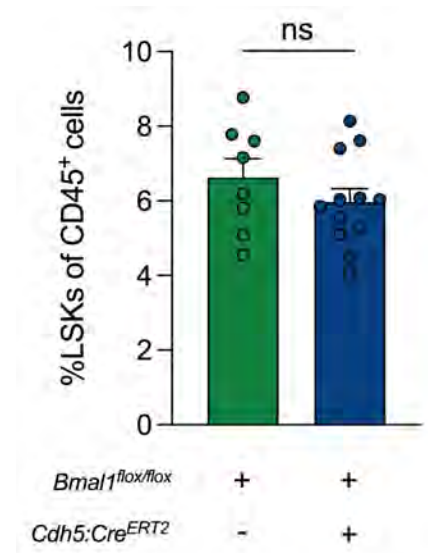
ns
10
8
6
4
2
0
%LSKs of CD45+ cells
Bmal1flox/flox + +
Cdh5:CreERT2 - +

D

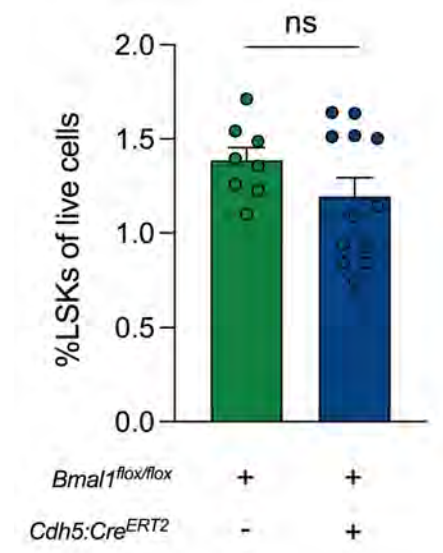
ns
2.0
1.5
1.0
0.5
0.0
%LSKs of live cells
Bmal1flox/flox + +
Cdh5:CreERT2 - +

E

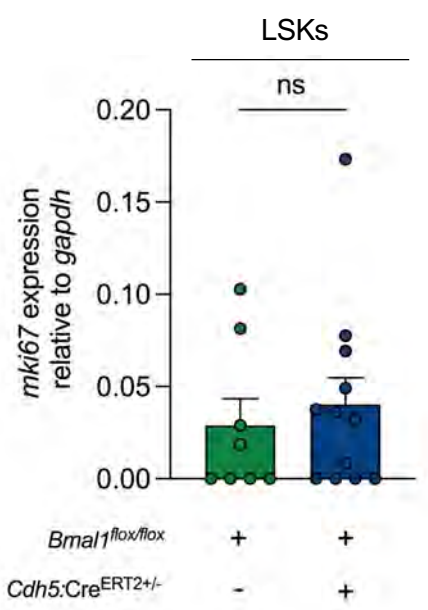
LSKs
ns
0.20
0.15
0.10
0.05
0.00
mki67 expression relative to gapdh
Bmal1flox/flox + +
Cdh5:CreERT2+/- - +

F

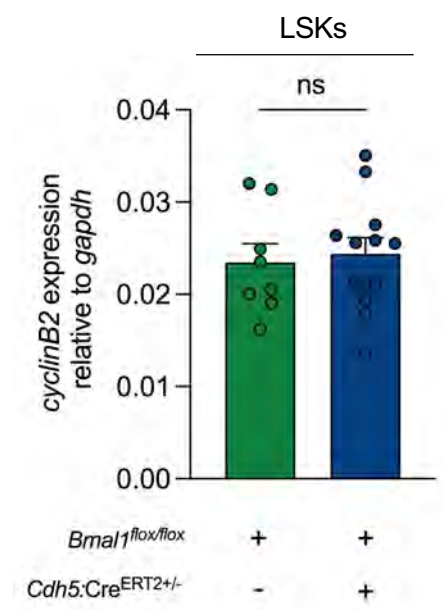
LSKs
ns
0.04
0.03
0.02
0.01
0.00
cyclinB2 expression relative to gapdh
Bmal1flox/flox + +
Cdh5:CreERT2+/- - +

Fig. S15. Endothelial-specific deletion of *Bmal1* in mouse does not alter LSK (HSPC) numbers in the fetal liver or *Bmal1* expression in LSKs. A. *Cdh5* expression in mouse fetal liver LSKs and endothelial cells at E13.5, as measured by qPCR. **B.** *Cmyb* expression in mouse fetal liver LSKs and ECs at E13.5, as measured by qPCR. **C.** %LSKs of $CD45^+$ cells in *Cdh5*:Cre^{ERT2}:$Bmal1^{flox/flox}$ embryos and controls at E13.5, as measured by flow cytometry. **D.** %LSKs of live cells in *Cdh5*:Cre^{ERT2}:$Bmal1^{flox/flox}$ embryos and controls at E13.5. **E.** *Mki67* expression in fetal liver LSKs of *Cdh5*:Cre^{ERT2}:$Bmal1^{flox/flox}$ embryos and controls at E13.5, as measured by qPCR. **F.** *Ccnb2* expression in fetal liver LSKs of *Cdh5*:Cre^{ERT2}:$Bmal1^{flox/flox}$ embryos and controls at E13.5, as measured by qPCR. Statistical significance between two groups was calculated using unpaired two-tailed Student's *t*-tests assuming equal variance.

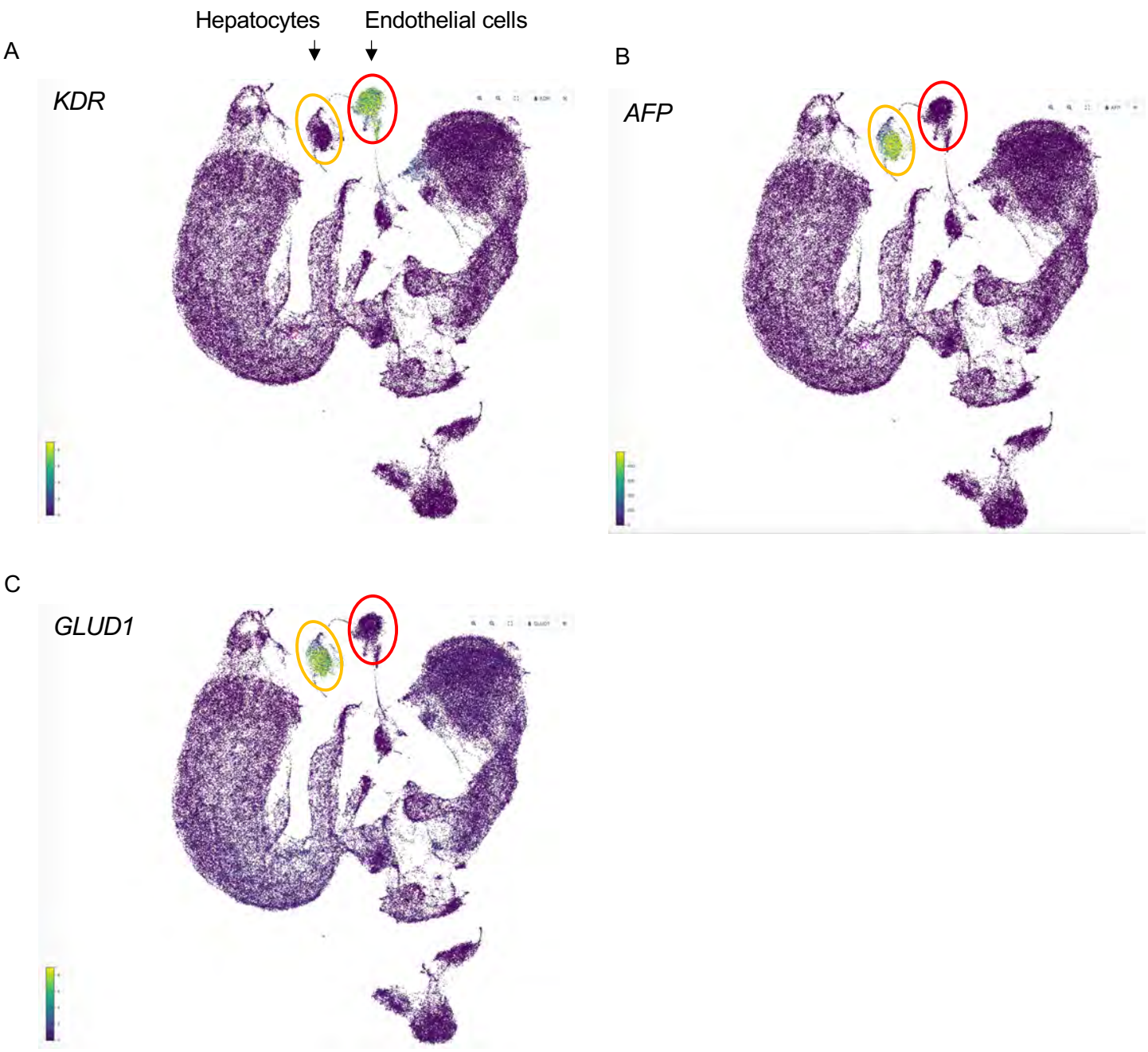

Fig. S16. *GLUD1* is expressed specifically in hepatocytes in human fetal liver. A. *KDR* expression defines the endothelial cell cluster. **B.** *AFP* expression defines the hepatocyte cell cluster. **C.** *GLUD1* is specifically expressed in hepatocytes of the human fetal liver. Yellow and red ovals denote the hepatocyte and the endothelial cell clusters respectively.

Table S1. Primers used for *in situ* hybridization probe generation

Gene	Forward	Reverse
bmal1a	AGAACAGCTGTCATCGTCAG	TCAAGCATACTGCCCGAAAC
bmal1b	CTTCATTAGTGCCTACCTGC	ACTCATAGAAAGACGTGCCC
clocka	TCATCTGTACAGACAGCAGG	TGCTGCTGTTGGAGTTGTTG
glud1a	ACAGCCAACCGGTATAACCT	ATCTGTCCCAAGAAGCAGCA
glula	ATCTCCCATTTACTGGACTG	TGCGACTTTGTACCGCACAA
glulb	GCTAGCATACGAATTCCACG	AGTCAGCGCCATACAAGTAC
slc1a5	CTGGACCCAAACCTTGTGAA	CCGGCATCTGAGGTGTTTTA
slc38a5a	TGGGTCAATGGAAAGCAGTC	GGGGGGCTAATAATTCTGAC
slc38a5b	GAGAGAATCGAAGTGGAGGA	TGGGGACAACAGAAAACTGG

Table S2. Primers used for generating dominant-negative *bmal1a* lines

line	Forward	Reverse
DN-bmal1a	AAGAATTCACCATGGCAGACC AAAGAATGGA	AACTCGAGTTATCCTTCAAG CATACTGCCC
R88A-DN-bmal1a	GGCACACAGTCAAATAGAGAA GAGAGCAAGGGATAAAATGAA CAG	CTGTTCATTTTATCCCTTGCT CTCTTCTCTATTTGACTGTG TGCC

Table S3. Primers used for genotyping

Primer	Forward	Reverse
UAS	AAAGCGGCCGCGGGATCACG CGGCCATCA	AAAACTAGTCGTGTGGAGG AGCTCAAAG
Cre	CGATGCAACGAGTGATGAGG	CGCATAACCAGTGAAACAG C
Bmal1 (flox)	ACTGGAAGTAACTTTATCAAA CTG	CTGACCAACTTGCTAACAAT TA

Table S4. qPCR Primers used in this study

Gene	Forward	Reverse
bmal1a	AAGACATTACGAGGGGCCAC	AGAGGAAACCATCAGCAGCC
bmal1b	ATGGCCGTCCAGCATATGAA	TGGCCAATCAGGTCATTCTG
per2	CCTTCTCGAGACATCCAGAA	ATGCACGCCTTGATGTCGAT
glud1a	GTGCAGTTGTAGATGTGCCT	AACGTCTTGTCTCCAAACCC
slc1a5	GCTGCTTTTCAGTCGTATGC	AGGTGCATACCACATGATCC
slc7a5	ACTCCTCTGCCTTCACTCAT	GGGCAGCAGAATATTGACCT
slc38a3a	CCTCTTCAACCTCAACTCAC	GCTCGGCTTCTACCTTATCA
slc38a3b	GCTGCATGGTTTTCTTCCTC	GATGGTGTAAGCAGTCTGTG
slc38a5a	CATCAACCCACAGACTGCAT	CAAAGATAGCAGTCAGCAGG
slc38a5b	ACGCAATCCCACAAAGAGAC	AACAGAAGCTGAAGAAGGGC
slc7a8a	GAACTGGTCGACCCTTATGT	ACCAAACGTCACAGCTACAG
slc7a8b	CATCCCAGCTTTGCTCATCA	CAAGCTCACTTTGATTGGCC
slc7a9	CACCTTCTCCAGCTCTAATG	ATGACTATCGGCACCTTGAC
slc7a6	GAAAGGAACCTTCCTCTGTC	TCCCACGAAAAACAACCTGG
slc7a7	TATTCCAGGGTTACACCCAG	CAGAGGGAGATTTCTCTCTG
slc38a2	AATATAGCCCTGGATCTGCG	CTCCTTCATTGGCCGTTTTG
slc38a7	CTTCAGATGTGCATGATGGC	TTATTGCGCCGATCAGCTTG
slc38a8a	TTTCAGTGTCATGAGGCCTG	GGATCACAGATCTTCCAAGC
slc38a8b	AGATGGTGAGTCTGGTGTTC	CGTACAGAGACAGACACAAC
glula	CTGCCAGTTCTCAGTTGAGT	GGTGGTTGGTTTCTGCAGTT
glulb	CCTGCAGAAACCAATCTTCG	GAAAGGATGACCATCTGTGC

Supplementary Table 4 continued.

Gene	Forward	Reverse
Bmal1	AGAGGTGCCACCAACCCATA	TGAGAATTAGGTGTTTCAGTTC GTCAT
Mki67	GAAGTCAAAGAGCAAGAGGC	CTTTCCAAGGGACTTTCCTG
Ccnb2	TGGCGAAGAAACCTCAGAAC	CTCTCTTCCTTCATGGAGAC
Glud1	AAGGGAGGTATCCGTTACAG	TAAAACCCTTCTTGGCCAGC
Glul	AACCTGCAGAGACCAACTTG	AAGCCATTGGAAGGCCAACC
Cdh5	CCCGTCTTTACTCAATCCAC	TGGGTTTGATGATACCCTCG
Cmyb	AATTATCTGCCCAACCGGAC	GCTTCGGACCATATTTCTGG
Rpl32	ACAATGTCAAGGAGCTGGAG	TTGGGATTGGTGACTCTGATG

Table S5. Differentially expressed genes in FACS-sorted CHT ECs from *kdrl:GAL4;UAS:DN-bmal1a;kdrl:EGFP* embryos and controls at 36 hpf, as determined by RNA-sequencing.

Gene	logFC	logCPM	PValue	FDR
ngs	-4.2227112	6.294271	2.78E-20	2.84E-16
zic2a	-13.462472	4.05282394	3.34E-16	1.71E-12
nr4a1	-2.5461074	8.11258794	7.82E-16	2.67E-12
stab2	-1.9659453	10.1521358	2.62E-12	6.69E-09
hbbe1.1	1.91447154	9.86835633	1.28E-11	2.62E-08
aplnrb	-1.8823056	8.45007857	3.38E-10	5.76E-07
sik1	-1.8327877	7.88526296	6.36E-09	9.29E-06
si:ch211-216l23.1	-2.2823842	6.48303109	1.18E-08	1.51E-05
ptgdsb	2.17830784	6.62134324	1.39E-08	1.58E-05
smyhc1	4.33630728	4.59961487	6.62E-08	6.78E-05
cxcl12a	-2.5511105	5.89194563	9.97E-08	9.27E-05
wu:fc13c02	-9.7672145	3.31158611	1.92E-07	0.00016332
frem1b	-1.6236739	7.87019329	2.35E-07	0.000185
dusp6	-1.7808807	7.08233982	2.66E-07	0.0001946
ctssa	-10.085346	3.20651378	2.88E-07	0.00019631
LOC795545	-1.3814214	9.93810679	6.61E-07	0.00042242
tle2	-1.8720053	6.60458259	9.31E-07	0.00056006
nr2f2	-1.9603837	6.34853658	1.69E-06	0.00091012
egr1	-2.0423472	6.18489191	1.69E-06	0.00091012
capn2b	-10.459604	2.95071324	1.89E-06	0.00096503
hbbe3	1.35327496	9.10362903	2.20E-06	0.00107276
stab1	-1.3210491	9.62758311	2.34E-06	0.00108907
hbae1	1.28745843	10.1074129	3.05E-06	0.00135584
skib	-2.1780644	5.89299564	3.91E-06	0.00164902
slit3	-1.668227	6.81155323	4.03E-06	0.00164902
si:ch73-173h19.3	-11.991945	2.58945236	5.13E-06	0.00201838
smarcc1b	-8.5224499	3.09332138	8.36E-06	0.00316861
igf2b	-1.4247733	7.58946146	9.34E-06	0.00341326
hapln3	-1.3483609	7.98459912	1.20E-05	0.00422076

Table S5 continued.

entpd1	-1.5350104	6.92570873	1.40E-05	0.00477225
dct	-11.794301	2.39319136	1.73E-05	0.00569727
sash1a	-1.4526771	7.10920245	2.05E-05	0.00655526
ptrfb	-1.4655101	7.04984696	2.15E-05	0.00666733
nr1d2a	-9.9449156	2.65478555	2.76E-05	0.00831725
flrt3	-1.3230721	7.64312653	3.35E-05	0.00963465
zgc:91999	-7.4565272	3.09902905	3.39E-05	0.00963465
col2a1a	-1.5410953	6.61662363	4.25E-05	0.01176571
ghrb	-1.9204009	5.85182775	4.99E-05	0.0130612
tnw	-2.8881499	4.75933569	5.09E-05	0.0130612
si:ch211-5k11.12	1.13522648	9.3816389	5.18E-05	0.0130612
apoeb	-1.1182255	9.89213685	5.23E-05	0.0130612
znf710a	-1.3288282	7.28693991	5.72E-05	0.01393695
sncga	-3.9252708	4.06357129	7.57E-05	0.01801995
ccdc85a	-11.470047	2.07218449	8.32E-05	0.01853683
flt4	-1.1488373	8.57667548	8.33E-05	0.01853683
fosab	-1.2294515	7.82183536	8.33E-05	0.01853683
hbae3	1.0771241	9.87548144	9.71E-05	0.02113708
glud1a	-1.3051016	7.14805821	0.00010911	0.02325963
fbn2b	-1.3149663	7.09098638	0.00011514	0.02404266
si:ch211-69i14.4	-1.8851976	5.73117113	0.00011783	0.0241127
zcchc24	-1.2066872	7.72374425	0.00013075	0.02581496
spry2	-1.8703444	5.73358479	0.00013119	0.02581496
sema3ab	-1.1772064	7.88471207	0.00014631	0.02824682
lin28a	-8.8878815	2.51873033	0.00015801	0.02947478
cyp26b1	-1.8893798	5.65418847	0.00015844	0.02947478
scpp8	1.23554338	7.3266291	0.00016735	0.03037753
ntmt1	-1.4818366	6.44268729	0.00016923	0.03037753
akap12b	-1.0861426	8.73653694	0.00017413	0.03071826
il1b	-2.0077729	5.47585413	0.00018434	0.03130001
tgfbi	-1.0721957	8.90402292	0.00018597	0.03130001

Table S5 continued.

il17rd	-11.2423	1.84741532	0.00018805	0.03130001
vwf	4.75498715	3.63264619	0.00018966	0.03130001
pdgfra	-11.223959	1.82911133	0.0001967	0.03166759
atp2a1	-1.2892976	6.99990615	0.00019808	0.03166759
ta	-8.8552072	2.40927091	0.00022605	0.03504386
aqp8a.1	-1.0174992	9.82666529	0.00023203	0.03543533
ces2	-11.111798	1.71843824	0.00025704	0.03798151
mxra8a	-11.101019	1.70836313	0.00026338	0.03798151
hsd17b7	-11.085498	1.69338638	0.00027295	0.03798151
cpped1	-11.083675	1.6906642	0.00027453	0.03798151
stm	-1.2355997	7.10261247	0.0002747	0.03798151
cblc	-11.081277	1.6883886	0.00027602	0.03798151
zgc:165518	-9.4820472	2.22821577	0.00028393	0.03798151
socs3b	-1.4709307	6.32326783	0.00028943	0.03798151
col8a2	-1.320044	6.71255685	0.00029253	0.03798151
sall3b	-11.05418	1.66119419	0.00029414	0.03798151
lgals1l1	-11.049469	1.65673299	0.00029726	0.03798151
me3	-1.9549936	5.45013514	0.00030067	0.03798151
cep128	-11.033951	1.64172523	0.00030792	0.03842249
gpm6aa	-11.007728	1.616281	0.00032673	0.03955676
fosl2	-1.0866873	8.09271064	0.00032788	0.03955676
mhc1zda	-8.4993627	2.40207262	0.00032861	0.03955676
zgc:103530	-10.990438	1.5997528	0.00033955	0.04014961
gpd1a	-1.6993266	5.81883835	0.00034413	0.04014961
jak2b	-1.6526955	5.90573966	0.00034531	0.04014961
hic1	-10.976555	1.58520585	0.00035087	0.04033766
ctnnd2b	-10.962689	1.57137887	0.00036209	0.04114331
fynb	-10.95777	1.56688254	0.00036591	0.04114331
lrrn1	-1.1362806	7.5681016	0.0003831	0.0423112
rac3a	-10.933996	1.54303941	0.00038616	0.0423112
ccdc80	-1.2564882	6.85549113	0.0004036	0.04346987
frs2a	-10.881646	1.49211823	0.00043318	0.04616994
tuba8l3	-1.0591881	8.11275729	0.00044618	0.04706509
gch2	2.41132159	4.80728949	0.00045687	0.04770096
myl10	2.14991059	5.07959741	0.00047787	0.0493893